C.P. No. 301
(18,124)
A.R.C. Technical Report

C.P. No. 301
(18,124)
A.R.C. Technical Report

MINISTRY OF SUPPLY

AERONAUTICAL RESEARCH COUNCIL

CURRENT PAPERS

Fin-and-Rudder Loads in a Yawing Manoeuvre: Effect of Direct and Power Assisted Rudder Movement

By

D. R. Puttock, D.C.Ae.

LONDON: HER MAJESTY'S STATIONERY OFFICE

1956

SEVEN SHILLINGS NET

C.P. No. 301

U.D.C. No. 629.13.014.4 : 533.69.048.1

Technical Note No. Structures 169

July, 1955

ROYAL AIRCRAFT ESTABLISHMENT

Fin-and-rudder loads in a yawing manoeuvre: effect of direct and power assisted rudder movement

by

D. R. Puttock, D.C.Ae.

SUMMARY

The severity of a yawing manoeuvre specified[1] for design purposes is investigated. It is found that the manoeuvre does not always represent the most critical case, higher fin-and-rudder loadings being obtainable when the specified frequency of rudder movement is changed. The inclusion of a power unit in the circuit may however impose restrictions on the rudder movement, leading to a reduction in the severity of the loading.

The analytical treatment includes the derivation of exact expressions for the angle of sideslip, fin-and-rudder load and rudder hinge moment induced by a sinusoidal rudder movement of arbitrary frequency. These expressions are analysed to determine how the maxima of each of the quantities are affected by variations in the frequency of the rudder movement. Computational charts are included to simplify the determination of these effects in particular instances.

The problems are illustrated with reference to a numerical example.

LIST OF CONTENTS

LIST OF APPENDICES

LIST OF TABLES

LIST OF ILLUSTRATIONS

1 Introduction

One of the present design requirements[1,2] stipulates that all aircraft shall have sufficient strength to permit the execution of two yawing manoeuvres. In one of these manoeuvres the rudder is to be moved sinusoidally through 1 or $1\frac{1}{2}$ cycles at a frequency equal to the damped natural yawing frequency of the aircraft, with an amplitude corresponding to a specified pedal force.

It will be noted that with the manoeuvre defined in this manner, the maximum rate of rudder movement needed for its execution is also implicitly determined. However, if the rudder circuit contains a power unit, the maximum rate of rudder movement is, in general, limited, and may well be less than that required for the above manoeuvre. The question then arises whether the associated design requirement, which normally determines the design loads for the fin-and-rudder, is not too severe in these cases.

The present note is primarily concerned with any limitations that a power unit may impose on the fin-and-rudder design conditions. Additionally, however, it also contains the results of a detailed study of the effects of the frequency of manual or power assisted sinusoidal rudder movement on the fin-and-rudder loading conditions. This study, which was a necessary preliminary to the main objective, has yielded some significant information on the manoeuvre executed without power assistance, and therefore, the results are presented and discussed.

The investigation is treated throughout from the airworthiness standpoint, so that the chief interest lies in the maximum loading conditions for a given effort during manoeuvres which the pilot is <u>able</u> to perform. No consideration is given to the determination of the most <u>likely</u> yawing manoeuvre, i.e. the one occurring most frequently.

2 Details of the investigation

For the preliminary study, exact analytical solutions, based on the equations of motion of the aircraft as used in response theory, were derived for the angle of sideslip, fin-and-rudder load and rudder hinge moment produced by a sinusoidal rudder movement of unit amplitude and arbitrary frequency (see Appendix I para.A.3). These solutions were analysed to determine how the quantities were affected by variations in the frequency of movement, attention being concentrated on their local maxima. The range of frequencies considered was from 0.5 to 1.5 times the damped natural yawing frequency of the aircraft. It was found that, for conventional aircraft, this range was sufficient to cover all the critical loading conditions.

In the presentation of this part of the investigation, the effects of frequency of rudder movement on the local maxima of the angle of sideslip are illustrated graphically. Unfortunately no such general approach is possible for the associated effects on the fin-and-rudder load and rudder hinge moment because of the increased number of significant parameters affecting these two quantities. However, with the use of approximate formulae, it has been possible to minimize the labour required to determine these effects in particular instances. A further simplification results from the use of a number of computational charts (see Appendix III). The effects of frequency are illustrated with the aid of a typical example, the data for which are given in Table I.

With a knowledge of the foregoing results the effects of the inclusion of a power unit into the rudder circuit have been assessed. Here too, a completely general presentation has been precluded by the number of

significant parameters involved, but the trends are illustrated by an extension of the above example (see Table I and para.3.4).

3 Discussion:

3.1 General note

The following paragraphs cover the most important aspects of the problem. A more detailed discussion of these aspects is presented in Appendix II. The suffix m is used throughout to denote local maxima of the various quantities.

3.2 Effect of frequency of rudder movement on the response in yaw

3.21 Introduction

The design yawing manoeuvre is specified in terms of a pedal force, which, in the absence of a power unit, is a function of the rudder angle and the response of the aircraft in yaw, itself a function of the rudder angle. Again, if a power unit is present, and limitations are imposed on the fin-and-rudder design conditions, it is probable that, the limitations will, in the first instance, relate to the amplitude and frequency of the specified rudder movement. It is therefore clear that, as a first step the response of the aircraft in yaw to unit sinusoidal rudder movement of different frequencies should be derived.

In this note the frequency of the rudder movement is, by definition, proportional to the parameter f, which is the ratio of the frequency of rudder movement to the damped natural yawing frequency of the aircraft (see Appendix I eqns. 3 and 4). Thus, when the response of the aircraft is expressed in terms of the amplitude of rudder movement, a change in f indicates a proportional change in both the frequency, and maximum (initial) rate of that movement. When the response is expressed in terms of pedal force, however, a change in f still indicates a proportional change in the frequency of the rudder movement, but the maximum rate depends upon the amplitude of the movement, which in turn depends on the hinge moment characteristics of the rudder. The case f = 1 corresponds to movement of the rudder at a frequency equal to the damped natural frequency of the aircraft (designated the damped resonant frequency) i.e. the frequency specified for the design manoeuvre.

3.22 Response per unit amplitude of rudder movement (See also Appendix II para B.1.2)

The response of an aircraft in angle of sideslip, β, to sinusoidal rudder movement is dependent (see Appendix I equation 5) on the frequency of the rudder movement, proportional to f, and on the ratio $\frac{R}{J}$, which is a measure of the aerodynamic characteristics of the aircraft. The influence of f on the response of a particular aircraft (i.e. at a particular value of $\frac{R}{J}$) is illustrated in Fig.(1), whilst its influence, and that of $\frac{R}{J}$, on the magnitude of the three local maxima which occur during a manoeuvre of $1\frac{1}{2}$ cycles of rudder movement, and which are of primary interest in the present note, is illustrated in Figs.(2), (3), (4) and (8). Fig.(8) relates to a specific example, the data for which are contained in Table I. Since the equation describing the lateral motion of the aircraft in the present problem, see Appendix I equation 2 and 4, is identical in form to that of a simple mass-spring-damping system subjected to a sinusoidal disturbance, it is therefore to be expected, and in fact confirmed by the figures, that the peak values of the local maxima occur with a frequency closer to the damped resonant frequency (f = 1) as the manoeuvre proceeds, and also that, at low frequencies of rudder movement, the first or second local maximum (in time) may be the absolute maximum in the manoeuvre.

The associated response in fin-and-rudder load, P, (see Appendix I equation 9 and Fig.(10)) is similar to that in β except for the insignificant maximum which occurs at the beginning of the manoeuvre, and, by comparing Fig.(8) and (11) it will be seen that the general effects of f on the significant P_m are similar to those on the β_m. Any qualitative differences between Figs.(8) and (11) are primarily dependent on the magnitude of the ratio $\frac{a_1}{a_2}$, but for conventional aircraft the differences will be small.

The response in rudder hinge moment, C_h (see Appendix I equation 17) is also illustrated in Fig.(10) and the variations of its local maxima with f are shown in Fig.(12). Here it should be noted that the values of f associated with the peak values of the C_{h_m} are much higher than in either of the cases covered above, cf. Figs.(8), (11) and (12). The dotted line in Fig.(12) represents the special case $b_1 = 0$ and divergence from it at any value of f is entirely due to $b_1\beta$ i.e. the effect of the response in sideslip on the hinge moments of the aircraft. In this connection the sign and magnitude of the ratio $\frac{b_1}{b_2}$ is of importance (see Appendix II para.B.1.2.3); with the value used in the derivation of Fig.(12) the response of the aircraft relieves the hinge moment due to rudder angle alone at low values of f.

The general equations for P and C_h are complex and somewhat unwieldy for use in detailed calculation of the local maxima, and in Appendix I para.A4 and A5 respectively approximate but more rapid methods are devised. The associated computational charts, are given in Appendix III. The accuracy of the approximate methods may be gauged from Fig.(10).

3.23 Response per unit maximum hinge moment or pedal force
(See also Appendix II para. B.1.3)

So far, the discussion has been confined to the effects of f on the β_m and P_m per unit rudder movement. The results presented in support of this discussion may now be re-examined to determine the effects of f on the β_m and P_m per unit maximum rudder hinge moment. These effects are illustrated in Figs.(19) and (20). The important difference to be noted between these Figs and Figs.(8) and (11) is that the peak values of the β_m and P_m no longer occur in the neighbourhood of f = 1. Consequently the damped resonant condition, which forms a basis for the determination of the design loading condition[1], does not necessarily represent the most critical loading condition. In the present example, see Table I, a load on the fin-and-rudder some 15% greater than the design load is obtained by moving the rudder sinusoidally with a frequency equal to 0.84 of the damped resonant frequency. This is due to the relieving effect of the aircraft response in yaw on the rudder hinge moments at low frequencies, and the ratio $\frac{b_1}{b_2}$ has, therefore, a significant effect on the absolute maximum loading condition. Other significant parameters are $\frac{R}{J}$ and $\frac{a_1}{a_2}$, but they affect the picture to a minor extent only.

3.3 Effect of a power unit on the rudder movement
(See also Appendix II para B.1.2)

To determine what limitations a power unit may impose on the fin-and-rudder design conditions, it is first necessary to consider what limitations, if any, the power unit will place on the rudder movement when an attempt is made to execute the specified manoeuvre. The precise limitations are difficult to assess, but for a qualitative investigation refined assumptions are probably not necessary, and in this note the rudder movement is assumed to be as illustrated in Fig.(22a), i.e. the frequency remains the same, but the amplitude is reduced. It is further assumed that the pedal force is proportional to rudder angle. However, to complete the picture it is desirable to consider also the effect of change in the frequency of the assumed movement, see Fig.(22b), on the response of the aircraft and to determine the critical conditions with the power unit present. The results of the preceding paragraphs are of use in this respect. The general effect of frequency changes on the amplitude of rudder movement, under the foregoing assumption, is illustrated in Fig.(23).

3.4 Effect of a power unit on the response of an aircraft
(See also Appendix II para.B.3)

To illustrate these effects the example of Table I has been extended to cover the case with a power unit in the rudder circuit. The characteristics of the power unit are assumed to be such that its maximum rate is reached when f = 0.7.

Thus below this frequency the power unit does not restrict the amplitude of movement, but above it the amplitude is reduced according to the relevant curve in Fig.(23).

The curves of the β_m and P_m per unit pedal force for a range of frequencies are given in Figs.(24) and (25) respectively. The full curves relate to the original example, i.e. without power unit, whilst the dotted and chain dotted curves relate to the example with power unit present, applying the assumed rudder displacement of para.3.3 and another, less realistic, and unconservative, approximation (see Appendix II para.B2) respectively. In practice it is to be expected that the actual curve would lie between the dotted and chain dotted curves.

The sets of curves indicate that, if a power unit restricts the movement of the rudder such that the design conditions cannot be met, the critical β_m and P_m obtained are lower than those associated with the specified design conditions. Further these critical conditions do not necessarily occur at the damped resonant frequency of the aircraft.

4 Conclusions:

(1) If the design manoeuvre is defined in terms of the amplitude of the rudder movement, the absolute maxima of the angle of sideslip and fin-and-rudder load occur, as would be expected, when the frequency of the rudder movement is very close to the damped natural yawing frequency of the aircraft, i.e. close to the damped resonant conditions.

(2) The absolute maximum hinge moment for usual values of b_1 and b_2 i.e. $\frac{b_1}{b_2}$ positive and b_2 negative, occurs at a much higher frequency than the damped resonant frequency, depending on the value of $\frac{b_1}{b_2}$. At low frequencies the response of the aircraft has a relieving effect on the

hinge moments, through b_1, which allows the application of greater rudder amplitudes for a given pedal force than would be predicted from a knowledge of the hinge moment due to rudder angle alone.

(3) If the design manoeuvre is defined in terms of a maximum hinge moment or pedal force, the absolute maxima of the angle of sideslip and fin-and-rudder load occur at frequencies much below the damped resonant frequency, the precise values depending on $\frac{R}{J}$, $\frac{a_1}{a_2}$ and $\frac{b_1}{b_2}$.

(4) It follows from (3) that the present design requirement, which calls for movement of the rudder at the damped resonant frequency up to a specified pedal force, does not always form the critical case. In some cases greater angles of sideslip and fin-and-rudder loads may be obtained by a slight reduction in the frequency of rudder movement.

(5) If a power unit limits the rudder movement such that the design conditions cannot be realised the ensuing fin-and-rudder loads are in general lower than those of the present design requirement.

NOTATION

A,B,C	coefficients in equation 9
$a_1 = -\frac{\partial C_{Yf}}{\partial \beta}$	(including effects of local sidewash at the tail)
$a_2 = \frac{\partial C_{Yf}}{\partial \zeta}$	
b	wing span
$b_1 = -\frac{\partial C_h}{\partial \beta}$	(including effects of local sidewash at the tail)
$b_2 = \frac{\partial C_h}{\partial \zeta}$	
C_h	rudder hinge moment coefficient
C_{Yf}	lateral force coefficient of the fin and rudder
f ratio	$\frac{\text{frequency of the sinusoidal rudder movement}}{\text{natural frequency of the damped yawing oscillations of the aircraft}}$
g	gravity constant
H	rudder hinge moment
H_e	amplification factor in equation 5
i_c	coefficient of inertia about the z axis
J	non-dimensional damped natural circular frequency of the aircraft in yaw

ℓ	fin-and-rudder arm
ℓ_R	distance of C.P. of fin-and-rudder load due to rudder deflection to C.G. of aircraft
$\overline{M}_r$	response factor, see equations 21 and 27
n_v	static stability derivative
n_r	damping derivative in yaw
P	fin-and-rudder load
Q_r $Q_{\pi/2}$	response factors, see Figs.2, 3, 4 and 13
R	non-dimensional damping factor of the lateral oscillation
$\hat{r}$	non-dimensional angular velocity in yaw
S	wing area
S"	fin-and-rudder area
t	time in seconds
$\hat{t} = \frac{W}{g\rho SV}$	unit of aerodynamic time in seconds
V	velocity of C.G. of the aircraft
$\overline{V}_R = \frac{S''\ell_R}{Sb}$	fin-and-rudder volume coefficient
W	weight of the aircraft
$\overline{X}$, $\overline{Y}$	response factors, see equation 15
x_r	variable in approximate equation, see equations 12, 18 and 23
$\overline{x}_r$	value of variable for which the approximate equations give maximum values
$\overline{y}_v = - y_v$	lateral force derivative due to β
$\overline{y}_\zeta = \frac{1}{2}\frac{S''}{S} a_2$	lateral force derivative due to ζ
β	sideslip angle
δ_n	non-dimensional rudder effectiveness
ε_r, $\varepsilon_{r-1,r}$	phase angles, see Figs.5, 6, 7, 15 and 16
ζ	rudder angle
μ_2, μ_3	non-dimensional mass of the aircraft - alternative expressions

$\nu_n = -\frac{1}{i_c} \cdot n_r$ non-dimensional damping parameter in yaw

ρ air density

τ non-dimensional aerodynamic time

φ_r frequency factor, see equation 24

$\omega_n = \frac{1}{i_c} \cdot \mu_2 \cdot n_v$ non-dimensional static stability parameter

Suffices

e maximum rudder angle

m local maxima

r pertaining to the r^{th} maximum of the response quantities r = 1,2 and 3

REFERENCES

No.	Author	Title, etc.
1		Design Requirements for Aeroplanes. (A.P.970, Vol.I and II).
2	T. Czaykowski	Dynamic Fin-and-Rudder Loads in Yawing Manoeuvres. R.A.E. Report Structures 76. June 1950.
3	J.P. Den Hartog	Mechanical Vibrations. McGraw-Hill Book Co., Inc. 1947.
4	D.R. Puttock	Effect of Rolling on the Fin-and Rudder Loads in Yawing Manoeuvres. Current Paper No.153. January, 1953.
5	S. Neumark	A Simplified Theory of the Lateral Oscillations of an Aircraft with Rudder Free Including the Effect of Friction on the Control System. R & M 2259, May 1945.

Attached: Appendices I, II and III
Table I
Figs.1 - 27
Drg. Nos. SME 77654/R - 77670/R inclus.
Detachable Abstract Cards

APPENDIX I

Analysis

A.1 Equations of motion

The non-dimensional equations of lateral motion of an aircraft may be written in the form, with the notation of ref.5.

$$\frac{d\beta}{d\tau} + \bar{y}_v\beta + \hat{r} = 0 \qquad (1a)$$

$$-\omega_n\beta + \frac{d\hat{r}}{d\tau} + \nu_n\hat{r} = -\delta_n\zeta \qquad (1b)$$

The underlying assumptions are that:

1. the forward speed is constant throughout the manoeuvre,
2. the fin-and-rudder force derivative due to rudder displacement ($\bar{y}_\zeta$) is negligible in equation (1a),
3. the vertical principal axis of inertia of the aircraft coincides with the z axis,
4. all rolling motion is neglected.

Equation (1a) and (1b) may be expressed in the form

$$\left.\begin{aligned} &\frac{d^2\beta}{d\tau^2} + (\bar{y}_v + \nu_n)\frac{d\beta}{d\tau} + (\omega_n + \nu_n\bar{y}_v)\beta = \delta_n\zeta \\ \text{or}\quad &\frac{d^2\beta}{d\tau^2} + 2R\frac{d\beta}{d\tau} + (R^2 + J^2)\beta = \delta_n\zeta \end{aligned}\right\} \qquad (2)$$

where

$$\left.\begin{aligned} R &= \tfrac{1}{2}(\bar{y}_v + \nu_n) = \text{non-dimensional damping factor of the oscillatory motion.} \\ J &= \sqrt{\omega_n - \tfrac{1}{4}(\nu_n - \bar{y}_v)^2} = \text{non-dimensional damped natural circular frequency factor of the oscillatory motion.} \end{aligned}\right\} \qquad (3)$$

It has been shown[4] that, with the present trends in aircraft design, the assumption of zero rolling motion is tending to become invalid. However, it is also shown that the main effect of neglect of the rolling is to modify the numerical values of the parameters R and J, and that the effect of rolling may be taken into account by using the exact values of R and J in all the response formulae obtained from the simplified approach. Fundamentally, it is necessary to add a further equation, an equation of rolling moments, to equations (1a) and (1b), and solve the resulting quartic to obtain the exact values of R and J. In practice, however, a method of factorization introduced by Neumark[5] may be used for this purpose. In the analysis of

particular cases where neglect of rolling if likely to incur appreciable error, it is suggested that equation 3 should not be used to calculate the values of R and J. Instead the formulae presented in Ref.4 should be used.

A.2 Definition of the manoeuvre:-

Consider a general fish-tail manoeuvre induced by the rudder, in which the rudder is moved to and fro in a sinusoidal motion at a frequency proportional to the natural frequency of the damped yawing oscillations of the aircraft then

$$\zeta = \zeta_e \sin Jf\tau \tag{4}$$

where the non-dimensional frequency of the rudder motion is Jf and

$$f = \frac{\text{frequency of rudder movement}}{\text{damped natural frequency of yawing oscillations of the aircraft}} .$$

A.3 Solution for the Angle of Sideslip

The solution of equation 2 for β , including equation 4, is

$$\beta = \delta_n \zeta_e H_e \left\{ fe^{-\frac{R}{J}J\tau} \left[2\frac{R}{J} \cos J\tau + \left(\frac{R^2}{J^2} - 1 + f^2\right) \sin J\tau \right] - 2\frac{R}{J} f \cos Jf\tau + \left(\frac{R^2}{J^2} + 1 - f^2\right) \sin Jf\tau \right\} \tag{5}$$

then

$$\frac{d\beta}{d\tau} = \delta_n \zeta_e H_e J \left\{ fe^{-\frac{R}{J}J\tau} \left[-\frac{R}{J}\left(\frac{R^2}{J^2} + 1 + f^2\right) \sin J\tau - \left(\frac{R^2}{J^2} + 1 - f^2\right) \cos J\tau \right] + 2\frac{R}{J} f^2 \sin Jf\tau + f\left(\frac{R^2}{J^2} + 1 - f^2\right) \cos Jf\tau \right\} \tag{6}$$

and

$$\frac{d^2\beta}{d\tau^2} = \delta_n \zeta_e H_e J^2 \left\{ fe^{-\frac{R}{J}J\tau} \left[-2\frac{R}{J} f^2 \cos J\tau + \left\{ \left(\frac{R^2}{J^2} + 1\right)^2 + f^2\left(\frac{R^2}{J^2} - 1\right) \right\} \sin J\tau \right] + 2\frac{R}{J} f^3 \cos Jf\tau - f^2\left(\frac{R^2}{J^2} + 1 - f^2\right) \sin Jf\tau \right\} \tag{7}$$

$$H_e = \frac{1}{J^2\left[\frac{R^2}{J^2} + (1+f)^2\right]\left[\frac{R^2}{J^2} + (1-f)^2\right]} .$$

These equations are valid for the ranges of f above and below resonance conditions (f = 1), but much of the following analysis only applies to the range f < 1.

Czaykowski[2] has considered a particular case of the fish-tail manoeuvre in which f = 1. For this particular case he was able to simplify the equation for the angle of sideslip and present graphically all the local maxima required for design purposes. In the general case, however, many of the simplifications are not valid and it is necessary to resort to numerical solution of the equation for β to obtain the required information for design. This involves the solution of the transcendental equation,

$$e^{-\frac{R}{J}J\tau} = \frac{2\frac{R}{J}f\sin Jf\tau + \left(\frac{R^2}{J^2} + 1 - f^2\right)\cos Jf\tau}{\frac{R}{J}\left(\frac{R^2}{J^2} + 1 + f^2\right)\sin J\tau + \left(\frac{R^2}{J^2} + 1 - f^2\right)\cos J\tau} \qquad (8)$$

which is the condition for the local maxima of β for any set of the parameters $\frac{R}{J}$ and f. In the present note the effect of f on the magnitude and times of occurrence of the first three local maxima of β have been calculated for a wide range of $\frac{R}{J}$ and the results are presented in Figs. 2, 3, 4, 5, 6 and 7. For convenience, the times of occurrence of the maxima are expressed in terms of a phase angle ε_r; the difference in positions of the corresponding maxima of β and ζ. Since $\zeta = \zeta_e \sin Jf\tau$, this is equivalent to measuring the angular position of each maximum of β from a datum $Jf\tau = \frac{\pi}{2}(2r - 1)$, where r (= 1, 2 and 3) signifies the particular maximum under consideration. The magnitudes of the maxima are given in terms of $Q_r = (-1)^{r+1} \cdot \frac{J^2}{\delta_n} \cdot \left(\frac{\beta_m}{\zeta_e}\right)_r$. Defined in this way Q_r is always positive. The range of f covered, $0.5 < f < 1.0$ is considered to be the most important range likely to be met in practice.

A.4 Fin-and-Rudder Load:

A.4.1 General formulae

The aerodynamic load on the fin-and-rudder during a lateral manoeuvre may be written (cf. Ref. 2)

$$\frac{P}{A} = -B\beta - C\frac{d\beta}{d\tau} + a_2\zeta \qquad (9)$$

where $A = \frac{1}{2}\rho V^2 S''$ $\qquad C = \frac{1}{\mu_3}a_1$

$$B = \left(1 + \frac{\bar{y}_v}{\mu_3}\right)a_1 \qquad \mu_3 = \frac{W}{g\rho S\ell}.$$

The condition for the maximum fin-and-rudder load is

$$- B \frac{d\beta}{d\tau} - C \frac{d^2\beta}{d\tau^2} + a_2 \frac{d\zeta}{d\tau} = 0. \qquad (10)$$

Using equations 4, 6 and 7 this condition may be rewritten as

$$e^{-\frac{R}{J}J\tau} = \frac{\left\{ f\left[\frac{2BR}{J} - CJ\left(\frac{R^2}{J^2}+1\right)\right] + CJ\, f^3 \right\} \sin Jf\tau + \left\{ f^2\left(\frac{CJ2R}{J} - B\right) + B\left(\frac{R^2}{J^2}+1\right) - \frac{a_2}{\delta_\eta H_e} \right\} \cos Jf\tau}{\left\{ f^2\left[B \cdot \frac{R}{J} - CJ\left(\frac{R^2}{J^2}+1\right)\right] + \left(\frac{R^2}{J^2}+1\right)\left[B \cdot \frac{R}{J} - CJ\left(\frac{R^2}{J^2}+1\right)\right] \right\} \sin J\tau + \left\{ f^2\left(\frac{2R}{J} CJ - B\right) + B\left(\frac{R^2}{J^2}+1\right) \right\} \cos J\tau} \qquad (11)$$

It is obvious that this equation is too complex to be of any practical value. The complexity is due to the nature of the equations for β and $\frac{d\beta}{d\tau}$, and, as implied in the previous paragraph, it is not possible to introduce general simplifications into the equations for β and $\frac{d\beta}{d\tau}$. However, it is possible to replace them locally by simpler functions for use in equations 9 and 10. In this way the labour can be kept to a minimum without any great loss in accuracy.

A.4.2 Approximate formulae for the fin-and-rudder load

Calculations have indicated that, in the general case, the component of the fin-and-rudder load which is dependent on $\frac{d\beta}{d\tau}$ has a marked influence on the precise positions of the maxima of the total load, although the magnitudes of these maxima are not appreciably affected. It is usually necessary to know both the total fin-and-rudder load and the load due to the rudder alone, and, since the load due to the rudder displacement alone is directly proportional to the position of the rudder at the P_m, it appears that the position of the P_m should be determined as accurately as possible. It is felt, therefore, that the term proportional to $\frac{d\beta}{d\tau}$, which may be neglected in the particular case $f = 1$ (cf. Ref.2), should be retained in the general case.

An analysis of the time histories of β and P in the general manoeuvre - see Fig.10 for example - suggests that, with the usual ranges of parameters, the various maxima of P occur later in the manoeuvre than the corresponding maxima of β (i.e. if the first small maximum of P is ignored). However, the phase angle between them is usually small. The new functions for β and $\frac{d\beta}{d\tau}$ need only be accurate, therefore, in the regions of the corresponding maxima of β and P. The response in β is oscillatory in character and a suitable function to describe the motion locally is found to be a circular function in which the coefficients and phase angles are chosen to give the local maxima exactly both in position and magnitude. The frequency of the new function may be assumed to be the same as that of the rudder movement. For convenience a separate datum is considered for each maximum. For the r^{th} maximum the local function for β is, using the notation of Fig.9

$$\frac{J^2}{\delta_n \zeta_e} \cdot (\beta)_r = (-1)^{r+1} Q_r \cos\left(Jf\tau - (2r-1)\frac{\pi}{2} - \varepsilon_r\right)$$

$$= (-1)^{r+1} Q_r \cos(x_r - \varepsilon_r) \qquad (12)$$

where $x_r = Jf\tau - (2r - 1)\frac{\pi}{2}$ and the particular datum is at $Jf\tau = (2r-1)\frac{\pi}{2}$. The first derivative of β may be obtained from equation 12 by differentiation.

The rudder movement about the new datum may be described as

$$\frac{J^2}{\delta_n \zeta_e}(\zeta)_r = (-1)^{r+1}\frac{J^2}{\delta_n}\cos x_r. \tag{13}$$

In these equations r(= 1, 2 and 3) indicates the particular local maximum under consideration. The angle ε_r is the phase angle between corresponding maxima of β and ζ and is considered positive when the β_m occurs after the corresponding ζ_m. Substituting these new functions in the general expression for P, equation 9, we have

$$\frac{J^2}{AB\delta_n}\left(\frac{P}{\zeta_e}\right)_r = (-1)^{r+1} Q_r\left[\frac{CJ}{B} f \sin(x_r - \varepsilon_r) - \cos(x_r - \varepsilon_r)\right] + \frac{a_2 J^2}{B\delta_n}\cos x_r$$

$$\text{or } \frac{1}{A}\left(\frac{P}{\zeta_e}\right)_r = (-1)^{r+1}\left[\bar{X}_r \sin(x_r - \varepsilon_r) + \bar{Y}_r \cos(x_r - \varepsilon_r) + a_2 \cos x_r\right] \tag{14}$$

$$\text{where} \quad \bar{X}_r = C \cdot \frac{\delta_n}{J} \cdot Q_r \cdot f$$

$$\bar{Y}_r = -B \cdot \frac{\delta_n}{J^2} \cdot Q_r \cdot \tag{15}$$

The equation for the position of the P_m is then

$$\bar{x}_r = Jf\bar{\tau}_r - \frac{\pi}{2}(2r - 1)$$

$$= \tan^{-1}\frac{\bar{X}_r \cos\varepsilon_r + \bar{Y}_r \sin\varepsilon_r}{a_2 + \bar{Y}_r \cos\varepsilon_r - \bar{X}_r \sin\varepsilon_r}. \tag{16}$$

Thus, for a given value of f, the only response quantities required for the calculation of the magnitude and position of a particular maximum of P are Q_r and ε_r. The values of these quantities, for a wide range of $\frac{R}{J}$ and f have been calculated from equations (5) and (8), and are given in Figs.2, 3, 4, 5, 6 and 7. The ringed points in Fig.10 indicate the accuracy of the new approach. The computational charts presented in Appendix III may be used for rapid estimation of the P_m.

A.5 Hinge Moment

The rudder hinge moment coefficient at any point in a lateral manoeuvre is

$$C_h = -b_1\beta + b_2\zeta. \tag{17}$$

The condition for the C_{h_m} is rather unwieldy, and the investigation of a particular case would be tedious. However, using the same technique as has been used in the previous section, approximate formulae may be derived to reduce the labour in such instances without any great loss in accuracy. All the maxima except the first may be obtained from a general formula.

1st Maximum:-

With typical values of b_1 and b_2, the first maximum of C_h occurs close to $Jf\tau = \frac{\pi}{2}$. In this region the response in β varies approximately as $(1 - \cos Jf\tau)$. If the new function for β is chosen such that it is exact at $Jf\tau = 0$ and $\frac{\pi}{2}$, we have, assuming the frequency of the motion to be the same as the frequency of the rudder displacement

$$\frac{J^2}{\delta_n}\left(\frac{\beta}{\zeta_e}\right) = Q_{\pi/2} \cdot (1 - \cos x_r) \tag{18}$$

where $x_r = Jf\tau$ and $r = 1$.

Equation (17) becomes

$$\left(\frac{C_h}{\zeta_e}\right)_1 = -\frac{\delta_n}{J^2} \cdot b_1 \cdot Q_{\pi/2} \cdot (1 - \cos x_1) + b_2 \sin x_1 \tag{19}$$

$$= \bar{M}_1 (1 - \cos x_1) + b_2 \sin x_1 \tag{20}$$

where $\bar{M}_1 = -\frac{\delta_n \cdot b_1}{J^2} \cdot Q_{\pi/2}$. (21)

The position of the maximum is at

$$\bar{x}_1 = \tan^{-1}\left(-\frac{b_2}{\bar{M}_1}\right). \tag{22}$$

Further Maxima:-

The dominant term in the equation for C_h, equation (17), is $b_2\zeta$. Thus for normal values of b_1 and b_2, the maxima in C_h will occur close to the corresponding maxima in ζ and the phase angle between corresponding maxima of β and C_h may be large. The function previously used to replace β locally (A.4.2) is only accurate in the region of each β_m. A more general function is therefore needed if accurate values of the remaining C_{h_m} are to be obtained.

A suitable general function is a sine function which gives exactly, the positions of $\beta = 0$ and the following β_m (in the region of the C_{h_m} in question) and also the magnitude of the β_m. The frequency of the new function is then automatically defined.

The function is (see also Fig.9)

$$\frac{J^2}{\delta_n}\left(\frac{\beta}{\zeta_e}\right)_r = (-1)^{r+1} Q_r \sin \varphi_r (x_r - \varepsilon_{r-1,r}) \tag{23}$$

where the local datum is at $Jf\tau = \pi(r-1)$ and $r = 2, 3$ etc.

$(\varepsilon_{r-1,r})$ is the phase angle between the positions of the corresponding $\beta = 0$ and $\zeta = 0$, considered positive when $\beta = 0$ occurs after $\zeta = 0$ and

$$\varphi_r = \frac{\text{local frequency of the response in } \beta}{\text{frequency of applied rudder movement}}$$

$$\simeq \frac{\pi/2}{\pi/2 + \varepsilon_r - \varepsilon_{r-1,r}} \tag{24}$$

Also

$$\frac{J^2}{\delta_n}\left(\frac{\zeta}{\zeta_e}\right)_r = (-1)^{r+1} \frac{J^2}{\delta_n} \cdot \sin x_r. \tag{25}$$

Hence equation (17) becomes

$$\left(\frac{C_h}{\zeta_e}\right)_r = (-1)^{r+1}\left(- Q_r \cdot \frac{\delta_n}{J^2} \cdot b_1 \cdot \sin \varphi_r(x_r - \varepsilon_{r-1,r}) + b_2 \sin x_r\right)$$

$$= (-1)^{r+1} (\overline{M}_r \sin \varphi_r (x_r - \varepsilon_{r-1,r}) + b_2 \sin x_r) \tag{26}$$

where
$$\overline{M}_r = - Q_r \cdot \frac{\delta_n}{J^2} \cdot b_1 . \tag{27}$$

The positions of the maxima are given by the following equation

$$\frac{\cos \overline{x}_r}{\cos \varphi_r(\overline{x}_r - \varepsilon_{r-1,r})} = - \frac{\overline{M}_r \varphi_r}{b_2} . \tag{28}$$

Within the ranges of $\frac{R}{J}$ and f considered in this note the range of φ_r is $0.8 < \varphi_r < 1.2$. For such cases

$$\cos \varphi_r(\overline{x}_r - \varepsilon_{r-1,r}) \simeq \cos(\overline{x}_r - \varepsilon_{r-1,r}) \tag{29}$$

and equation (28) may be simplified to

$$\frac{\cos \bar{x}_r}{\cos(\bar{x}_r - \varepsilon_{r-1,r})} = -\frac{\bar{M}_r \varphi_r}{b_2} . \qquad (30)$$

The solution to an equation of this type is given in Fig.27 for a considerable range of parameters.

Thus for rapid estimation of the C_{h_m}, the only additional response quantities, over and above those used in the estimation of the P_m, are $Q_{\pi/2}$ and $\varepsilon_{r-1,r}$. These may be found from equation (5). The values have been derived in the present note for a wide range of $\frac{R}{J}$ and f; the results are given in Figs.13, 15 and 16.

Fig.10 gives the exact response in β, P and C_h to a fish-tail manoeuvre for the aircraft considered in Table I. The ringed points are the maxima of P and C_h as calculated by the above formulae. It is seen that the approximate values are accurate to within 5%.

APPENDIX II

Detailed Discussion

The primary object of the present investigation has been to examine the effects of direct and power assisted rudder movement in relation to the design requirement[1]. This has necessitated a very detailed analysis of the general effects of rudder movement on the ensuing loading conditions. The chief points of interest are reported in para.3 of the main text, but the detailed discussion covering these points and further points of perhaps secondary interest from the airworthiness aspect are given in this Appendix. The Appendix is self contained and has the same general layout as para.3.

B.1 Effect of Frequency of Rudder Movement on the Response in Yaw

B.1.1 Introduction

To simplify the discussion, consideration is first given to the manner in which the various response quantities are affected by variations in the frequency of a sinusoidal rudder movement of constant amplitude (para.1.2). Then the quantities are considered in terms of a maximum pedal force for the same frequency range (para.1.3).

The rudder movement is defined as $\zeta = \zeta_e \sin Jf\tau$ where J is the non-dimensional, damped, natural circular frequency of the aircraft in yaw, and ζ_e is the amplitude of the movement. The non-dimensional circular frequency of the rudder movement is Jf, and f is, therefore, the ratio between the rudder frequency and the damped, natural yawing frequency of the aircraft. The case f = 1 corresponds to movement of the rudder at the damped resonant frequency of the aircraft in yaw. The non-dimensional rate of movement of the rudder is $\frac{d\zeta}{d\tau} = Jf\zeta_e \cos Jf\tau$ and the maximum (initial) rate is $Jf\zeta_e$. Thus when the response is expressed in terms of the amplitude of rudder movement, a variation in f indicates a proportional variation in both the frequency and maximum rate of movement of the rudder. However, if the response is expressed in terms of the maximum pedal force, a variation in f still indicates a proportional change in the frequency of the displacement, but the maximum rate of displacement depends on ζ_e, which, in turn, depends on the hinge moment characteristics of the rudder and, as will be seen later, on f itself although not proportional to it.

B.1.2 Response per unit amplitude of rudder movement

B.1.2.1 Angle of sideslip

The curves in Fig.1 give the response of an aircraft in angle of sideslip to sinusoidal movement of the rudder at four different frequencies. All the curves are presented with $Jf\tau = \left(\frac{Jf}{\hat{t}}\right) . t$, which is proportional to non-dimensional time, as a common base. In this way the disturbing movement, $\zeta = \zeta_e \sin Jf\tau$, appears as a single curve irrespective of the frequency. Plotted against $J\tau$, the curves of response would be considerably closer together with a resultant loss in clarity. It is seen that, while the general character of the curves is the same, both the positions and magnitudes of the local maxima are affected by variations in f. It is also apparent that the manner in which each of these maxima is affected depends on the particular local maximum in question.

For given values of δ_n, the rudder effectiveness, and J, the angle of sideslip is a function of $\frac{R}{J}$, f and time, (Appendix I equation (5)) and it is simple, although laborious, to determine the magnitudes and positions of its local maxima for different combinations of $\frac{R}{J}$ and f. The results of such an investigation are presented in Figs.2 to 4 and 5 to 7 respectively, and cover the three local maxima that occur in the duration of a manoeuvre of $1\frac{1}{2}$ cycles of rudder movement.

Examination of Figs.2 - 4, indicates that the magnitude of the individual maxima Q_1, Q_2 and Q_3 are all affected in a similar manner by the parameters $\frac{R}{J}$ and f, i.e. the maxima decrease if $\frac{R}{J}$ is increased, and increase to a peak and then decrease if f is increased. The effects become more pronounced as the manoeuvre develops, and the percentage change in Q_3 following a change in $\frac{R}{J}$ or f, or both, is much larger than the corresponding percentage change in Q_1. Also, as the manoeuvre develops, for a given value of $\frac{R}{J}$, the values of f associated with the peak values of Q_r tend towards the damped resonance value. Resonance conditions might be expected to give the peak value of Q_r, but there are two reasons why this is not so in any problem of the present type. Firstly, steady values are not reached in the specified duration of the manoeuvre, and secondly, the motion of the aircraft is damped. If the motion of a system is damped, the maximum response occurs at a frequency somewhat below resonance conditions, (cf. Ref.3) even if asymptotic conditions are reached. Further if the motion is overdamped, the maximum response drops away as the frequency is increased from zero, (cf. Ref.3 page 66), and no peak is apparent. In the case under consideration, where the damping is moderate, the peak values of Q_3 occur in the region of f = 0.9 to 0.95.

The positions of the maxima, see Figs.5 - 7, are all affected in a similar way by changes in $\frac{R}{J}$ and f, but not to the same extent. For a given value of $\frac{R}{J}$, the phase angles ε_1, ε_2 and ε_3 increase as f is increased. Thus, as the frequency of the displacement of the rudder is increased, the response in β tends to lag more and more behind the rudder displacement, cf. Fig.1. However, as the manoeuvre develops, the angles ε_r gradually decrease and approach a steady value. This value depends on $\frac{R}{J}$ and f, and may be obtained from a consideration of the asymptotic conditions (i.e. at $Jf\tau = \infty$). The positions of the maxima are not affected greatly by changes in $\frac{R}{J}$ except possibly at the lower end of the frequency range considered in this note.

The effects of $\frac{R}{J}$ and f on Q_r become more noticeable as the manoeuvre develops; this is best illustrated if the values of Q_r, for a given value of $\frac{R}{J}$, are plotted on the same frequency base, as in Fig.8, where the data of the example in Table I are used. It is seen that, at the lower end of the frequency range, Q_1 is the critical maximum for the manoeuvre. If the frequency is increased a point is reached at which Q_1 and Q_2 become equal. For a certain region beyond this frequency, Q_2 is the critical maximum and finally, as the damped resonance conditions are approached, Q_3 becomes the critical one. If the disturbing frequency is increased beyond f = 1, Q_2 and Q_1 in that order,

again become critical. The values of f, below the resonance conditions, at which Q_1 and Q_2 and Q_2 and Q_3 become equal are given in Fig.14, for a range of values of $\frac{R}{J}$. The values of f are little affected by $\frac{R}{J}$, except when this parameter is small.

The general equation for β, equation 5, contains trigonometrical functions of two distinct frequencies; one is the frequency of the disturbing motion, the other, the transient frequency, is the damped natural yawing frequency of the aircraft. With the range of f considered in this note, the two frequencies are of the same order. Where the initial effect of the transient response on the overall response is considerable, a condition approximating to the characteristic "beating" phenomenon is to be expected, i.e. motion with periodically varying amplitude. The transient response component is usually well damped, so that a true beating condition cannot develop. The remarks made above indicate that the amplitude of the response in β does vary in some complex way, and it appears that a form of beating is present in the sideslipping motion induced by sinusoidal rudder movement of frequencies close to the damped resonant yawing frequency of the aircraft.

B.1.2.2 Fin-and-rudder load

A time history of the fin-and-rudder load induced by sinusoidal rudder movement of a specific frequency is given in Fig.10 for the example of Table I. It is seen that the form of the response in P is similar to that in β, except at the beginning of the manoeuvre. The additional maximum that occurs in the initial stages of the manoeuvre is usually very small, and, for design purposes, may be disregarded. An examination of the general equation for P, equation (9), and the ranges of the parameters involved, indicates that the contribution to the total load of the component proportional to β is paramount. Thus, the fin-and-rudder load is affected by changes in $\frac{R}{J}$ and f in a similar way as the angle of sideslip, (cf. Figs.8 and 11) and, in the general case, it is necessary to have a knowledge of the three local maxima of P before the critical condition is stated.

Since P is greatly dependent on β, the corresponding maxima of these two quantities (disregarding the first, very small, maximum of P) occur at roughly the same times in the manoeuvre. With the usual values of the pertinent parameters, each maximum in β is closely followed by a maximum in P. The proximity of each pair of maxima depends on the value of f, i.e. on the frequency of the rudder displacement. For the particular case of $f = 1$, (see Ref.2), these maxima occur at $Jf\tau \simeq \pi$, 2π and 3π, i.e. when the rudder is central. In this special case, the contributions to the total loads of the components proportional to ζ and $\frac{d\beta}{d\tau}$ are negligible. However, for values of f other than unity, the maxima in β, and hence the maxima in P, do not occur in the region of $Jf\tau = \pi$ etc., but when the rudder is in a deflected position (cf. Fig.10). Thus, in the general case, each P_m contains a component due to the angular position of the rudder, and also, since the P_m occur after the corresponding β_m, a small component due to $\frac{d\beta}{d\tau}$ (see equation (9)).

Detailed calculations have indicated that the component of P due to $\frac{d\beta}{d\tau}$ has a marked influence on the precise positions of the P_m, although the magnitudes are not appreciably affected. Since the designer often needs to have a knowledge of the separate components of the P_m, as well as the values the P_m themselves, an accurate knowledge of the position of the P_m is also

desirable. The rudder angles associated with the P_m are usually small, although they vary appreciably with f, and the components of P_m due to the position of the rudder, which are proportional to $\zeta_e \sin Jf\tau$ are much affected by inaccuracies in the estimation of the rudder angles for the P_m. Thus it appears that the component of P due to $\frac{d\beta}{d\tau}$ should be retained in any computations involving the P_m and their components.

The general equation for P is complex, and rather unwieldy for use in detailed calculations of the maxima in P. This complexity arises from the presence of the components containing β and $\frac{d\beta}{d\tau}$. In Appendix I para.A.4.2, a method is developed to reduce the computational work involved in such a task. In this method, the exact equations for β and $\frac{d\beta}{d\tau}$ are replaced by simpler, approximate equations, which give good agreement with the exact equations in the neighbourhood of each β_m. A convenient expression for β_m is $Q_r \cos(Jf\tau-\varepsilon_r)$. The approximate equation for $\frac{d\beta}{d\tau}$ follows by differentiation. The two parameters Q_r and ε_r are precisely those used in para.B.1.2.1 to describe the β_m in magnitude and position. The accuracy of the new approach may be gauged from Fig.10. The "ringed" points are obtained from the computational chart. The curve shows exact values.

To illustrate the effect of f on the various maxima of P, all other factors considered constant, the example in Table I has been analysed. The results are obtained from the simplified formulae, and are presented in Fig.11. The curves confirm that the maxima in β and P are affected in a very similar manner by changes in f. The values of f for the peak values of the P_m are a little higher than those for the peak values of the β_m. These differences depend on the ratio $\frac{a_1}{a_2}$. If it is high the shape of the curves for the β_m and P_m are almost identical.

B.1.2.3 Rudder hinge moment

An example of the response in C_h to a sinusoidal rudder movement is given in Fig.10. Again the character of the response is similar to that in β. However, with the usual values of b_1 and b_2, the term $b_2\zeta$ in the equation for C_h, equation (17), is the dominant one, and the response in C_h follows the disturbance more closely than is the case with the response in β and P. Although the term $b_2\zeta$ is the dominant term, the effect of f on the response is considerable. This is mainly due to the changes in phase which occur between β and ζ when f is varied. This is especially marked when $\frac{b_1}{b_2}$ is positive and b_2 is negative, for, in such cases, the components of C_h, $b_1\beta$ and $b_2\zeta$, tend to oppose each other throughout the manoeuvre, and slight changes in phase between the two components cause considerable changes in the overall C_h response.

The effect of f on the various maxima of C_h for the example in Table I, is illustrated in Fig.12. The curves have the same general characteristics as the corresponding ones for the β_m and P_m. However, the values of f for

the peak values of the C_{h_m} are higher than in either of the other cases. The dotted line represents the maxima of C_h for the special case $b_1 = 0$ and divergence from this line, at any value of f, is entirely the effect of $b_1\beta$ i.e. the effect of the response of the aircraft in β. Below $f = 0.9$ in this particular example, the response of the aircraft reduces the hinge moment below the value obtained from the rudder alone. This tendency is likely to be present if $\frac{b_1}{b_2}$ is positive and b_2 is negative. The ratio $\frac{b_1}{b_2}$ has a controlling influence on the value of f at which the effect of the response of the aircraft changes sign. The significance of this feature will be discussed more fully in para.B.1.3.

The curves in Fig.12 indicate that it is necessary to calculate the values of all three C_{h_m} before stating the absolute maximum for the manoeuvre. However, the character of the equation for C_h, equation (17), is basically the same as that for P, and it is consequently unsuitable for use in detailed calculations because of the labour involved. In Appendix I para.A.5 further approximate equations for β are introduced to simplify the equation for C_h. For the 1st maximum of C_h, β is expressed as a function $Q_{\pi/2}(1-\cos Jf\tau)$ where $Q_{\pi/2}$ is a response factor involving the value of β at $Jf\tau = \frac{\pi}{2}$ (see Fig.13), and for the 2nd and 3rd maxima, β is expressed as a function of $Q_r \sin \varphi_r (Jf\tau - \varepsilon_{r-1,r})$. In both cases, the approximate equation for C_h may be tabulated for calculation of the maxima. The relevant charts are given in Appendix III. The accuracy of the approach may be gauged from Fig.10. The squared points are obtained from the approximate equations; the curve shows the exact values.

B.1.3 Response per unit maximum pedal force

So far the discussion has been confined to consideration of the effect of f on the response in β, P and C_h induced by unit amplitude sinusoidal rudder movement. The present design requirement specifies an amplitude of movement corresponding to a given pedal force being the maximum force applied in the manoeuvre. To compare the fin-and-rudder load for the design case $f = 1$, and the load induced by sinusoidal movement of the rudder at other frequencies, the effects of f on such quantities as the β_m and P_m per unit maximum C_h are required. Because of the large number of parameters involved, the effects are best illustrated by an example. In the previous paragraphs, the effects of f on $\frac{\beta_m}{\zeta_e}$, $\frac{P_m}{\zeta_e}$ and $\frac{Ch_m}{\zeta_e}$ have been given for the the example in Table I - see Figs.8, 11 and 12. At any value of f, the uppermost curve in each figure gives the absolute maximum value of each quantity produced in the full manoeuvre of $1\frac{1}{2}$ cycles of rudder displacement. If only one cycle of rudder displacement is to be considered, the curve for the third maximum $r = 3$, may be neglected in each case. If the reciprocal of the values on the upper boundary in Fig.12 are calculated, the resultant curve gives the value of ζ_e at each value of f, which must be applied to obtain unit C_{h_m} at some point in the manoeuvre. The curve is given in Fig.17. Any combination of ζ_e and f below this curve does not produce unit C_{h_m} at any time during the manoeuvre considered. Conversely, if a combination

above the curve is selected, unit C_{h_m} will be exceeded. It is seen that, as f is increased, the amplitude of rudder movement to produce unit maximum C_h decreases considerably. This effect is likely to occur in all cases where $\frac{b_1}{b_2}$ is positive and b_2 is negative. The rapidity with which ζ_e decreases as f is increased depends on the magnitude of $\frac{b_1}{b_2}$. The curve is discontinuous since it is based on the upper boundary in Fig.12. The points of discontinuity correspond to values of f at which the absolute maximum of C_h for the manoeuvre changes from one local maximum to the next (see para.B.1.2.3). The dotted line represents the special case $b_1 = 0$. The relieving effect of the aircraft response is clearly demonstrated.

If the combination of f and ζ_e at each frequency, to produce unit maximum C_h is known, the corresponding maximum (initial) rates of displacement of the rudder may be calculated since the maximum rate is proportional to $f\zeta$. The curve for the present example is given in Fig.18. The area below the curve corresponds to conditions which do not produce unit maximum C_h in the specified duration of the manoeuvre. The maximum rate increased to a peak and then drops as f is increased. In general, the position and magnitude of the peak depends on $\frac{b_1}{b_2}$.

The curves of the β_m and P_m per unit maximum C_h are plotted in Figs.19 and 20. They are similar in character to those for the β_m and P_m per unit ζ_e, but there is one important difference, namely that the peak values of the β_m and P_m per unit maximum C_h do not occur at or close to f = 1. Consequently, the damped resonance condition (i.e. the present design case) does not necessarily represent the critical loading case. In the present example, the greatest β_m, at f = 0.765, is 30% greater than the largest β_m at f = 1. Similarly the greatest value of P_m, at f = 0.84, is nearly 15% greater than the largest P_m at f = 1. A similar state exists if the duration of the manoeuvre is restricted to one cycle of rudder displacement.

Thus although the pilot may tend to displace the rudder at the damped natural yawing frequency of the aircraft if he executes a manoeuvre approximating to the fish-tail manoeuvre, he will be able, with conventional rudder controls and control characteristics, to apply a greater rudder amplitude for a given maximum pedal force than in the damped resonance condition by reducing the frequency of the displacement slightly (because of the relieving effect of the response of the aircraft on the hinge moments at low frequencies). Such an action will give rise to greater angles of sideslip and fin-and-rudder loads than those associated with the resonance case. The maximum rate of movement will be slightly higher than that associated with resonance conditions but, with direct control, it should be attainable without undue effort.

These remarks only apply strictly to the chosen example. The important parameters are a_1, a_2, b_1, b_2 and $^R/_J$, and provided these do not change much the overall picture will be similar.

B.2 Effect of a power unit on the rudder movement and pedal forces

In certain circumstances, the addition of a hydraulic power unit to the rudder circuit may impose restrictions on the movement of the rudder. In particular, there may be a restriction on the maximum rate at which the rudder can be moved. If the rudder pedals are moved sinusoidally at a low frequency, with low amplitude, the power unit is normally able to produce a corresponding movement at the rudder. However, if the frequency of the pedal movement is increased without altering the amplitude an initial rate of movement equal to the maximum rate of the power unit is eventually reached, cf. Fig.21.. Beyond this point, the pilot is not completely free to apply the movement he desires but is influenced by the characteristics of the power unit. The present design requirement specifies the frequency of the rudder movement, and also a pedal force (the maximum force applied in the manoeuvre). Implicit in this requirement is a maximum rate of rudder movement. If this rate cannot be realised through the power unit, the specified manoeuvre cannot be performed and the design requirement may then be too severe.

To examine this point, an assumption must be made with regard to the actual rudder movement obtained by the pilot when he attempts to perform the required manoeuvre. If the rudder is operated directly, the pilot is likely to move it at the damped natural yawing frequency of the aircraft. The addition of a power unit will probably not alter this tendency, although there is likely to be a small phase lag between the pedal and rudder movement. The phase lag is of no consequence however, in the present investigation since the aircraft response induced by the movement of the rudder is of primary interest. The effect of the power unit in restricting the rate of movement is probably to reduce the amplitude of the rudder displacement. Just how much the amplitude will be reduced is difficult to assess. A first approximation might be that the pilot moves the rudder sinusoidally at the specified frequency, with an initial rate equal to the maximum rate of the power unit. However, if he attempts to apply the specified movement of the rudder, corresponding to a pedal force of 100 lb, the amplitude may be greater than given by this approximation. In the absence of any flight or laboratory data to justify a more realistic approach it is assumed that the rudder is moved at a frequency equal to the damped natural yawing frequency of the aircraft, with an amplitude equal to the arithmetic mean of the specified amplitude and the amplitude given by the first approximation suggested above (see Fig.22a). Thus, the maximum initial rate of movement is higher than the maximum rate of the power unit. However, such an assumption is not unreasonable because it is usually possible, through the follow-up mechanism of the power unit, to boost up slightly the maximum rate a few percent. Also the movement of the rudder at a rate at, or close to the maximum rate of the power unit makes the execution of an exact sinusoidal movement difficult, and the initial movement is likely to be approximately linear rather than sinusoidal. Nevertheless the resultant rudder movement is assumed to be of sinusoidal form in order that use may be made of many of the graphs and charts already presented and discussed. Thus the conclusions reached are mainly qualitative, although they indicate the trends to be expected.

The specified amplitude of the rudder movement is that which can be obtained with a pedal force of 100 lb. The assumption with regard to the actual amplitude of movement of the rudder when a power unit is in the circuit, implies that the applied pedal force is less than this amount, provided that the relationship between pedal movement and pedal force is a linear one. However, if the pilot chooses to move the rudder at a lower frequency than the damped resonant frequency, he is able, without increasing the maximum rate of movement to obtain a bigger amplitude and consequently a bigger pedal force, i.e. a force closer to the specified 100 lb. This

reduction in frequency, which involves a corresponding increase in amplitude, may give rise to a greater fin-and-rudder load than could be obtained with the assumed movement - in much the same manner as in the case of the manoeuvre induced by direct operation of the rudder (para.8.1). If the maximum rate of the power unit is very much lower than the rate implicit in the specified manoeuvre, the power unit affects the pedal movement over a considerable range of frequencies. In this range, the effect of the power unit will be assumed to be as before, namely that and the amplitude is equal to the arithmetic mean of the specified amplitude and the amplitude corresponding to movement at the optimum rate of the power unit and the frequency in question (see Fig.22b). Thus the assumed rate of movement varies with the frequency of movement.

B.3 Effect of a power unit on the response of an aircraft

B.3.1 Example chosen

To illustrate the effects of a power unit, on the various response quantities, the previous example of Table I is extended to cover the case with a power unit in circuit. The characteristics of the unit are assumed to be such that its maximum rate is 0.7 of the maximum rate required to perform the specified fish-tail manoeuvre, i.e. the maximum attainable frequency of movement of the rudder, with the amplitude corresponding to a pedal force of 100 lb, is 0.7 of the damped natural yawing frequency of the aircraft, or simply, f = 0.7. At low frequencies, below f = 0.7, the pilot can apply the amplitude of movement corresponding to 100 lb pedal force, and the maximum initial rate of movement depends on the frequency he chooses to use. Above f = 0.7, with the influence of the power unit, the resultant amplitude of movement depends on the frequency as shown in Fig.23.

It is felt that the chosen characteristics of the power unit represent almost an extreme practical case, since it is not expected that the optimum rate of the unit will be much less than 0.7 of that required for the execution of the fish-tail manoeuvre. If it is, it will probably mean that the aircraft cannot be manoeuvred in the most efficient manner.

B.3.2 Angle of sideslip

Consider now Fig.24. The full line represents the case in which, for the range of frequencies considered, the power unit has no effect on the control motion i.e. the present design conditions, at f = 1, can be met. The β_m are expressed in terms of pedal force, and are obtained directly from Fig.8. In making this step it is assumed that the pedal force is proportional to pedal displacement. The dotted curve represents the case in which the power unit is added to the circuit. The amplitude of the rudder movement above f = 0.7 is reduced according to the relevant curve in Fig.23. The chain dotted curve has been produced by assuming that the rudder movement above f = 0.7 is sinusoidal but that the maximum rate is limited to the maximum rate of the power unit, i.e. the first approximation mentioned in para.B.2. In this case the amplitude of the movement decreases as the frequency is increased such that the maximum rate remains constant.

The curves indicate that, if the power unit restricts the movement of the rudder such that the design conditions cannot be reached, the maximum angle of sideslip obtainable is lower than that associated with the present design conditions. Also, this maximum may occur at a frequency considerably lower than the damped resonant frequency of the system.

B.3.3 Fin-and-rudder load

A similar set of curves has been produced for the fin-and-rudder load at various frequencies, Fig.25. The curves are very similar to those for the

angle of sideslip. If the assumed effect of the power unit on the pedal displacement is accepted rough quantitative conclusions may be drawn. In the example chosen, it is seen that the maximum load is approximately 18% lower than the specified design load. The maximum occurs when the rudder is moved at a frequency approximately equal to the damped resonant frequency. However, it is likely that in other examples, the critical frequency may differ from the damped resonant frequency.

B.3.4 Rudder hinge moment

The rudder hinge moment, which may be needed for the determination of the strength of components on the rudder side of the power unit, has also been calculated (see Fig.26). The effects of a power unit are similar to those found in the other two response quantities.

APPENDIX III

Computational Charts

The following charts may be used to calculate the local maxima of the fin-and-rudder load and rudder hinge moment produced by unit amplitude of sinusoidal rudder movement of a chosen frequency (αf), and the local maxima of the angle of sideslip and fin-and-rudder load per unit maximum C_h for the same frequency of movement. The corresponding maximum angle of sideslip per unit rudder movement may be obtained from Figs. 2, 3 and 4. If the duration of the manoeuvre is $1\frac{1}{2}$ cycles of rudder movement, three local maxima of each quantity are produced, corresponding to r = 1, 2 and 3 (for 1 cycle of movement the number of maxima is only two, r = 1 and 2), and for the chosen value of f, all three local maxima should be computed before stating the absolute maximum of the quantity for the chosen manoeuvre. The charts are based on the approximate formulae derived in Appendix I, namely

$$\frac{1}{\Lambda}\left(\frac{P_m}{\zeta_e}\right)_r = (-1)^{r+1}\left\{\bar{X}_r \sin(\bar{x}_r - \varepsilon_r) + \bar{Y}_r \cos(\bar{x}_r - \varepsilon_r) + a_2 \cos \bar{x}_r\right\}$$

$$r = 1, 2 \text{ and } 3$$

$$\left(\frac{C_{h_m}}{\zeta_e}\right)_r = \bar{M}_r(1 - \cos \bar{x}_r) + b_2 \sin \bar{x}_r$$

$$r = 1$$

$$\left(\frac{C_{h_m}}{\zeta_e}\right)_r = (-1)^{r+1}\left\{\bar{M}_r \sin \varphi_r (\bar{x}_r - \varepsilon_{r-1,r}) + b_2 \sin \bar{x}_r\right\}$$

$$r = 2 \text{ and } 3.$$

The charts may also be used to calculate the local and absolute maxima of the above quantities over a range of rudder movement frequencies thereby permitting the determination of the frequencies which produce the greatest angle of sideslip and fin-and-rudder load per unit rudder movement and maximum C_h, and the magnitudes of these quantities. In general, the critical frequency will lie in the range $0.5 \leq f \leq 1.0$.

The numerical values included in the charts illustrate the orders of magnitude of the quantities in the various columns etc.

Data required.

(see also List of Symbols):

a_1	ℓ_R	(ft)
a_2	n_v	

b	(ft)	n_r	
b_1		S	(ft^2)
b_2		S''	(ft^2)
f	a range	V	(ft/sec T.A.S.)
g	(ft/sec^2)	$\overline{V}$	
i_c		W	(lb)
ℓ	(ft)	y_v	

Basic formulae:

$$\mu_2 = \frac{W}{g\rho Sb} \qquad \delta_n = \frac{\mu_2 \overline{V}_R a_2}{i_c} \qquad A = \tfrac{1}{2}\rho V^2 S''$$

$$\mu_3 = \frac{W}{g\rho S\ell} \qquad R = \tfrac{1}{2}(\overline{y}_v + \nu_n) \qquad B = \left(1 + \frac{\overline{y}_v}{\mu_3}\right) a_1$$

$$\omega_n = \frac{\mu_2 n_v}{i_c} \qquad J = \sqrt{\omega_n - \tfrac{1}{4}(\nu_n - \overline{y}_v)^2} \qquad C = \frac{1}{\mu_3} a_1$$

$$\nu_n = -\frac{n_r}{i_c}$$

$$\overline{y}_v = -y_v$$

CHART I

Maximum Fin-and-Rudder Load Per Unit Amplitude of Simusoidal Rudder Displacement

1	a_2																							
2	$\frac{C \cdot \delta_n}{J}$		$\frac{-B \cdot \delta_n}{J^2}$	f	r	Q_r	ε_r (degrees)	$Q_r \cdot f$	$\bar{X}_r = \frac{C \cdot \delta_n}{J} \cdot Q_r \cdot f$	$\bar{Y}_r = \frac{-B \cdot \delta_n}{J^2} \cdot Q_r$	sin ε_r	cos ε_r	$\bar{X}_r \cos \varepsilon_r + \bar{Y}_r \sin \varepsilon_r$	$a_2 + \bar{Y}_r \cos \varepsilon_r - \bar{X}_r \sin \varepsilon_r$	$\tan \bar{x}'_r$	$\bar{x}'_r$ (degrees)	$(\bar{x}_r - \varepsilon_r)$ (degrees)	sin$(\bar{x}_r - \varepsilon_r)$	cos$(\bar{x}_r - \varepsilon_r)$	cos $\bar{x}'_r$	$\bar{X}_r \sin(\bar{x}_r - \varepsilon_r) + \bar{Y}_r \cos(\bar{x}_r - \varepsilon_r) + a_2 \cos \bar{x}'_r$	$(-1)^{r+1}.0$	$\frac{1}{A} \left(\frac{P_m}{\zeta_e}\right)_r$	$\left(\frac{P_m}{\zeta_e}\right)_r$
1																								
2	0.576		-4.00	0.6	1	1.23	66	0.984	0.566	-4.92	0.914	0.407	-4.26	-0.518	8.264	83.1	17.1	0.294	0.956	0.120	-4.30	1	-4.30	
"	"		"	"	2	1.75	53	1.400	0.806	-7.0	0.799	0.602	-5.11	-2.86	1.789	60.8	7.8	0.136	0.991	0.488	-5.85	-1	5.85	
"	"		"	"	3	1.88	45	1.503	0.867	-7.52	0.707	0.707	-4.70	-3.93	1.196	50.1	5.1	0.089	0.996	0.641	-6.13	1	-6.13	
"	"		"	0.8	1	"	"	"	"	"	"	"	"	"	"	"	"	"	"	"	"	"	"	
"	"		"	"	2	"	"	"	"	"	"	"	"	"	"	"	"	"	"	"	"	"	"	
"	"		"	"	3	"	"	"	"	"	"	"	"	"	"	"	"	"	"	"	"	"	"	
"	"		"	0.7	1	"	"	"	"	"	"	"	"	"	"	"	"	"	"	"	"	"	"	
"	"		"	"	2	"	"	"	"	"	"	"	"	"	"	"	"	"	"	"	"	"	"	
"	"		"	"	3	"	"	"	"	"	"	"	"	"	"	"	"	"	"	"	"	"	"	
						Figs 2,3,4	Figs 5,6,7	4 × 6	2 × 8	3 × 6	sin 7	cos 7	9×12+10×11	1 + 10 × 12 + 9 × 11	$\frac{12}{17}$	$\tan^{-1} 15$	16 - 7	sin 17	cos 17	cos 16	9×18+10×19 +1×20	$(-1)^{5+1}.0$	21 × 22	A × 23
						9	7	8	9	10	11	12	13	14	15	16	17	18	19	20	21	22	23	24

CHART IIa

Maximum Rudder Hinge Moment per Unit Amplitude of Sinusoidal Rudder Displacement (First Local Maximum)

b_1	b_2	$-\frac{\delta_n \cdot b_1}{J^2}$	f	r	$Q\pi/2$	$\bar{M}_1 = \frac{-\delta_n \cdot b_1}{J^2} \cdot Q\pi/2$	$\tan \bar{x}_1 = \frac{-b_2}{\bar{M}_1}$	$\bar{x}_1$ (degrees)	$\sin \bar{x}_1$	$\cos \bar{x}_1$	$1 - \cos \bar{x}_1$	$C_{h_1}/\zeta_e = \bar{M}_1(1 - \cos \bar{x}_1) + b_2 \sin \bar{x}_1$
					fig 13	3 x 6	$-2/7$	$\tan^{-1}$ 8	sin 9	cos 9	+(1 - 11)	7 x 12 + 2 x 10
1	2	3	4	5	6	7	8	9	10	11	12	13
-0.1	-0.3	0.127	0.6	1								
=	=	=	0.7	1								
=	=	=	0.8	1	0.59	0.075		76	0.970	0.242	0.758	-0.235

CHART IIb

Further Local Maxima of the Rudder Hinge Moment

b_1	b_2	$-\frac{\delta_n \cdot b_1}{J^2}$	f	r	Q_r	ε_r (degrees)	$\varepsilon_{r-1,r}$ (degrees)	$\bar{M}_r = \frac{-\delta_n \cdot b_1}{J^2} \cdot Q_r$	$\varphi_r = \frac{90}{90 + \varepsilon_r - \varepsilon_{r-1,r}}$	$-\frac{\bar{M}_r \varphi_r}{b_2}$	$\bar{x}_r$ (degrees)	$\bar{x}_r - \varepsilon_{r-1,r}$ (degrees)	$\varphi_r(\bar{x}_r - \varepsilon_{r-1,r})$ (degrees)	$\sin \varphi_r(\bar{x}_r - \varepsilon_{r-1,r})$	$\sin \bar{x}_r$	$\bar{M}_r \sin \varphi_r(\bar{x}_r - \varepsilon_{r-1,r}) + b_2 \sin \bar{x}_r$	$(-1)^{r+1.0}$	$\left(\frac{C_{h_m}}{\zeta_e}\right)_r$
					figs 2,3,4	figs 5,6,7	figs 15,16	3 × 14	$\frac{90}{90 + 15 - 16}$	$-\frac{17 \times 19}{2}$	fig.27	20 − 16	18 × 21	sin 22	sin 20	17 × 23 + 2 × 24	$(-1)^{5+1.0}$	25 × 26
1	2	3	4	5	14	15	16	17	18	19	20	21	22	23	24	25	26	27
−0.1	−0.3	0.127	0.6	2														
			"	3														
			0.7	2														
			"	3														
			0.8	2	1.75	53	53	0.222	1.0	0.740	50	−3	−3	−0.052	0.766	−0.241	−1	0.241
			"	3	1.88	45	48	0.239	1.034	0.824	36.5	−11.5	−11.9	−0.206	0.595	−0.228	1	−0.228

CHART III

Maxima of the Angle of Sideslip and the Fin-and-Rudder Load per Unit Maximum Rudder Hinge Moment

$\frac{\delta_n}{J^2}$	f	r	Q_r	$(-1)^{r+1}$	$(-1)^{r+1} \cdot \frac{\delta_n}{J^2} \cdot Q_r = \left(\frac{\beta_m}{\zeta_e}\right)_r$	$\frac{1}{A}\left(\frac{P_m}{\zeta_e}\right)_r$	$\left(\frac{C_{h_m}}{\zeta_e}\right)_r$	$\text{Maximum}\left(\frac{C_{h_m}}{\zeta_e}\right)$	$\left(\frac{\beta_m}{\text{Maximum } C_{h_m}}\right)_r$	$\frac{1}{A}\left(\frac{P_m}{\text{Maximum } C_{h_m}}\right)_r$
			figs 2,3,4	$(-1)^{3+1.0}$	1 x 4 x 5	Chart I	Chart II	Absolute maximum of 8 at each f considered positive	7/9	8/9
1	2	3	4	5	6	7	8	9	10	11
1.27	0.7									
=	=									
=	0.8	1	1.23	1	1.562	-4.30	-0.235		6.481	-17.83
=	=	2	1.75	-1	-2.223	5.85	0.241	0.241	-9.224	24.27
=	=	3	1.88	1	2.388	-6.13	-0.228		9.909	-25.44

TABLE I

Data for example

R	$= 0.664$	B	$= 2.527$
J	$= 3.775$	C	$= 0.115$
$\frac{R}{J}$	$= 0.175$	$\frac{a_1}{a_2}$	$= 1.39$
δ_n	$= 17.64$	a_2	$= 1.8$
$\frac{\delta_n}{J^2}$	$= 1.257$	b_1	$= -0.1$
		b_2	$= -0.3$
		$\frac{b_1}{b_2}$	$= 0.33$

WT.2078.CP.301.K3 - Printed in Great Britain

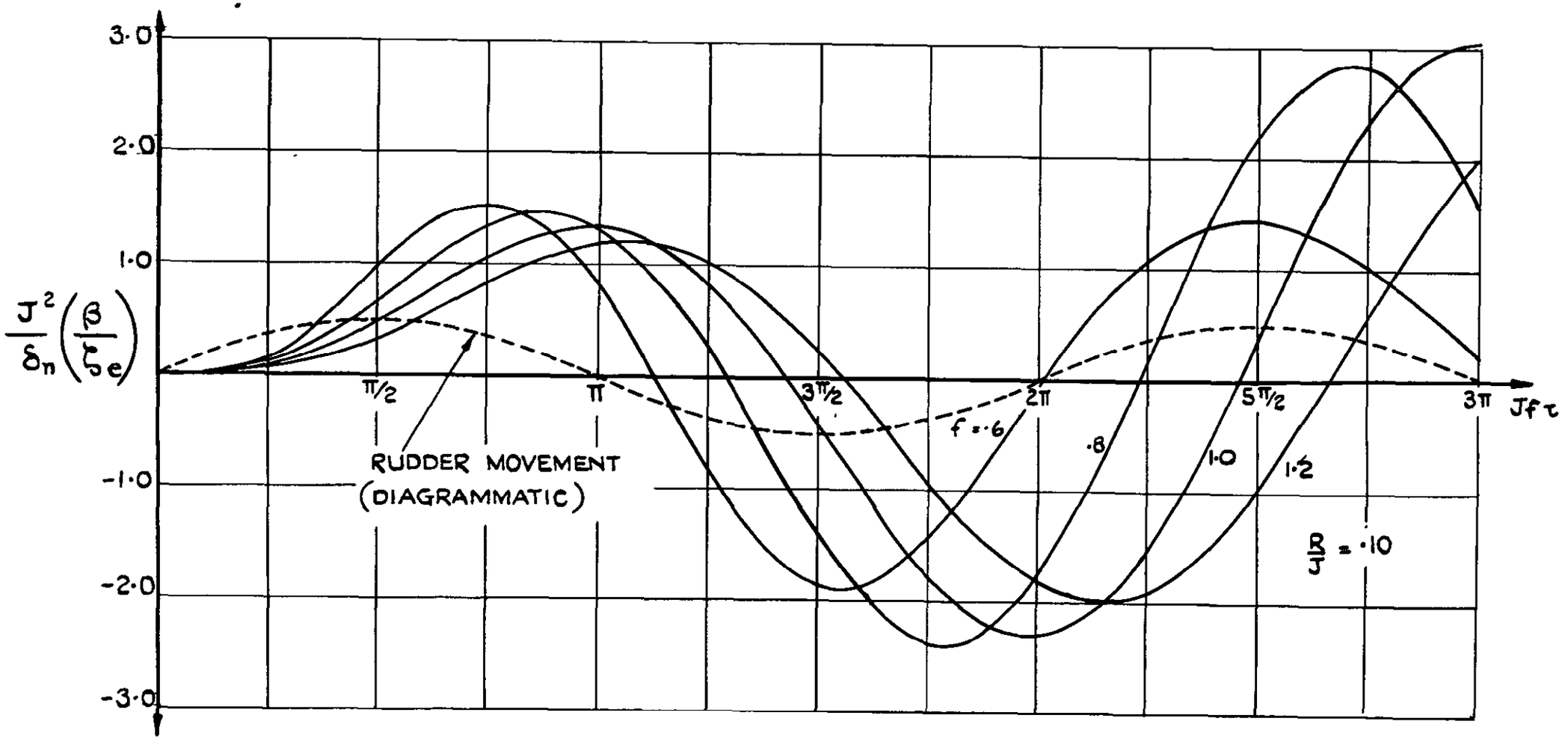

FIG. 1. EFFECT OF VARIATIONS IN THE FREQUENCY OF THE SINUSOIDAL RUDDER MOVEMENT ON THE RESPONSE IN ANGLE OF SIDESLIP.

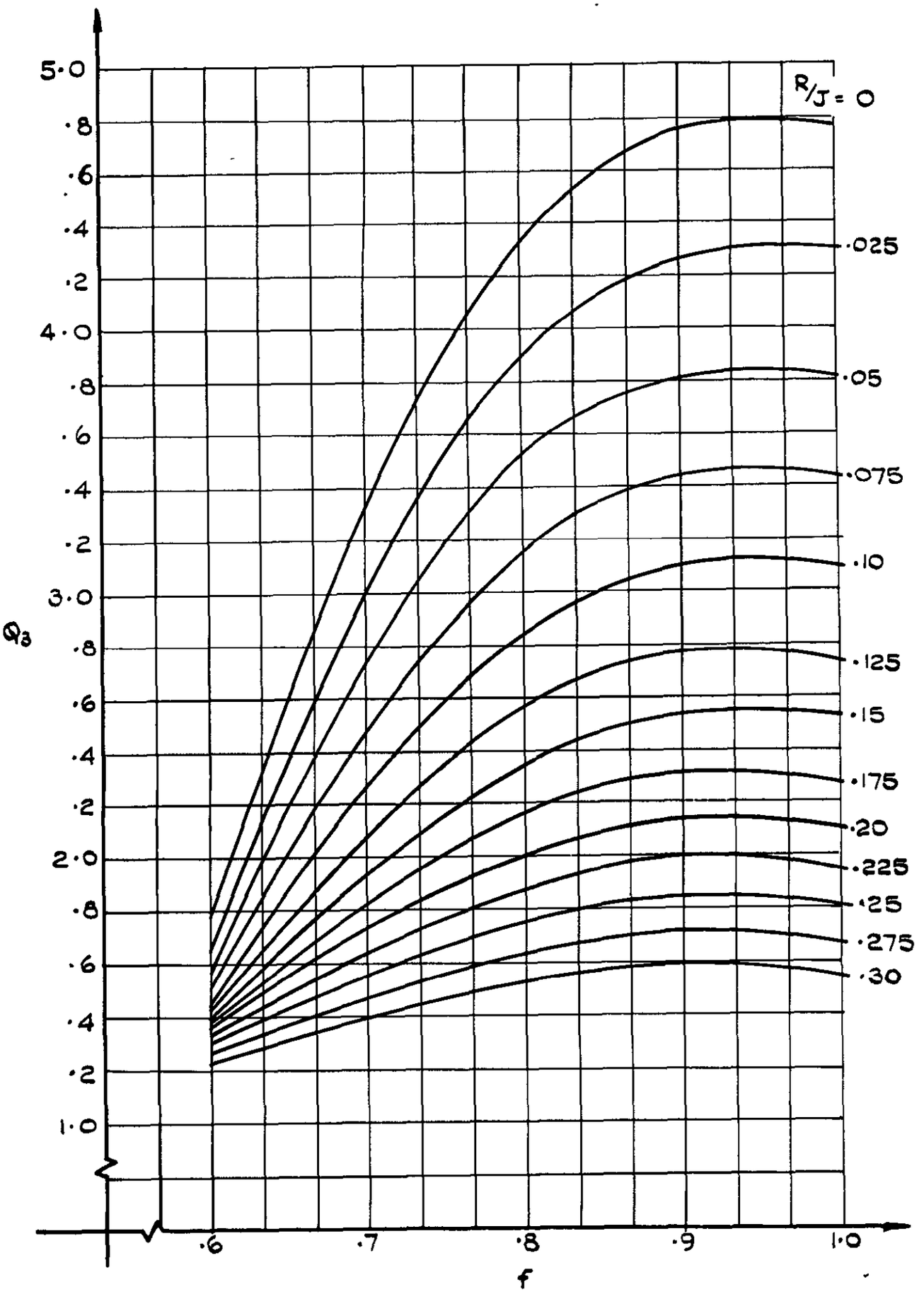

FIG. 2. RESPONSE FACTOR = $Q_r = (-1)^{r+1} \frac{J^2}{\delta n} \left(\frac{\beta m}{\zeta_e}\right)_r$:- r = 3

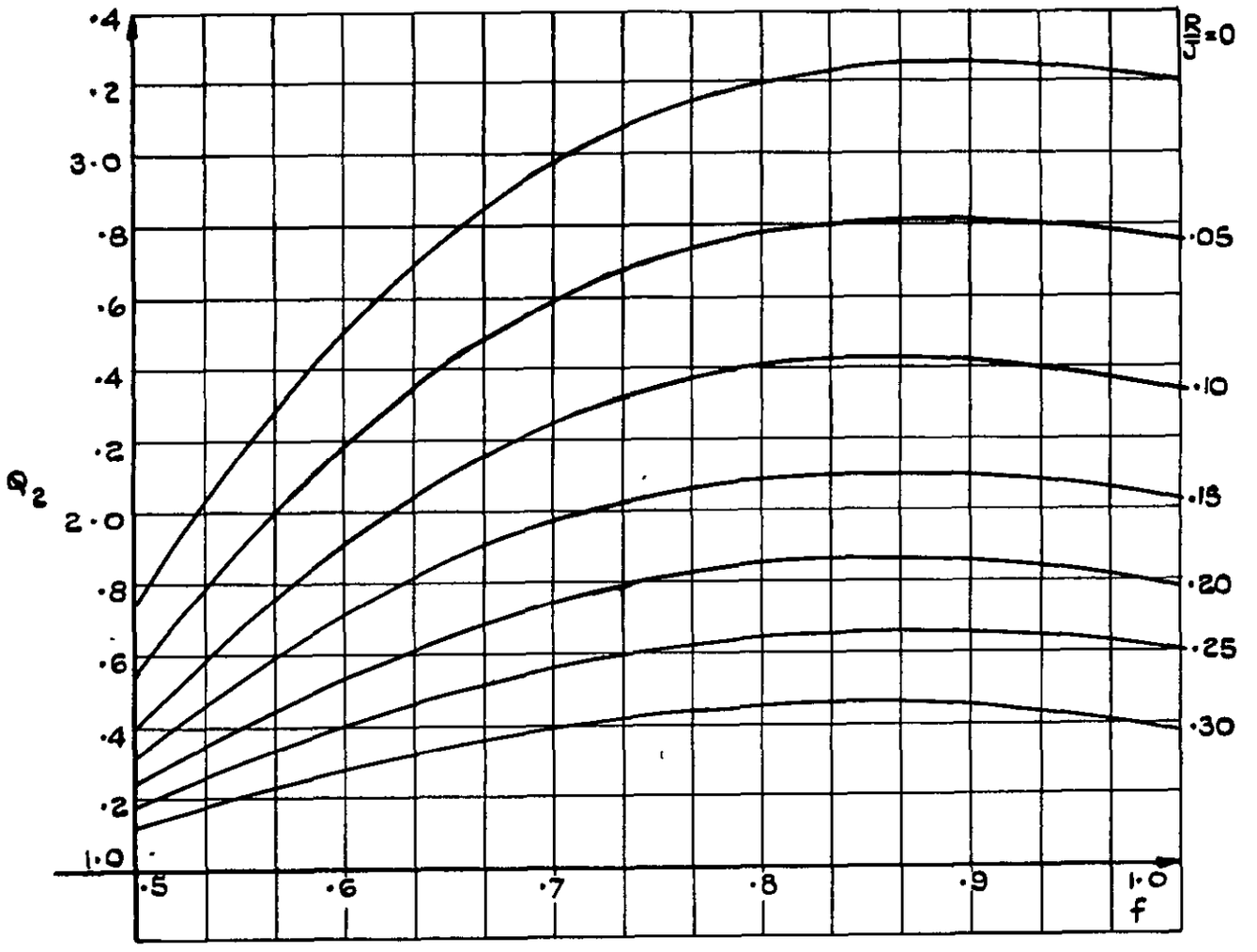

FIG. 3. RESPONSE FACTOR

$$Q_r = (-1)^{r+1} \frac{J^2}{\delta n} \left(\frac{\beta_m}{\zeta_e}\right)_r \quad :- \; r = 2$$

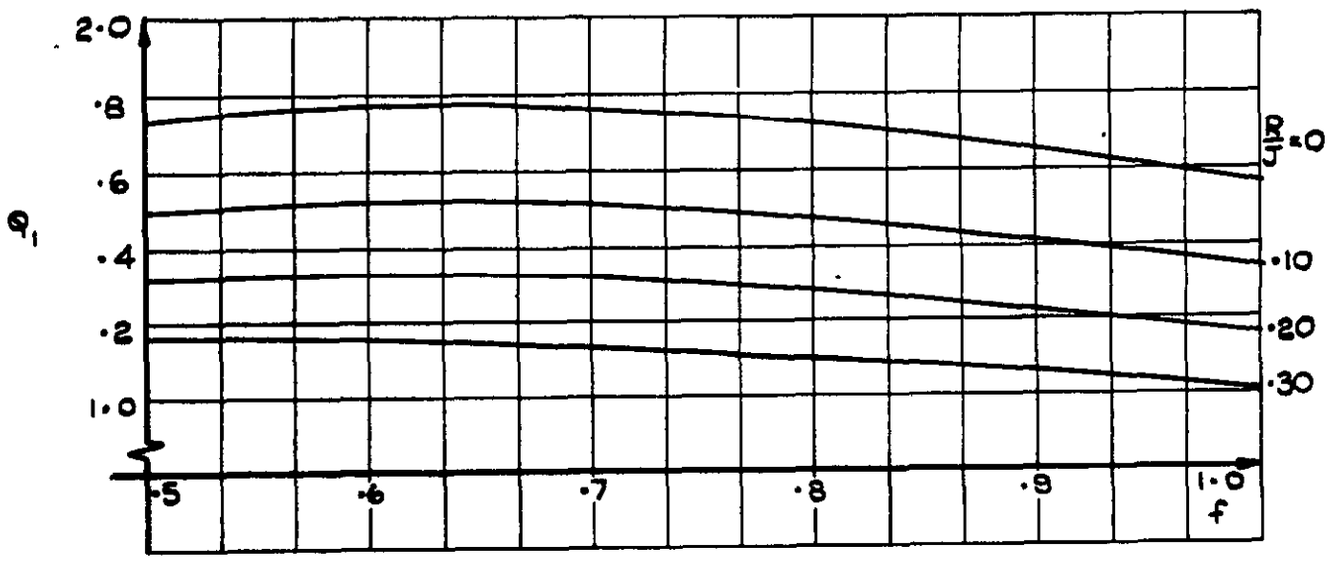

FIG. 4. RESPONSE FACTOR

$$Q_r = (-1)^{r+1} \frac{J^2}{\delta n} \left(\frac{\beta_m}{\zeta_e}\right)_r \quad :- \; r = 1$$

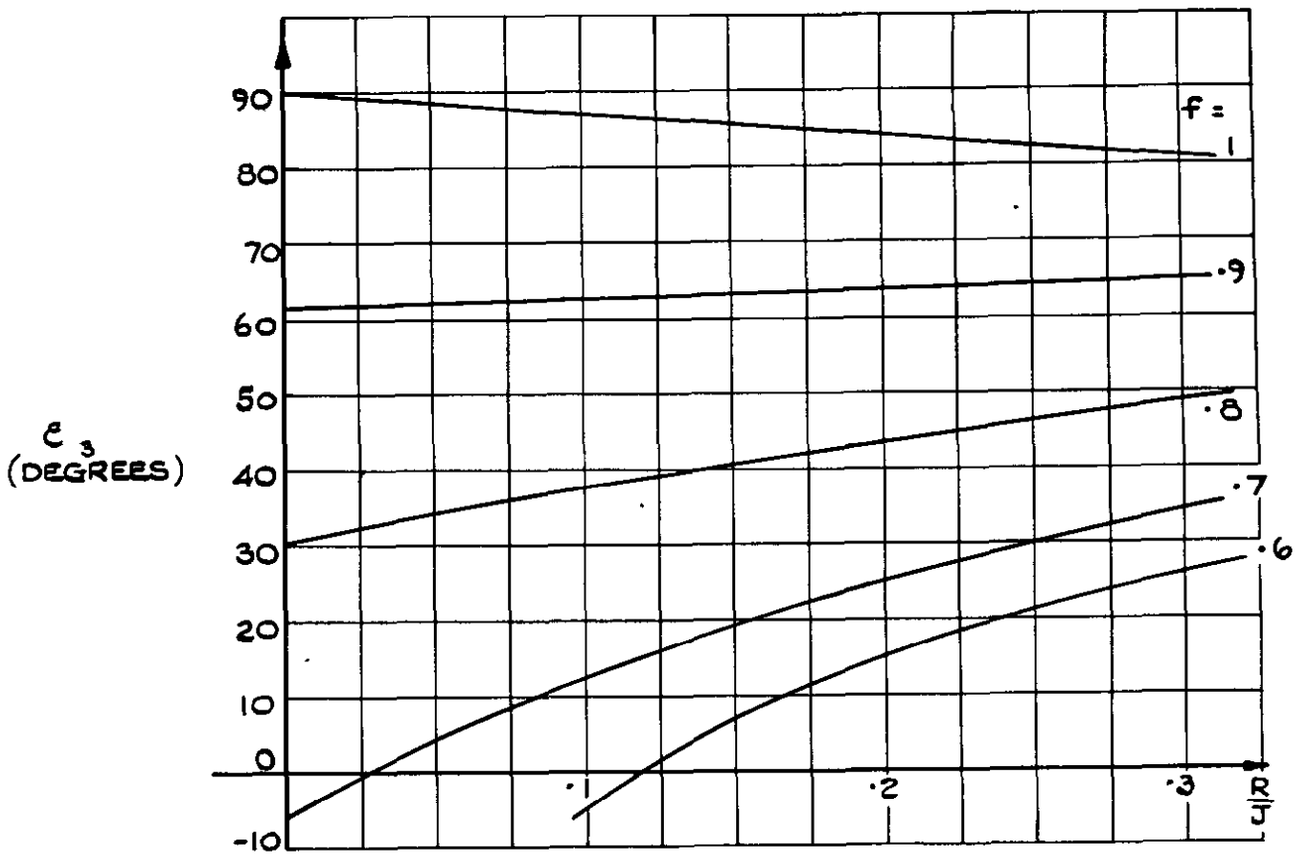

FIG. 5 PHASE ANGLE ε_r, $r = 3$

(APP. I § A3)

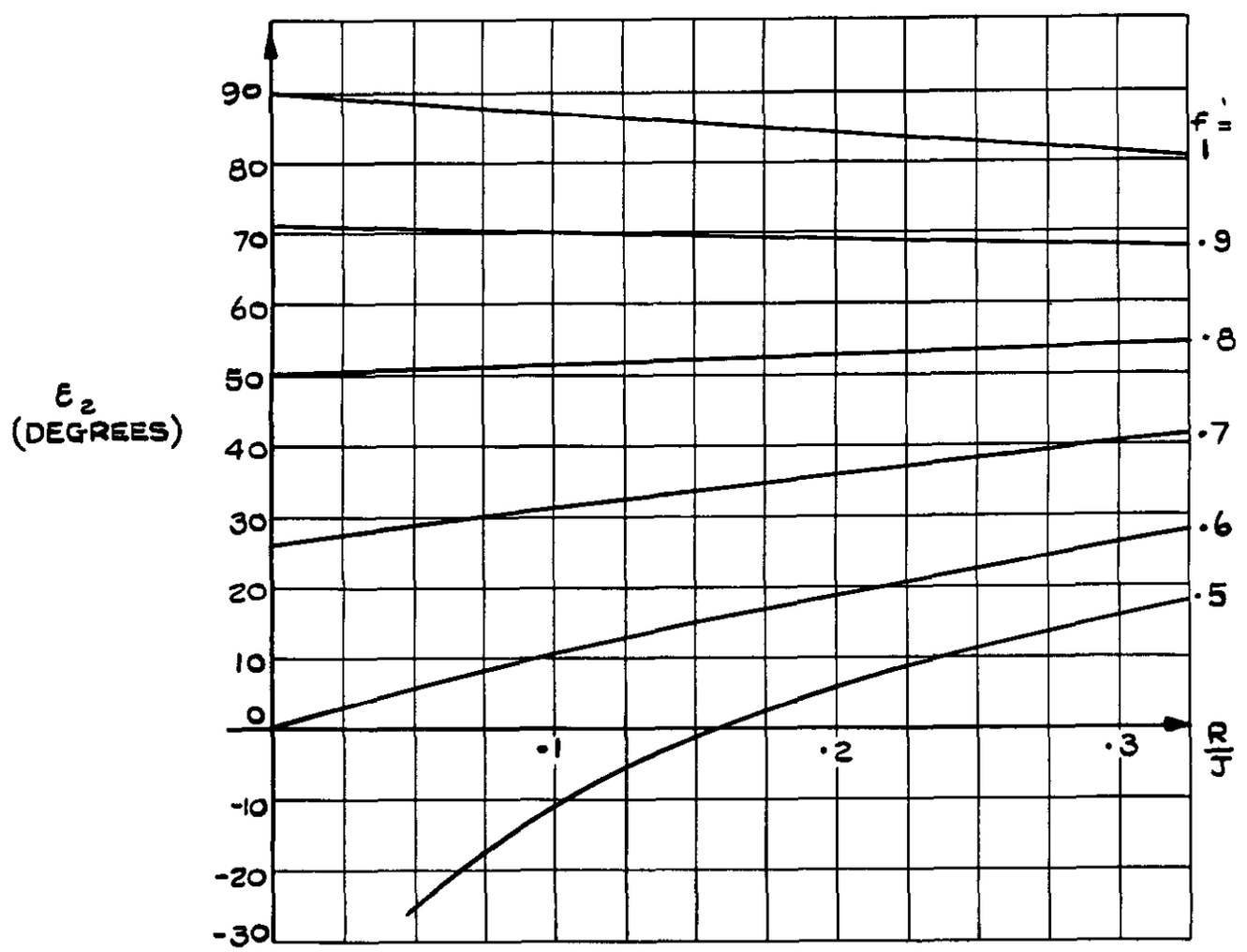

FIG. 6 PHASE ANGLE ε_r, $r = 2$

(APP. I § A3)

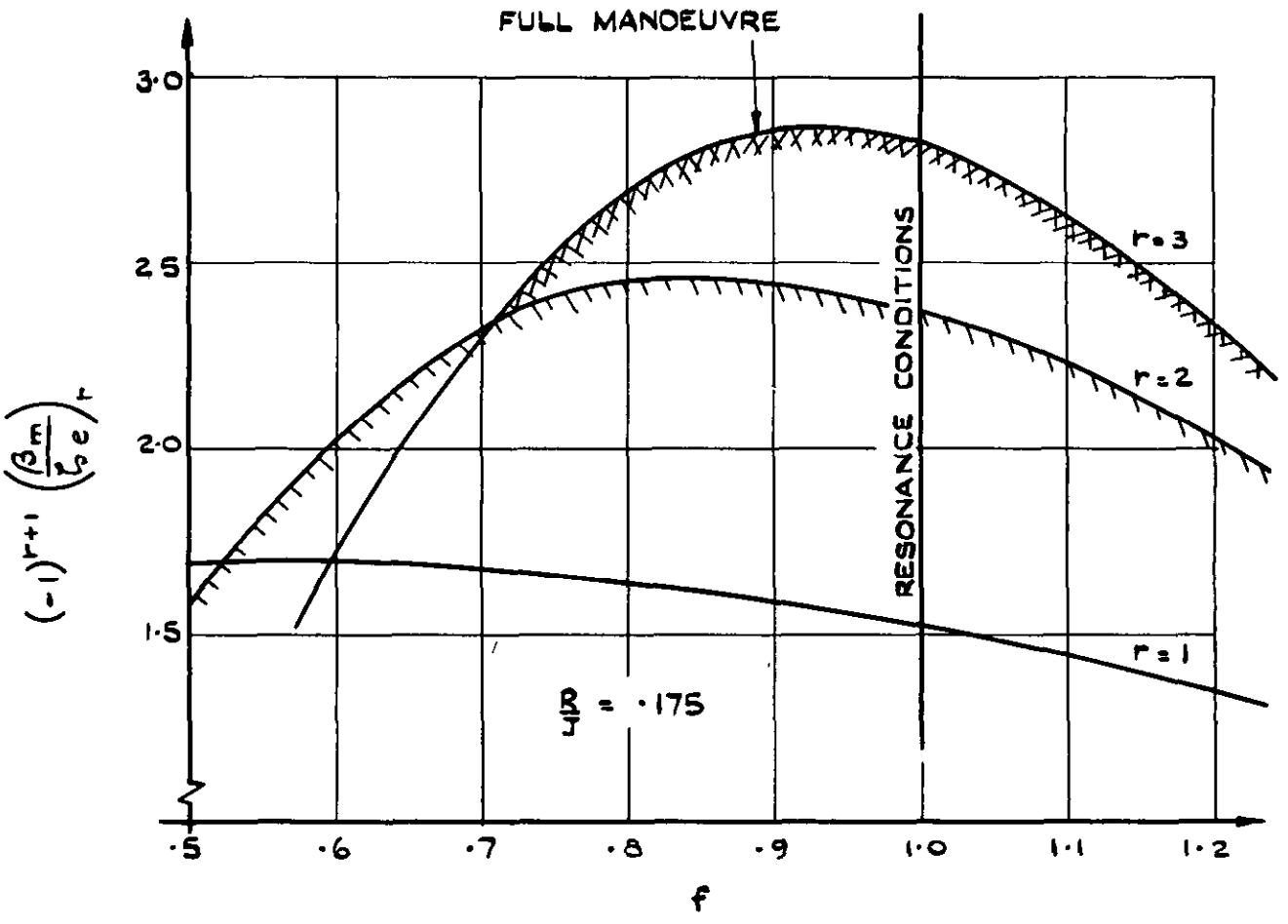

FIG. 8. AN EXAMPLE OF THE EFFECT OF f ON THE βm PER UNIT AMPLITUDE OF RUDDER MOVEMENT. DATA — TABLE I.

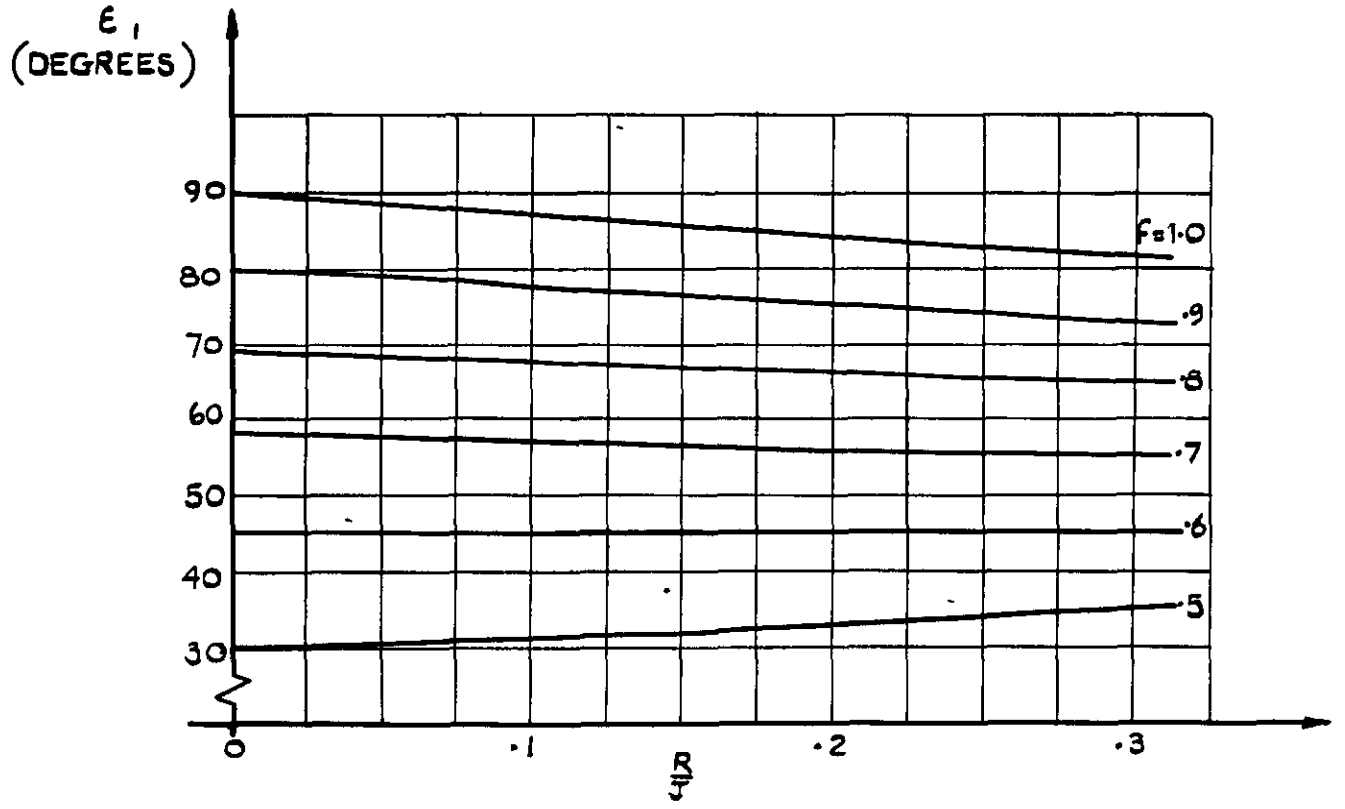

FIG. 7. PHASE ANGLE ε_r, r = 1
(APP. I. § A 3)

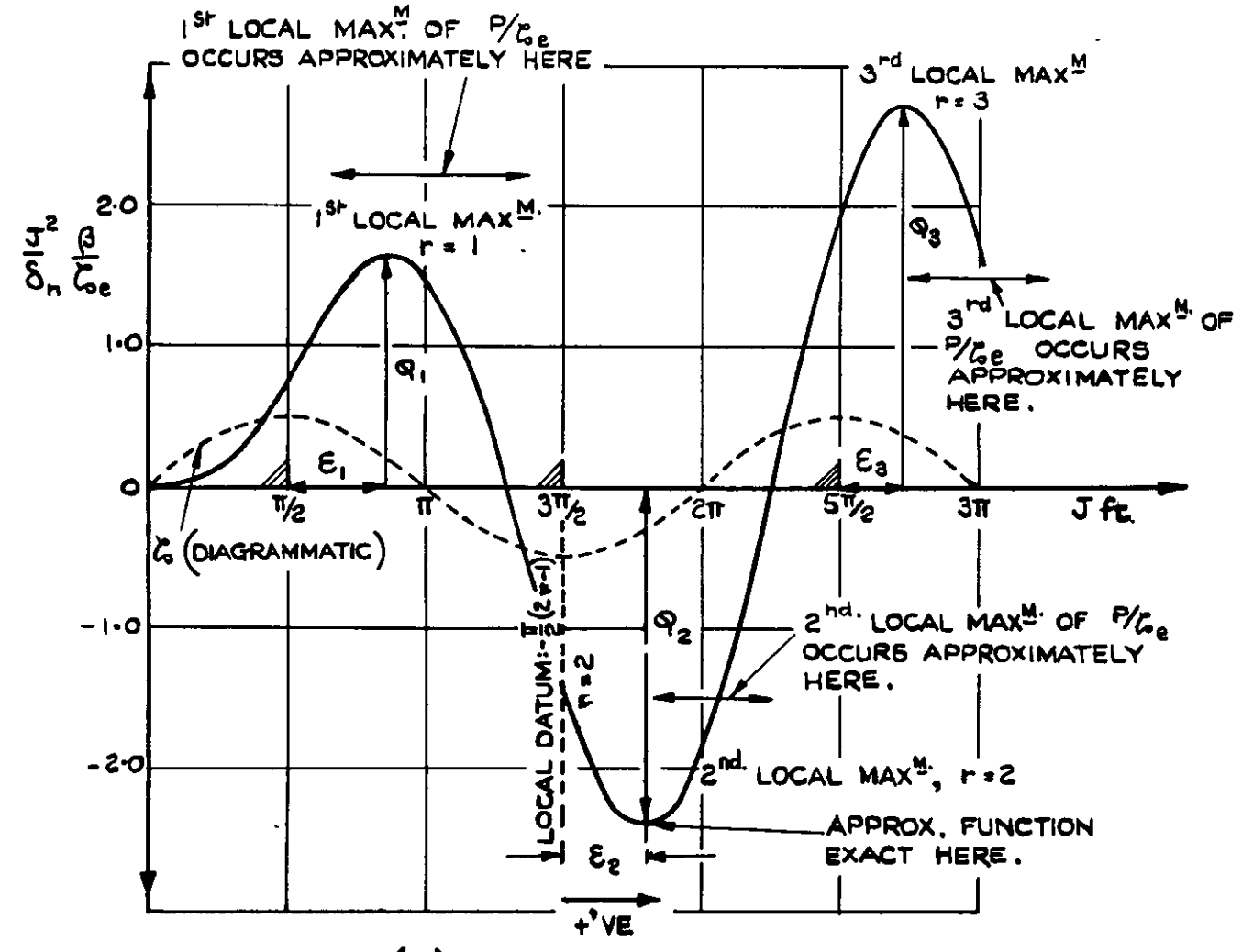

(a) FIN-AND-RUDDER LOADS.

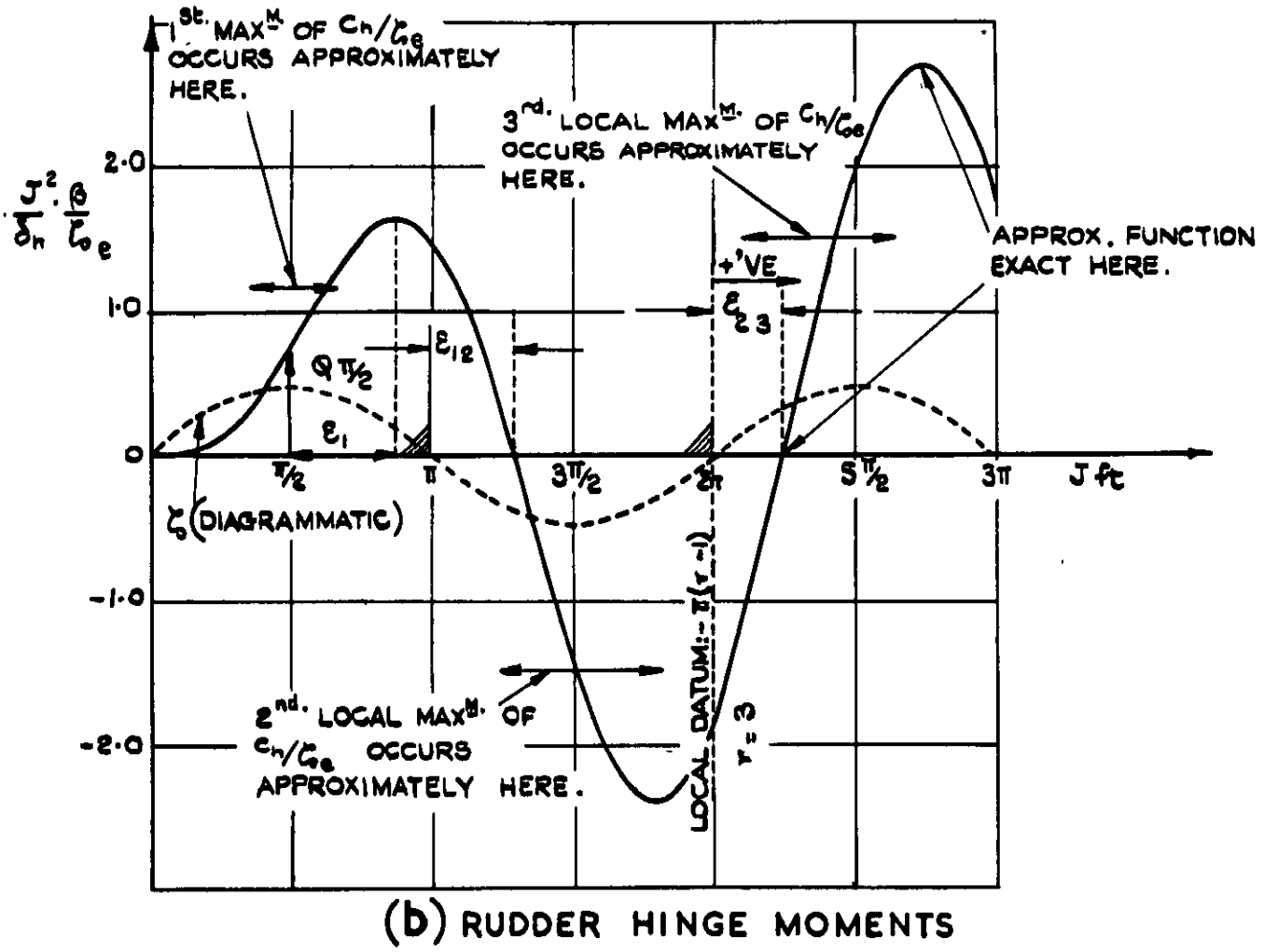

(b) RUDDER HINGE MOMENTS

FIG. 9(a & b) NOTATION AND SIGN CONVENTION USED IN THE DERIVATION OF THE APPROX. FORMULAE IN APPENDIX I.

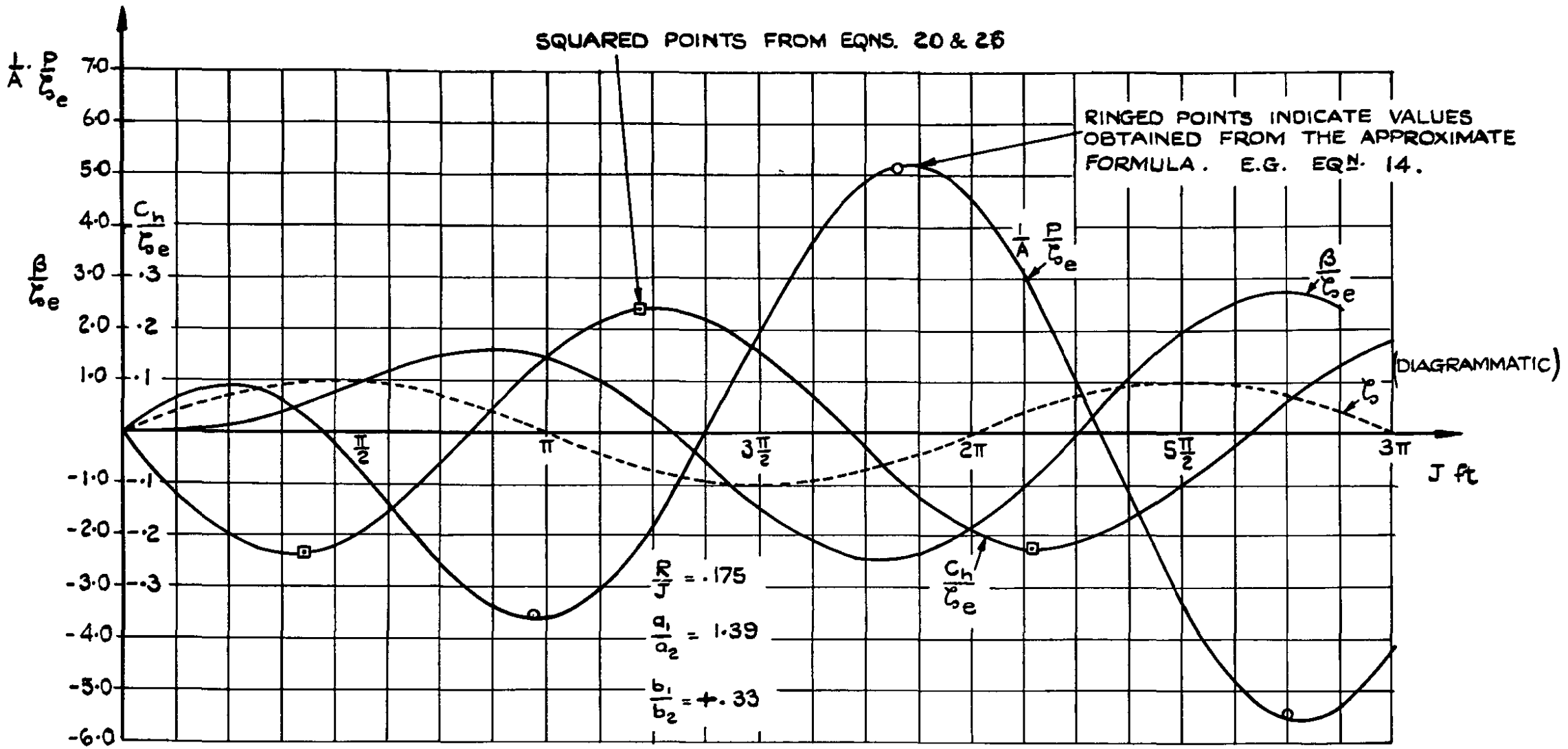

FIG. 10. TIME HISTORIES OF THE ANGLE OF SIDESLIP, FIN-AND-RUDDER LOAD & RUDDER HINGE MOMENT DUE TO SINUSOIDAL MOVEMENT OF THE RUDDER AT A PARTICULAR FREQUENCY :- f = 0.80 DATA IN TABLE I.

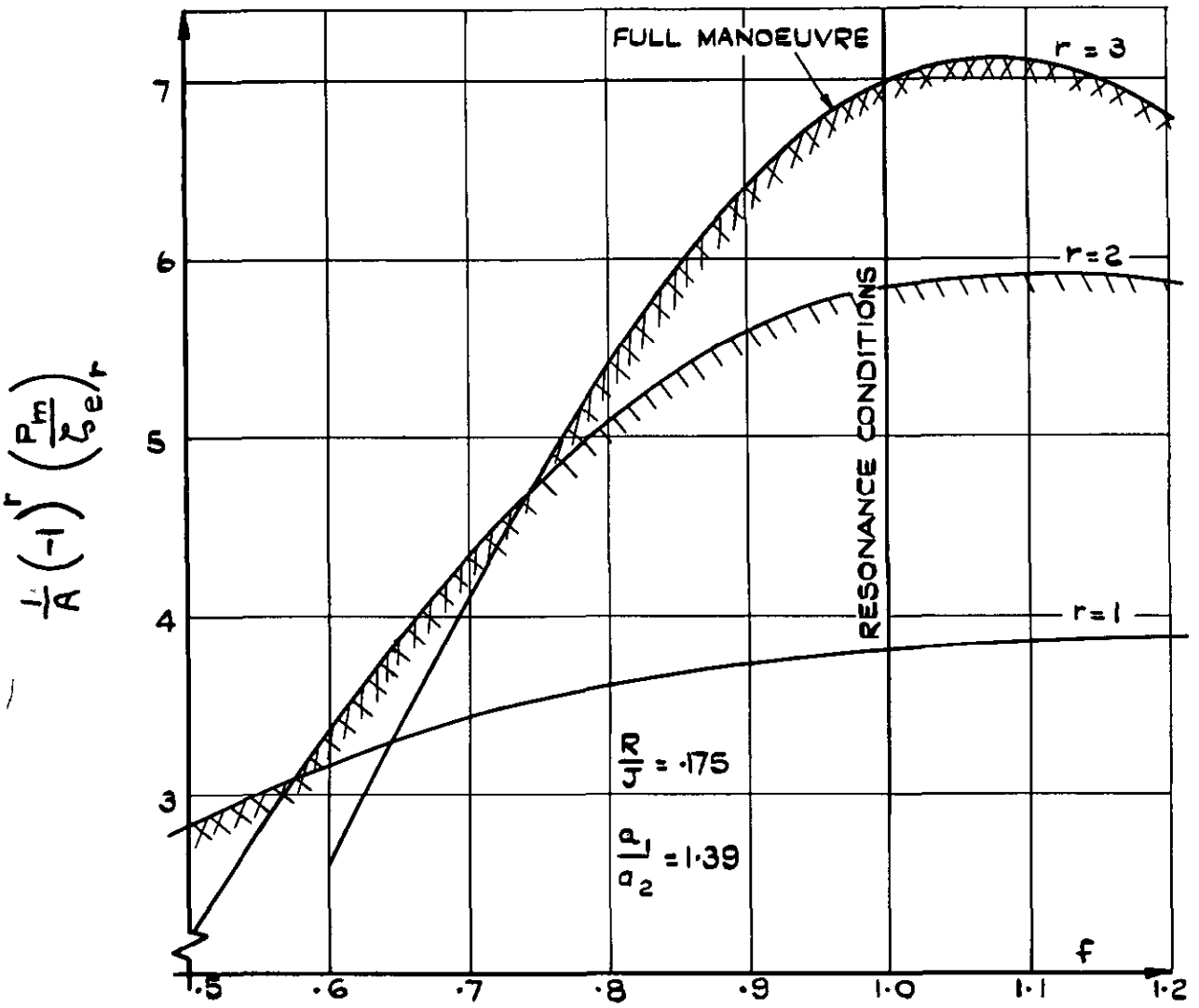

FIG. 11. AN EXAMPLE OF THE EFFECT OF f ON THE Pm PER UNIT AMPLITUDE OF RUDDER MOVEMENT. DATA - TABLE I.

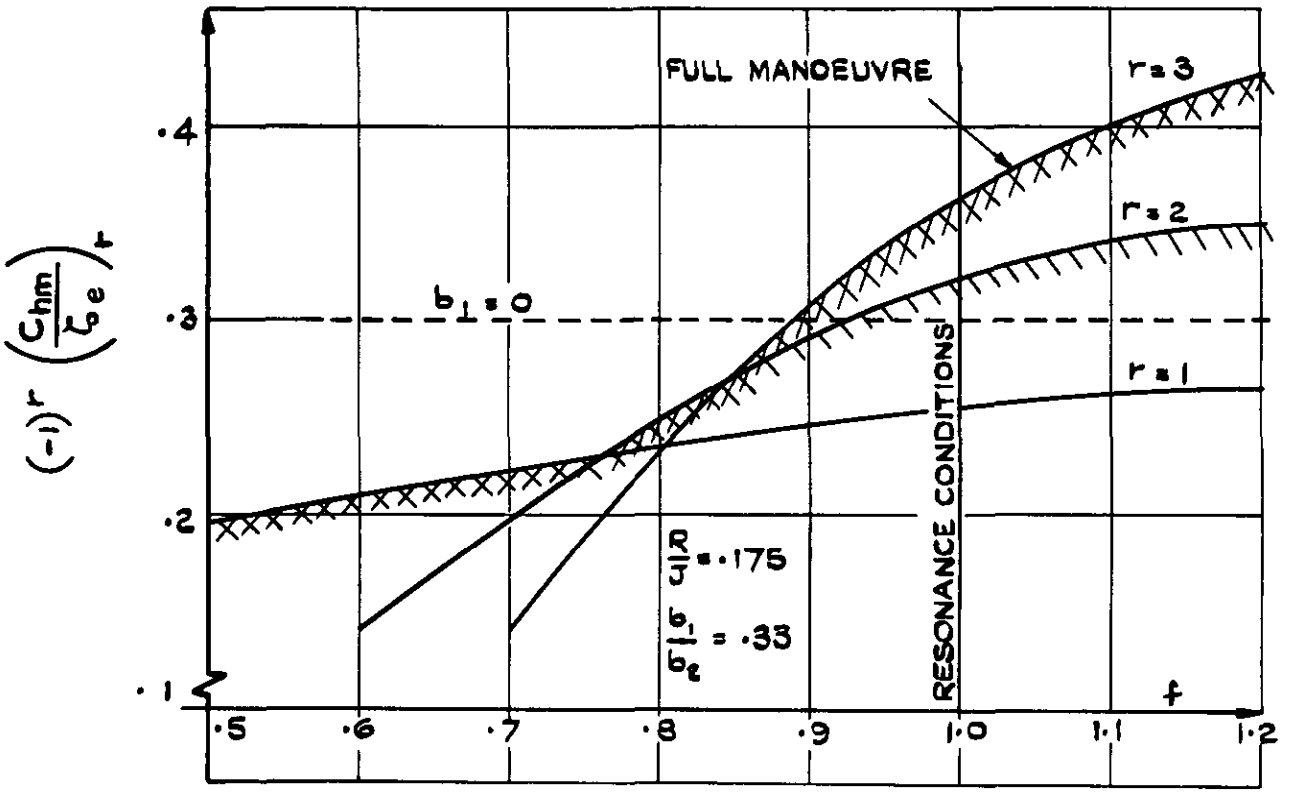

FIG. 12. AN EXAMPLE OF THE EFFECT OF f ON THE CHm PER UNIT AMPLITUDE OF RUDDER MOVEMENT. DATA - TABLE I.

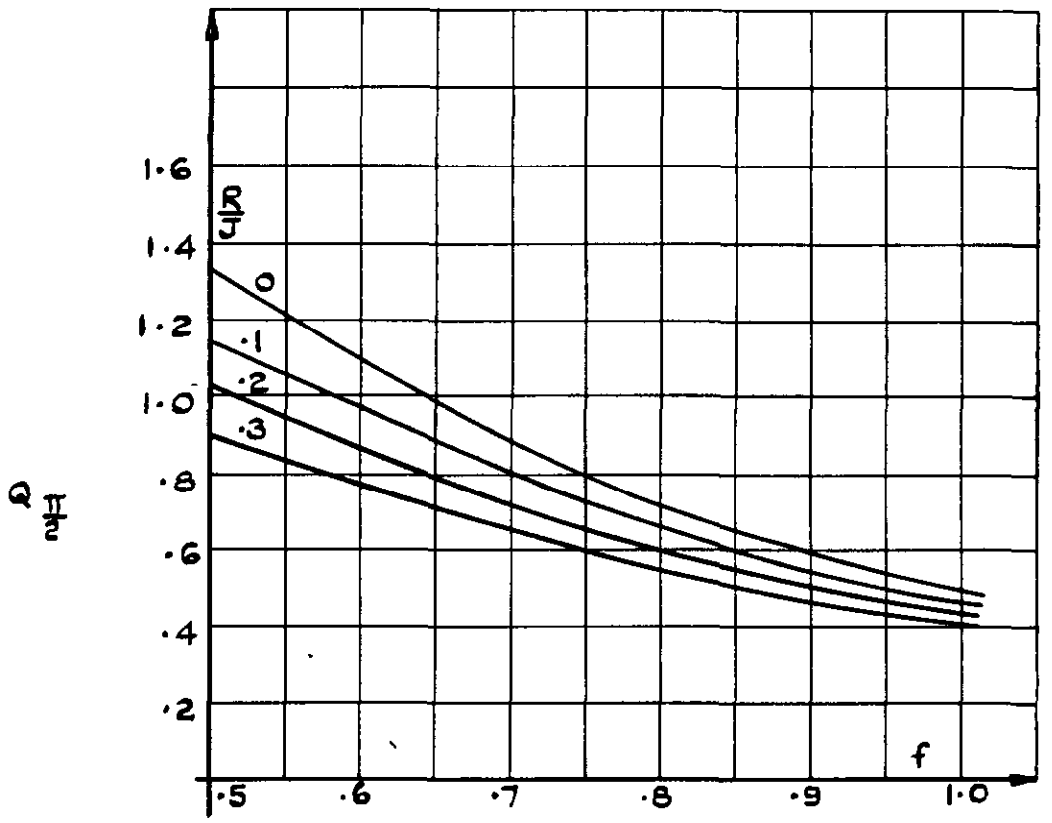

FIG. 13. RESPONSE FACTOR

$$Q_{\frac{\pi}{2}} = \frac{J^2}{\delta n}\left(\frac{\beta}{\zeta_e}\right) \quad J f \tau = \frac{\pi}{2}$$

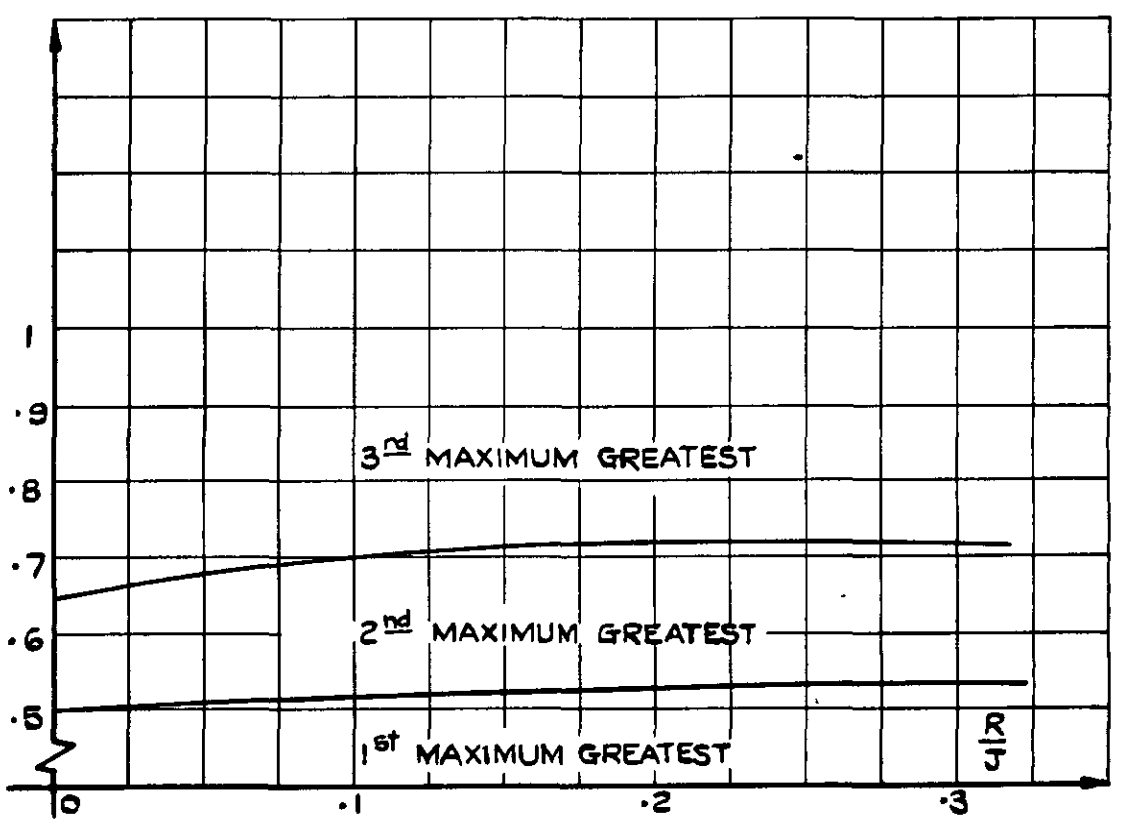

FIG. 14. VALUES OF f FOR WHICH 1st & 2nd & 2nd & 3rd LOCAL MAXIMA OF THE RESPONSE IN β ARE NUMERICALLY EQUAL.

$\varepsilon_{1,2.}$

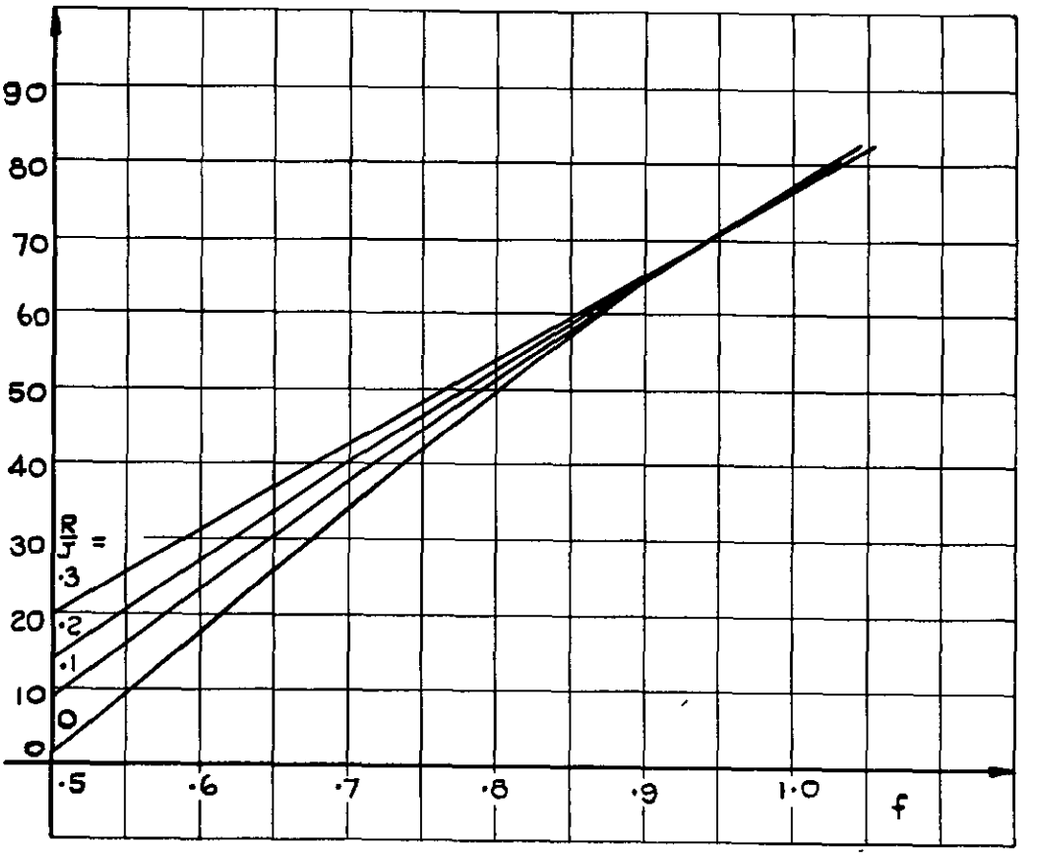

FIG. 15. PHASE ANGLE $\varepsilon_{r-1,\,r,\,r=2}$
(APP. § A5)

$\varepsilon_{2,3}$

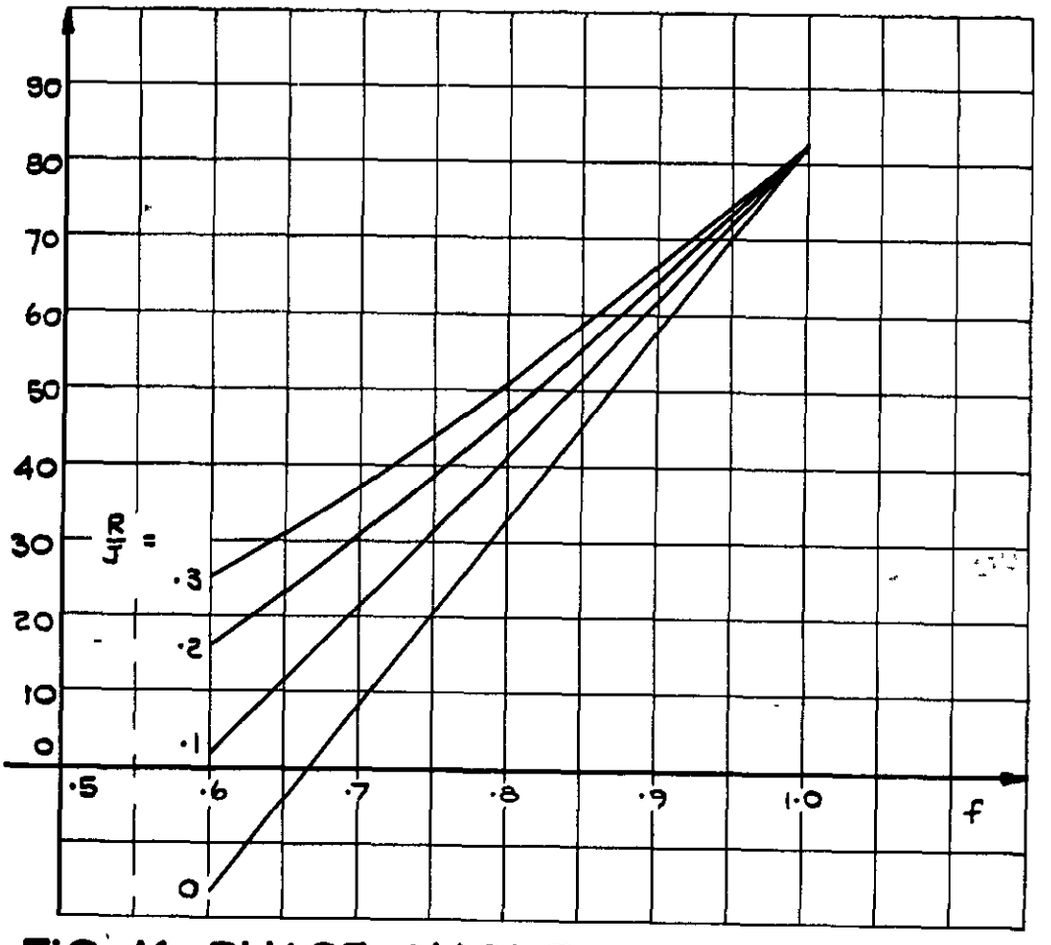

FIG. 16. PHASE ANGLE $\varepsilon_{r-1,\,r,\,r=3}$
(APP. § A5)

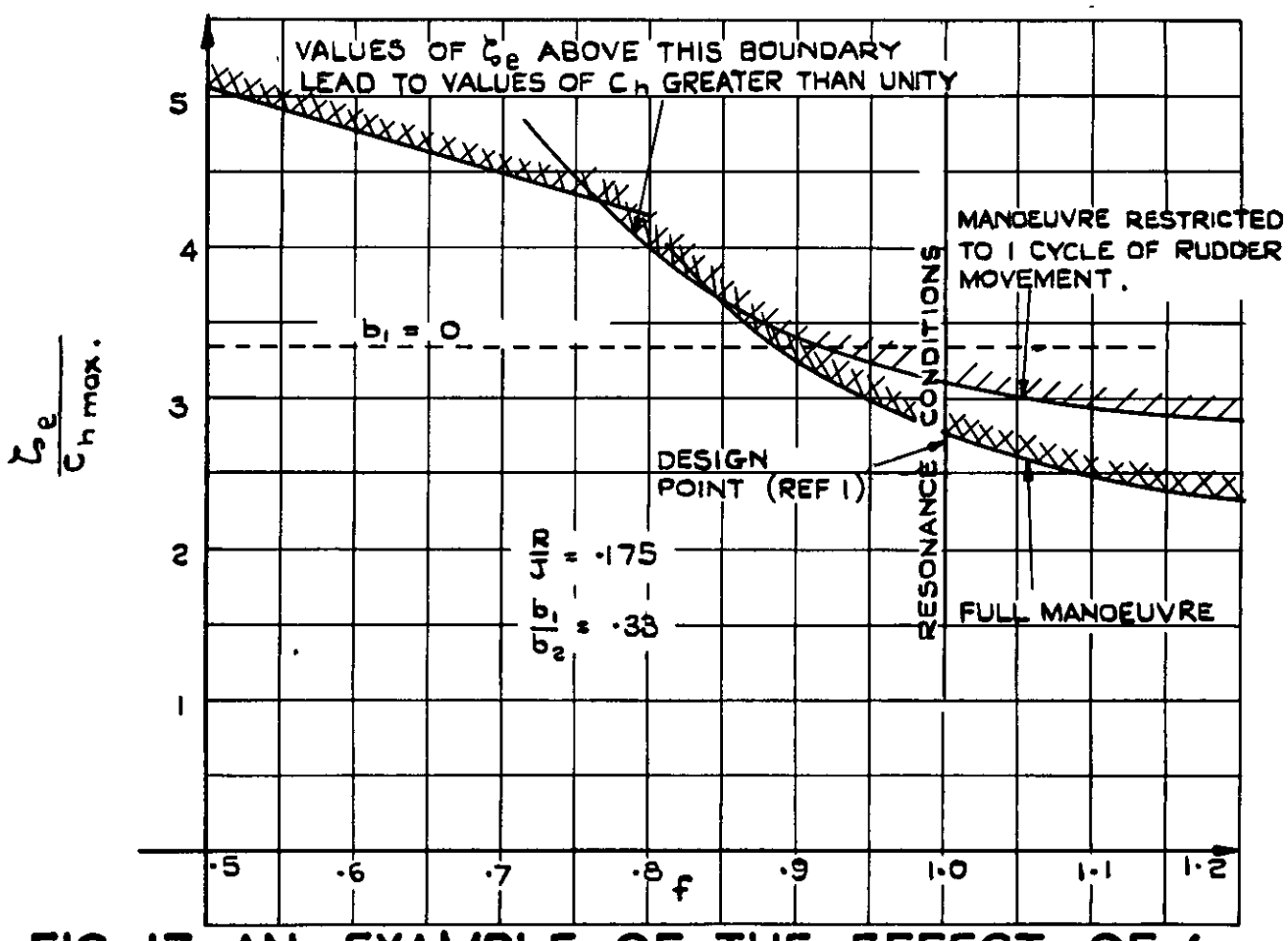

FIG. 17. AN EXAMPLE OF THE EFFECT OF f ON THE VALUE OF ζ_e REQUIRED TO REACH UNIT MAXIMUM C_h IN THE MANOEUVRE.
DATA :— TABLE I.

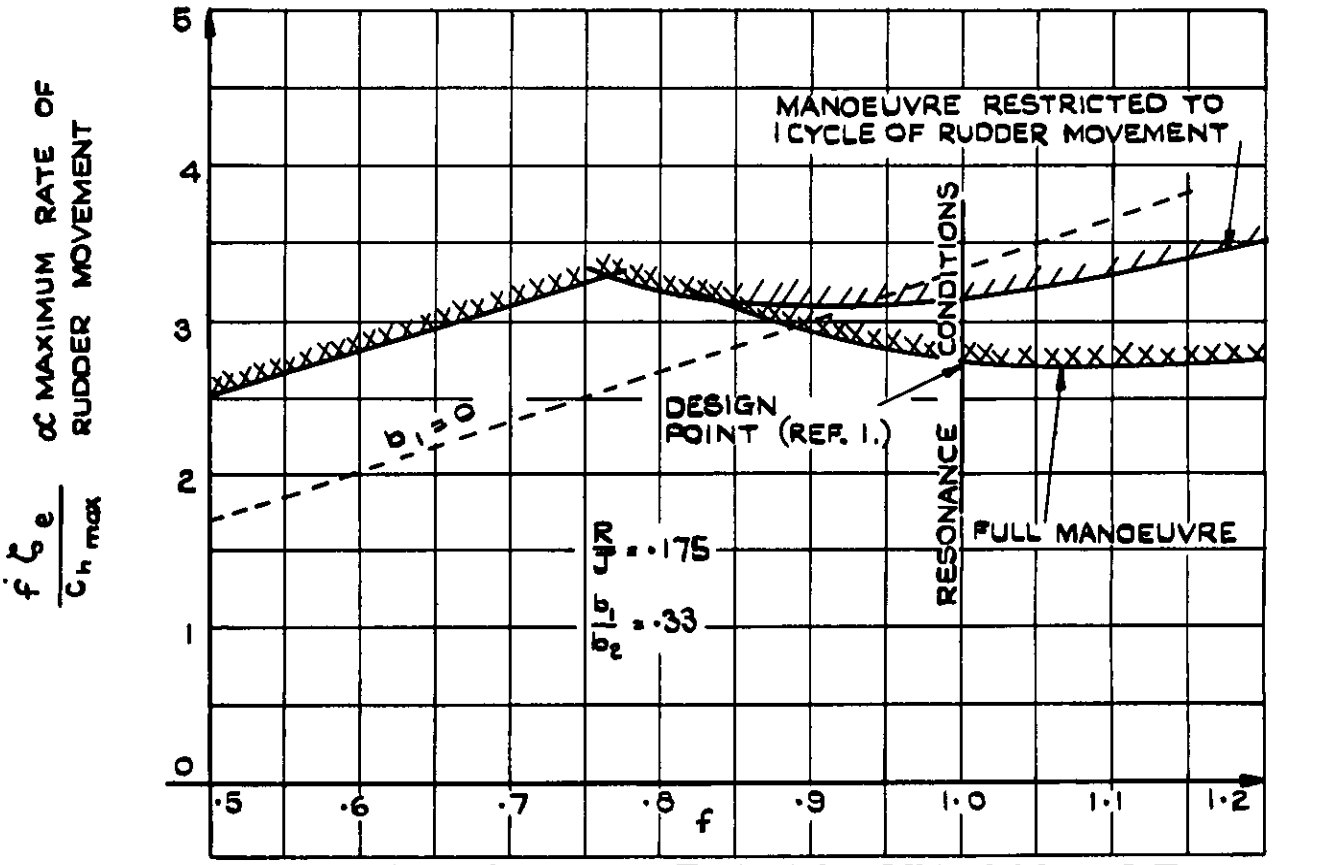

FIG. 18. AN EXAMPLE OF THE EFFECT OF f ON THE MAXIMUM (INITIAL) RATE OF RUDDER MOVEMENT ASSOCIATED WITH UNIT MAXIMUM C_h.
DATA :— TABLE I.

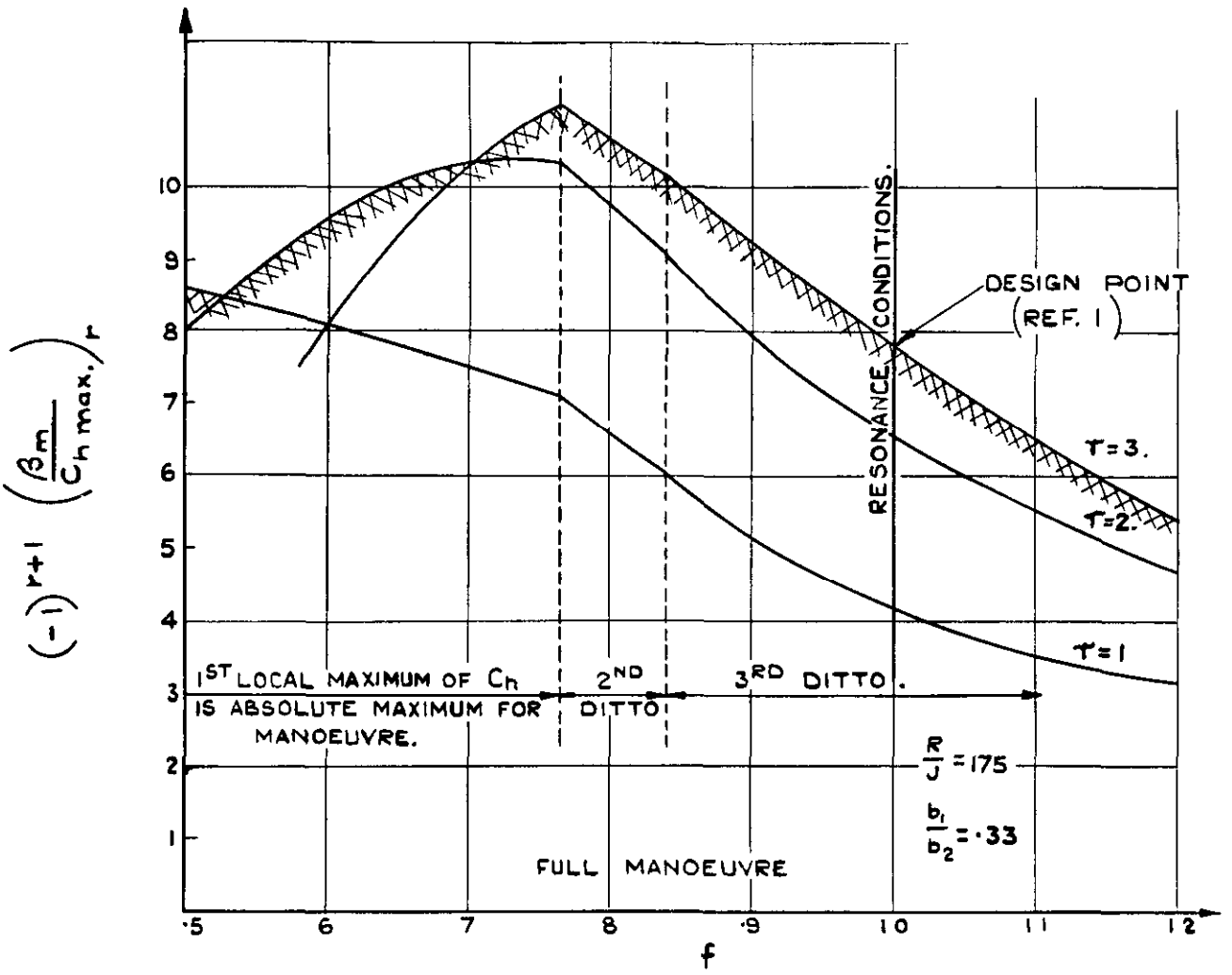

FIG. 19 AN EXAMPLE OF THE EFFECT OF f ON THE β_m PER UNIT MAXIMUM C_h, DATA IN TABLE I.

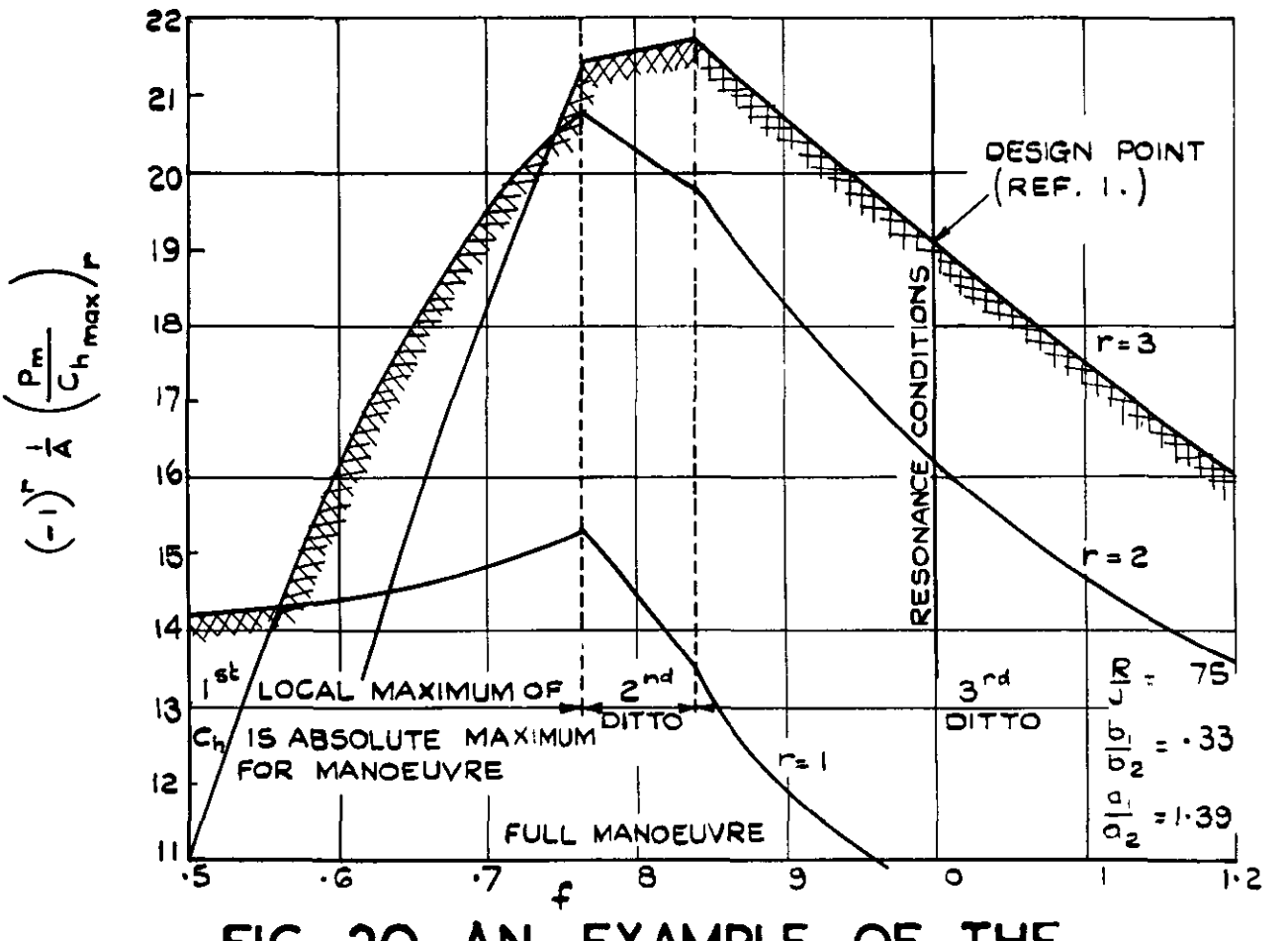

FIG. 20 AN EXAMPLE OF THE EFFECT OF f ON THE P_m PER UNIT MAXIMUM C_h, DATA IN TABLE I.

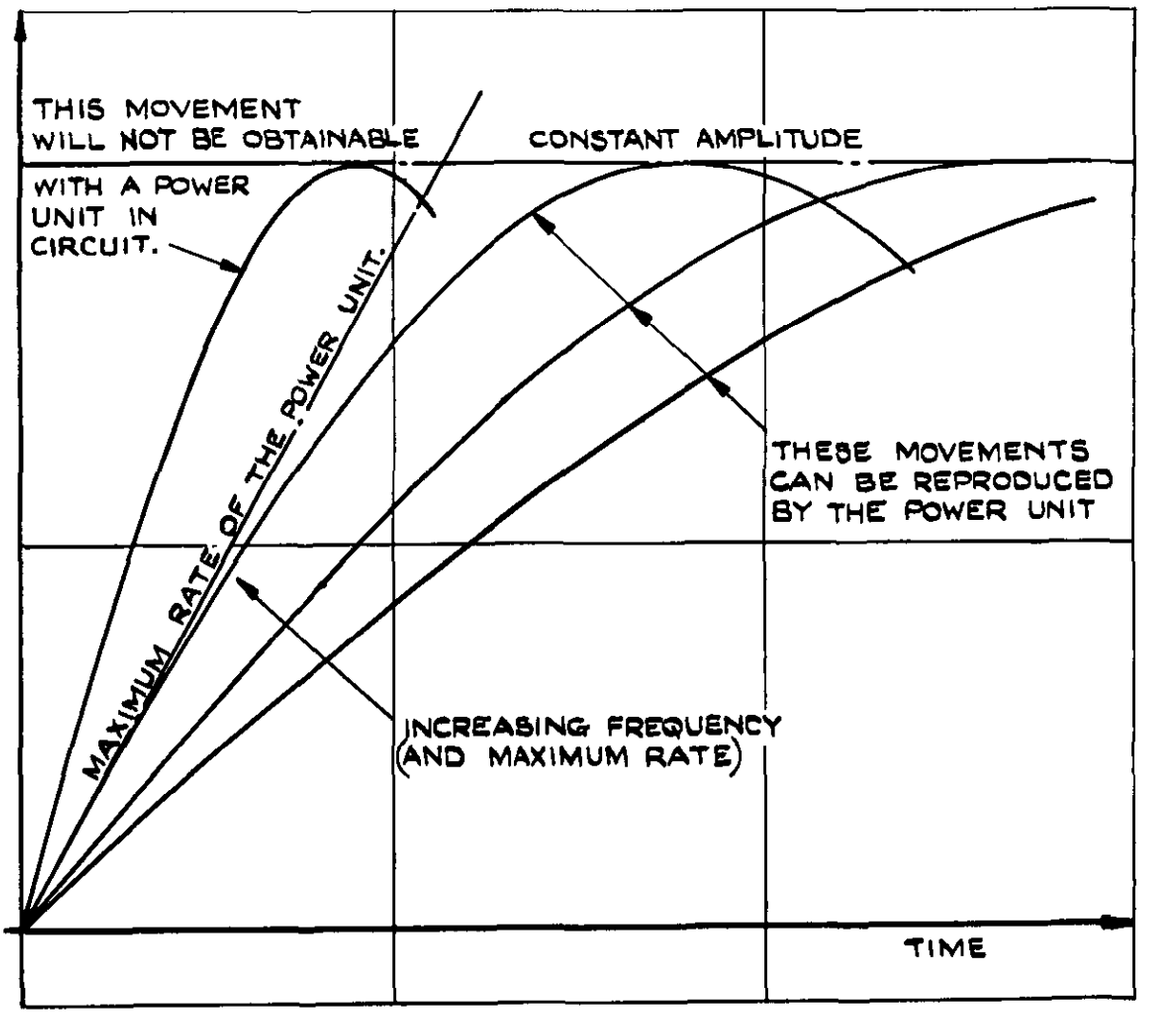

FIG. 21. EFFECT OF FREQUENCY ON THE MAXIMUM RATE OF MOVEMENT.

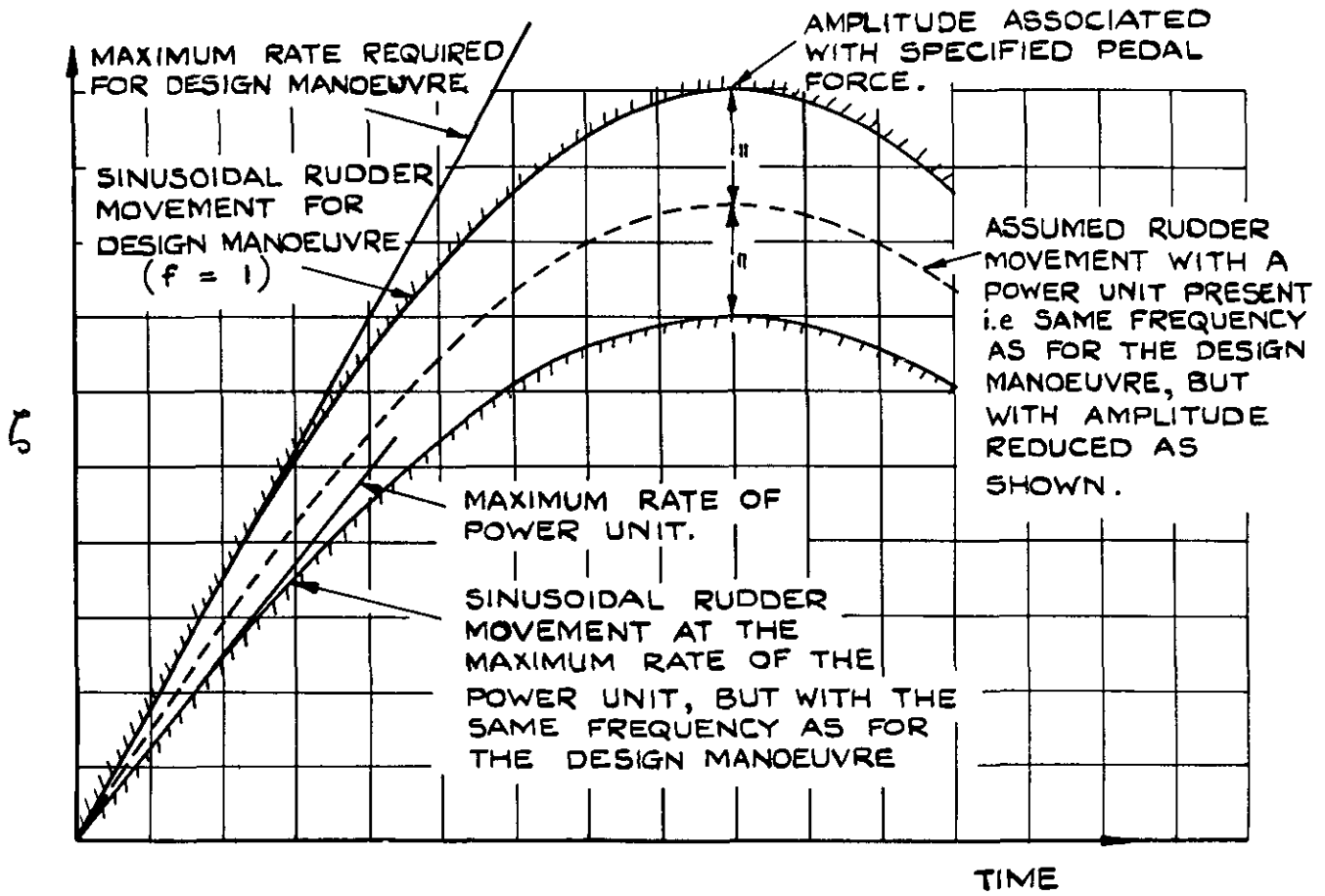

(a)

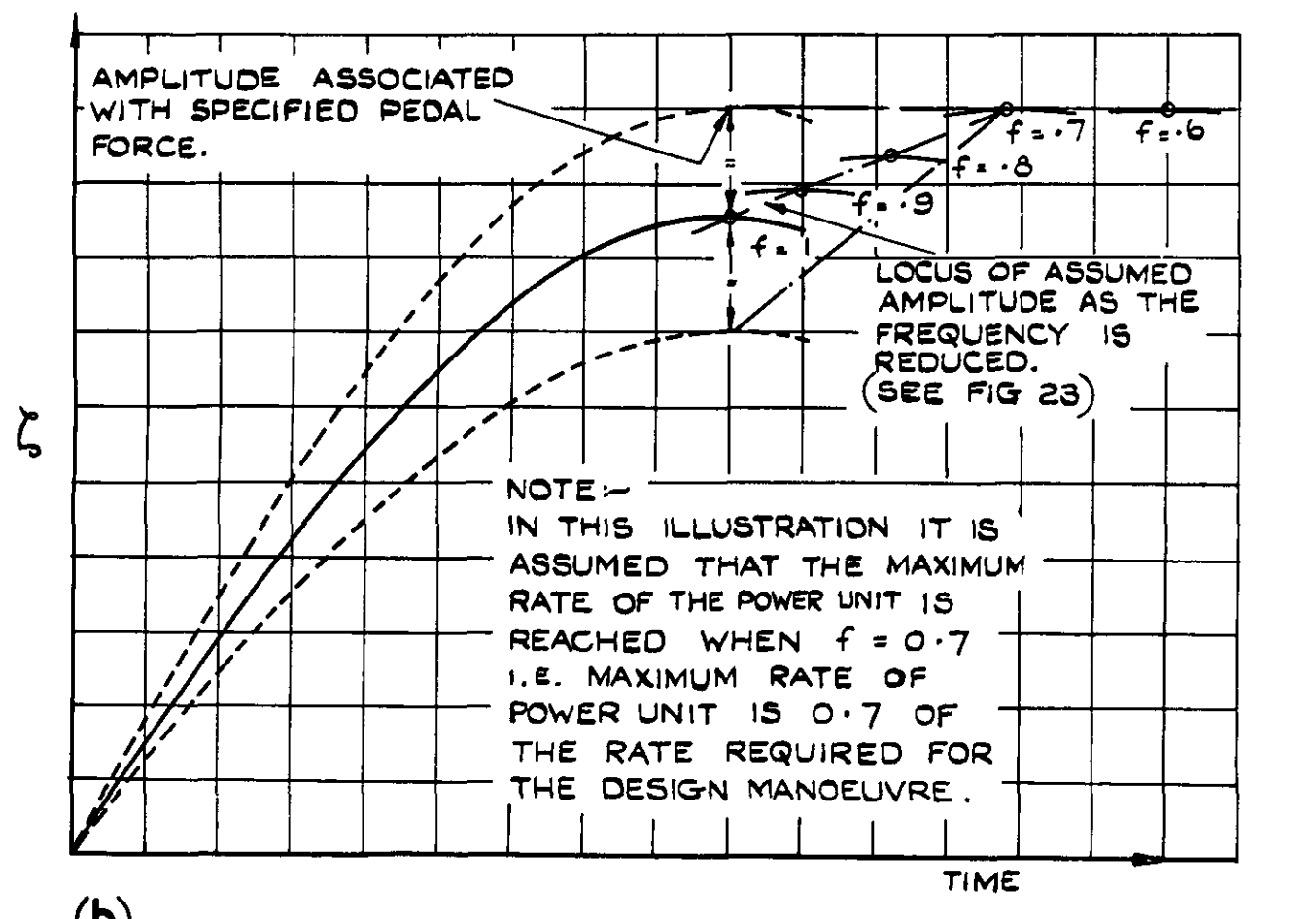

(b)

FIG. 22 (a & b) ASSUMED EFFECT OF A POWER UNIT ON THE RUDDER MOVEMENT WHEN AN ATTEMPT IS MADE TO EXECUTE THE DESIGN MANOEUVRE f = 1. AND ON THE MOVEMENT AT LOWER FREQUENCIES.

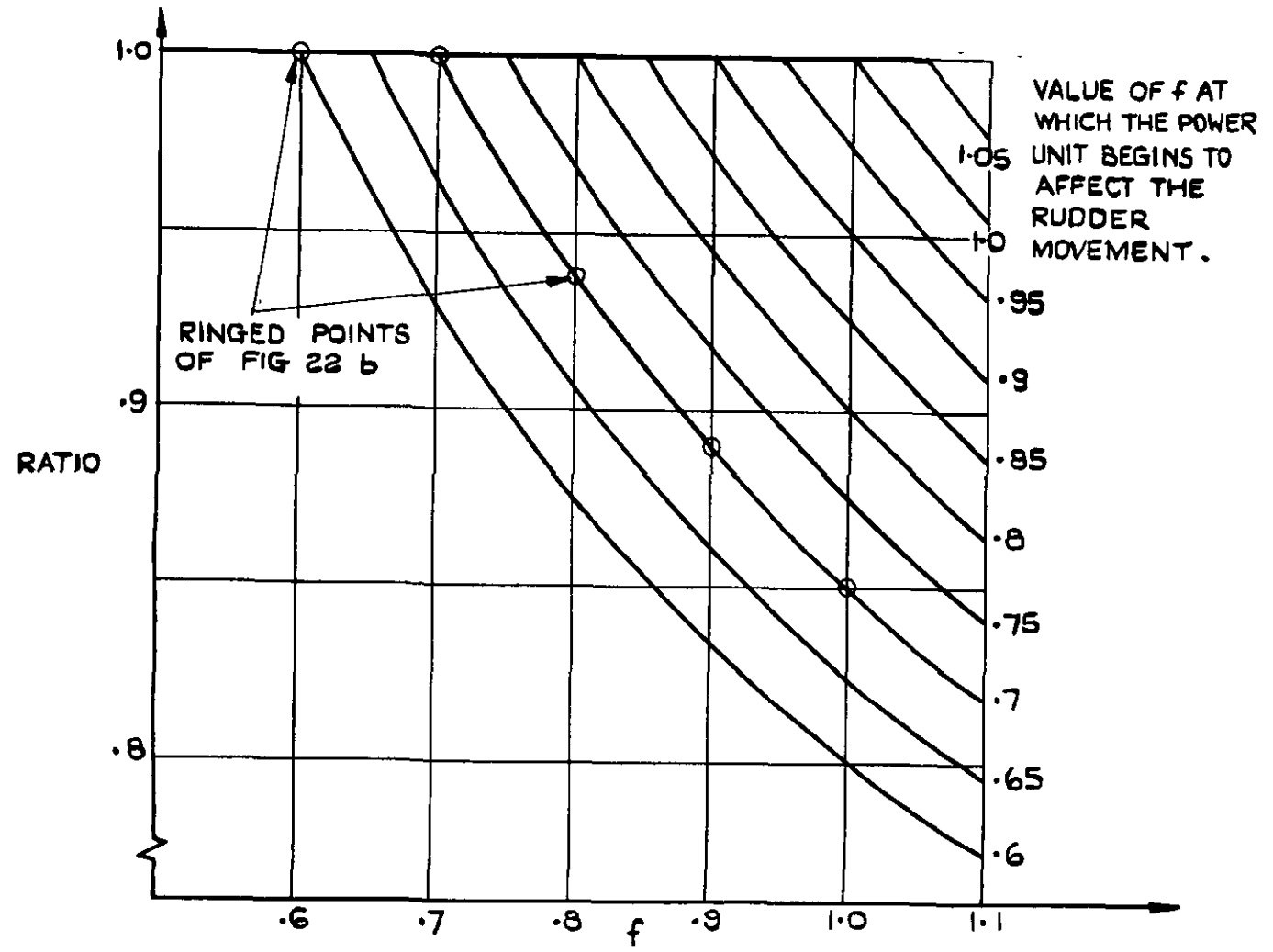

FIG. 23. RATIO

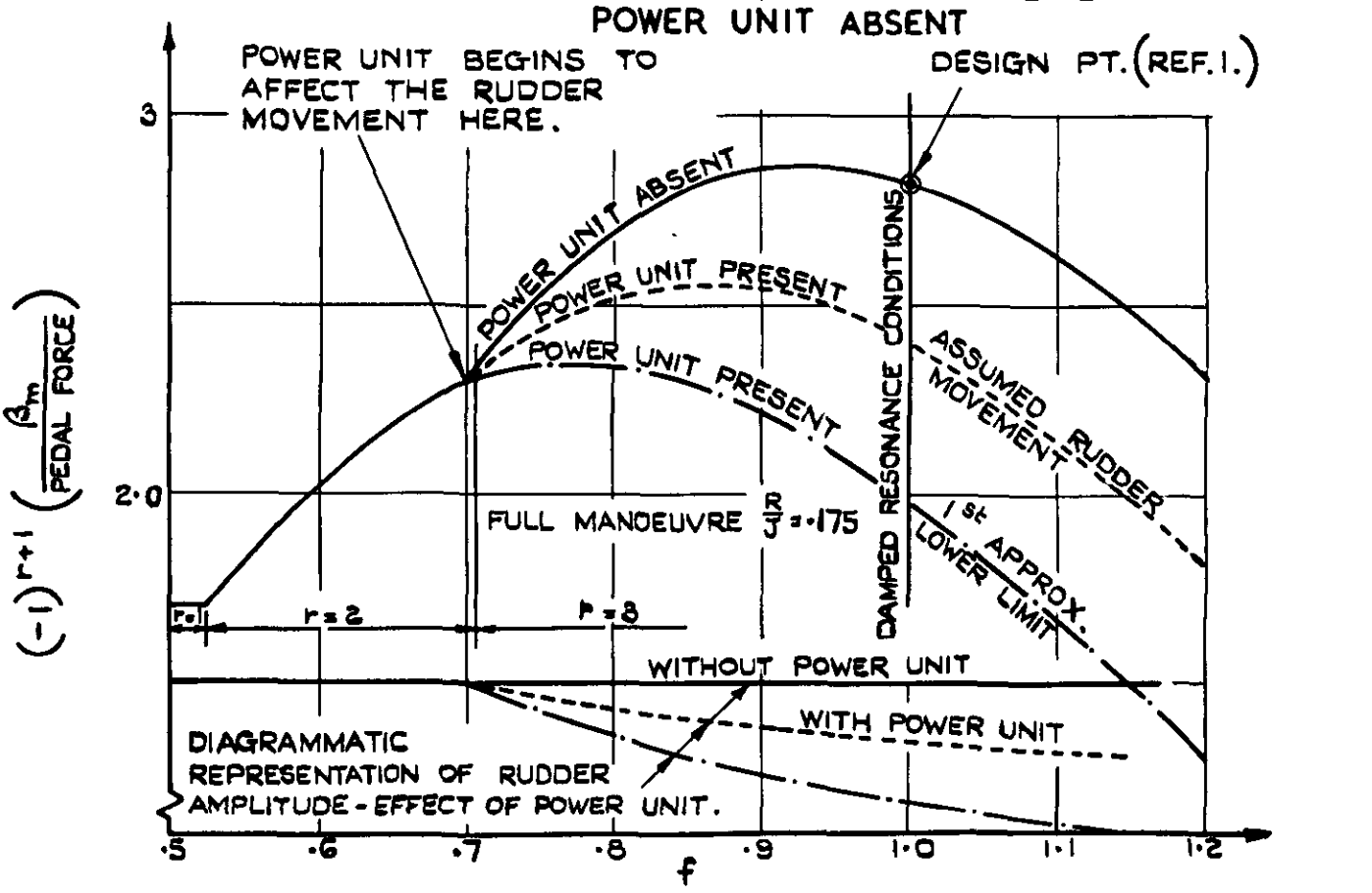

FIG. 24. EXAMPLE SHOWING EFFECT OF POWER UNIT ON THE β_m AT VARIOUS VALUES OF f. EXAMPLE DATA IN TABLE I.

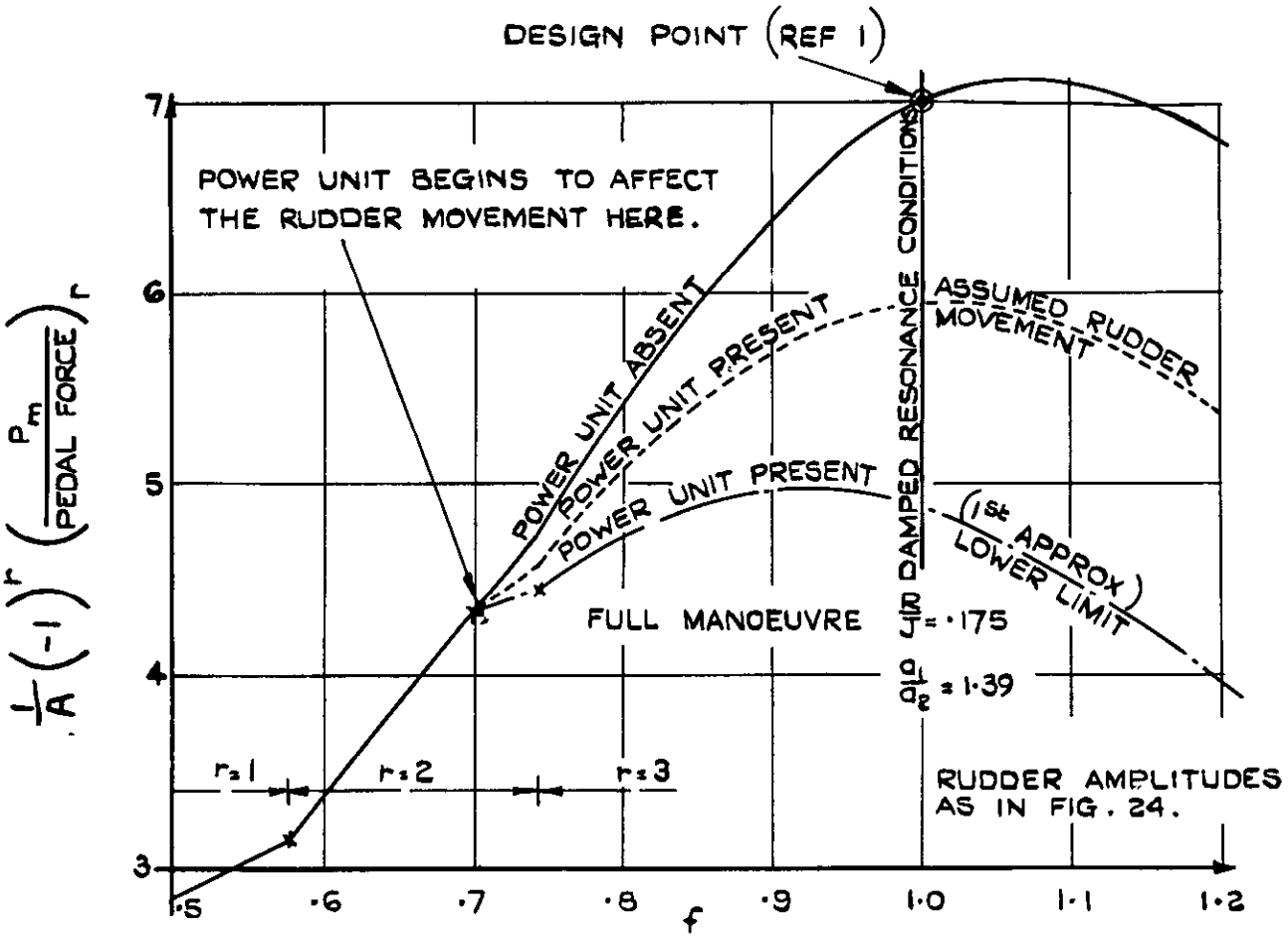

FIG. 25. EXAMPLE SHOWING EFFECT OF POWER UNIT ON THE P_m AT VARIOUS VALUES OF f. EXAMPLE DATA IN TABLE I.

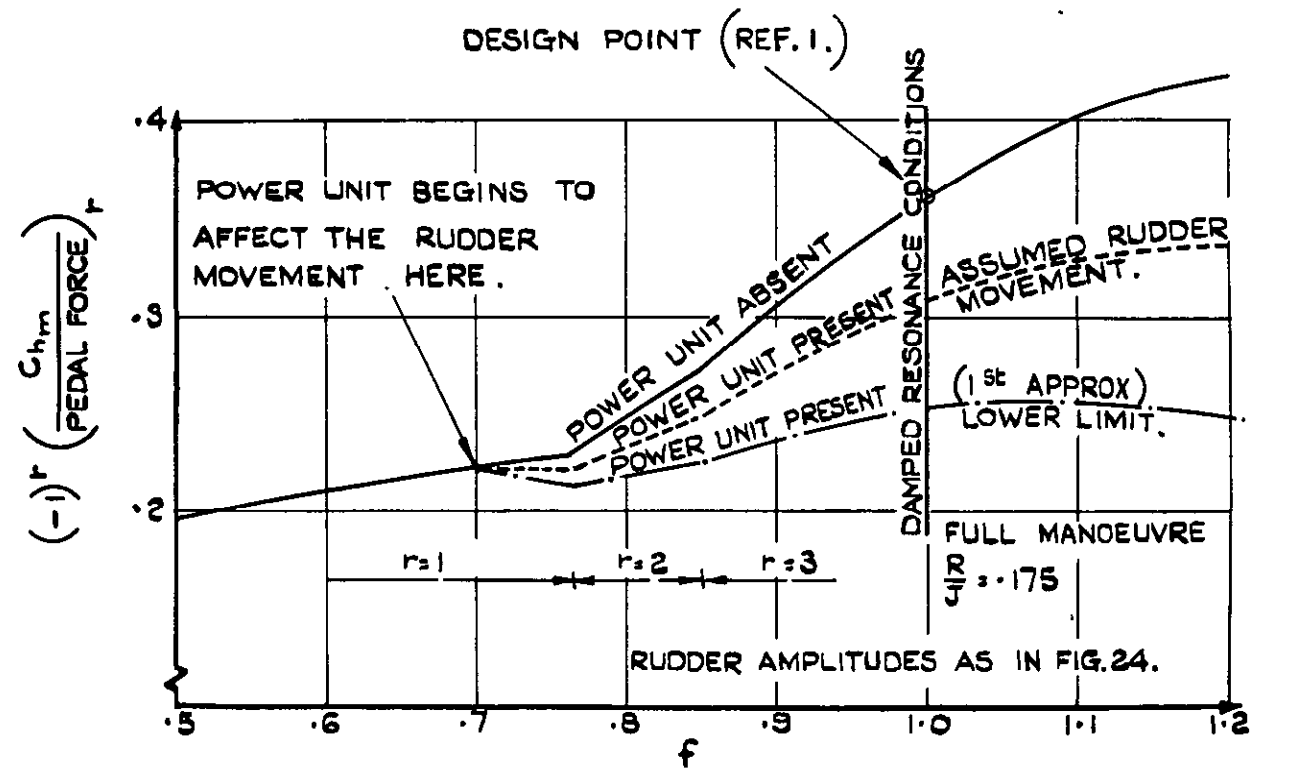

FIG. 26 EXAMPLE SHOWING EFFECT OF POWER UNIT ON THE C_{hm} AT VARIOUS VALUES OF f EXAMPLE DATA IN TABLE I.

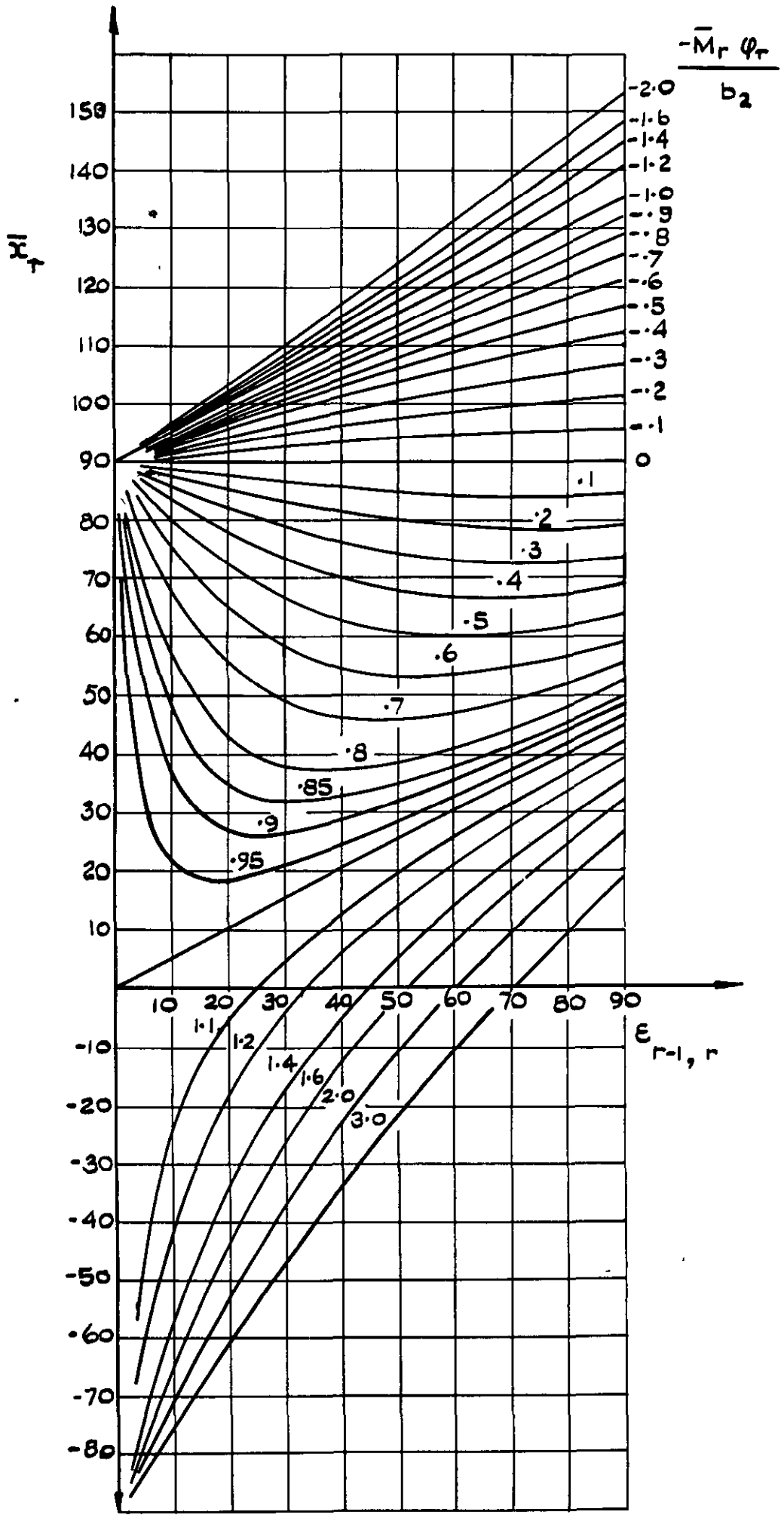

FIG. 27. SOLUTION OF THE EQUATION

$$\frac{\cos \bar{x}_r}{\cos\left(\bar{x}_r - \varepsilon_{r-1,r}\right)} = -\frac{\bar{M}_r \varphi_r}{b_2}$$

C.P. No. 301
(18,124)
A.R.C. Technical Report

Published by
HER MAJESTY'S STATIONERY OFFICE
To be purchased from
York House, Kingsway, London W C 2
423 Oxford Street, London W 1
P O Box 569, London S E 1
13A Castle Street, Edinburgh 2
109 St Mary Street, Cardiff
39 King Street, Manchester 2
Tower Lane, Bristol 1
2 Edmund Street, Birmingham 3
80 Chichester Street, Belfast
or through any bookseller

PRINTED IN GREAT BRITAIN

S.O. Code No. 23-9010-01

C.P. No. 301

C.P. No. 304
(17,990)
A.R C. Technical Report

C.P. No. 304
(17,990)
A.R.C. Technical Report

MINISTRY OF SUPPLY

AERONAUTICAL RESEARCH COUNCIL

CURRENT PAPERS

Three-Dimensional Wind-Tunnel Tests of a 30° Jet Flap Model

By

J. Williams, M.Sc., Ph.D., and

A. J. Alexander, B.Sc.,

of the Aerodynamics Division, N.P.L.

LONDON · HER MAJESTY'S STATIONERY OFFICE

1957

EIGHT SHILLINGS NET

Three-Dimensional Wind-Tunnel Tests of a 30° Jet Flap Model

- By -
J. Williams, M.Sc., Ph.D.
and
A. J. Alexander, B.Sc.
of the Aerodynamics Division, N.P.L.

9th November, 1955

SUMMARY

As a first investigation of finite aspect ratio effects in relation to the jet flap scheme, pressure plotting experiments were made on a small-scale model, with a 12½% thick wing section already tested under two-dimensional conditions at the N.G.T.E. The spanwise distribution of 'pressure lift' loading induced by T.E. blowing was evaluated by chordwise integration of the surface static pressures, and followed closely that which would be expected for a conventional wing at incidence (without T.E. blowing). The total lift, drag and pitching moments were derived for values of jet momentum coefficient C_J up to 2 at wing incidences between -5° and 20°, and up to 5 at zero incidence, by summing the corresponding integrated pressure forces and jet reaction components.

CONTENTS

1./

Published with permission of the Director, National Physical Laboratory

1. Introduction

The jet flap scheme developed at the N.G.T.E.[1] is essentially a means of producing an asymmetry of flow about a wing in order to increase lift at constant wing incidence, without recourse to mechanical devices such as large T.E. flaps. Air is ejected with high velocity at an angle θ to the chord-line, through a narrow spanwise slot at the wing T.E. In the so-called 'shrouded jet flap', a small hinged T.E. flap is included merely to turn the jet through the required angle by Coanda effect, instead of inclining the direction of the blowing slot to the chord line. The jet-flap scheme may be contrasted with blowing over normal size T.E. flaps, where the asymmetry of the flow is basically engendered by the flap deflection, and the blowing prevents flow separation over the flap nose, thus ensuring that the flap attains its theoretical efficiency* (see Fig.1 of Ref.3). Even in this case, if the blowing momentum is increased beyond that required to prevent flow separation, the lift is also further increased (supercirculation) by the effective extension of the flap chord (or downward displacement of the dividing streamline extending from the T.E. of the flap[4]).

Extensive two-dimensional wind-tunnel tests on 12½% thick elliptic sections have been made at the N.G.T.E.[2] for various jet deflection angles θ up to and including 90°. At the request of the A.R.C. Performance Sub-Committee, tests on a three-dimensional jet flap model were carried out at the N.P.L. to obtain quickly some idea of the magnitude of finite aspect ratio effects†. A small pressure-plotting model of rectangular planform, with a 12½% thick elliptic section and a jet angle of 31.3°, was provided by N.G.T.E. and was mounted with a plate at one end to give an effective aspect ratio slightly less than 3.0 (see § 2). The lift, drag and pitching moment forces were calculated from measurements of the surface static pressures and the jet reaction. For completeness, tests were also made on the same wing with a second end-plate added, in an attempt to approach two-dimensional flow conditions (see § 2).

2. Experimental Set-up

The model was made of metal, with a chord c of 8 inches and with a span s of 12 inches excluding the ellipsoidal tip fairing which added a further 0.25 inches. A turntable, attached at the model root, rotated about the mid-chord axis in a fixed end-plate as illustrated in Fig.1a; the end-plate extended about 0.8 chord upstream of the wing L.E., two chords downstream of the T.E. (jet exit), one chord vertically above the zero-incidence chord-line and two chords below. Fig.2a, which was derived from the theoretical results of Ref.4, gives the effective aspect ratio of the wing as 2.75 for the appropriate ratio of wing span to end-plate height. The set-up of the supplementary experiments, with the ellipsoidal tip removed and a second end-plate added, did not represent strictly two-dimensional conditions. With the present end-plate size, which was limited by

structural/

---

*The quantity requirements to achieve a moderate lift by blowing over a normal size T.E. flap are considerably less than those needed with the simple jet flap at the same angle.

†Provisional conclusions were communicated to the A.R.C. Performance Sub-Committee in February, 1954, immediately the tests were completed, and advance copies of some of the graphs contained herein have already been given very limited circulation.

structural and accessibility considerations, the loading was sensibly constant across the span but according to Fig.2a, the effective aspect ratio was only 6.8.

For the measurement of surface static pressures, 26 tappings were provided at each of the four spanwise stations 0.2s, 0.5s, 0.8s and 0.95s from the wing root, closely spaced near the L.E. and T.E. of the model. Some static pressure tappings were also included in the end-plate at the wing root but these were only useful for general guidance. Unfortunately, it was not possible to incorporate static tubes in the blowing slot walls. The upper lip of the blowing slot was located at the T.E. of the elliptic section with the lower lip just on the undersurface to give a mean slot width w of 0.025 in., i.e., w/c = 0.003; the spanwise variation was less than 0.0025 in. N.G.T.E. measurements showed that at zero wind-speed the jet issued at an angle 31.3° to the chord-line, with no observable variation spanwise or change with jet efflux over the practical range. The internal structure of the model is shown in Fig.1b.

The model was located centrally in the N.P.L. Low Turbulence Wind-Tunnel (regular 16-sided cross-section, 7 ft height), so that the tunnel interference effects were small. The general arrangement of the model and the external ducting to the Broom-Wade compressor unit is depicted in Fig.1a. A simple pitot comb traverse gear was employed to explore briefly the development of the jet wake (see Fig.1c). The jet could be straddled at any spanwise location and at distances downstream up to three chords behind the T.E; the axis of the comb could be aligned along the local mean direction of the jet flow. Detailed explorations were not possible, however, owing to shortage of tunnel time and lack of a sufficiently closely spaced pitot comb.

The calibration curve given in Fig.2b, of jet reaction J against the jet total pressure measured in the blowing duct, was used to derive the values of the non-dimensional jet reaction coefficient C_J ($\equiv J/\frac{1}{2}\rho_o U_o^2 S$). The curve was determined at the N.G.T.E. from balance measurements of thrust with the model at zero incidence and with zero wind-tunnel speed, a correction being applied to allow for the static pressure distribution arising from the flow induced about the model by the jet efflux.

3. Range of Tests and Reduction of Observations

Most of the wind tunnel tests were carried out at a windspeed of 100 ft/sec ($R = 0.1 \times 10^6$), when the available air supply permitted C_J - values up to 0.5 to be used. Higher values of C_J were obtained by reducing the windspeed to 50 ft/sec ($C_J < 2.1$) and to 30 ft/sec ($C_J < 4.8$). Observations were first made with the three-dimensional model at zero incidence and C_J - values up to 4.8. Transition wires were located on the front upper and lower surfaces of the model, at 0.2c behind the L.E., as far forward as possible without causing interference at the closely spaced static holes in the wing nose. Similar experiments were then made at incidences ranging between -5° and 20° for C_J values up to 2.1, both with and without transition wires. Unless otherwise stated the results discussed in the text and plotted in the graphs refer to those obtained with transition wires.

The lift coefficient C_L on the wing may be regarded as comprising the vertical component $C_J \sin(\theta + \alpha)$ of the jet reaction at the nozzle and the vertical 'pressure force' C_{Lp} arising from the airflow over the aerofoil surface. Thus we write

$$\left.\begin{aligned} C_L &= C_J \sin(\theta + \alpha) + C_{Lp} \\ C_D &= -C_J \cos(\theta + \alpha) + C_{Dp} \\ C_M &= -\tfrac{2}{c} C_J + C_{Mp} \end{aligned}\right\} \quad \ldots\ldots(1)$$

where/

where n is the perpendicular distance from the point about which moments are taken onto the extended centre-line of the jet nozzle. For moments about mid-chord, as quoted for the present tests, $n/c \simeq \frac{1}{2} \sin\theta$. The sectional pressure-force coefficients were obtained from the measured static pressures by chordwise integration. The overall force coefficients were then derived by integration across the span, and for convenience were based on the area S of the rectangular plan-form excluding the small ellipsoidal tip[x]. Some simplifying assumptions had to be made for the chordwise integration of the static pressures close to the T.E. since there were no static pressure holes inside the slot throat. Although the resulting error in the lift coefficients is insignificant, this may not be so for the pitching moment and drag coefficients under all conditions.

The quasi two-dimensional experiments, made with the ellipsoidal tip removed and a second end-plate added, covered roughly the same ranges of C_J and incidence as those tested on the three-dimensional model. It was first checked that the set-up gave sensibly constant loading across the span, i.e., nominally two-dimensional flow, for a few representative conditions. Then for the remainder of the tests, the static pressures were recorded only at the mid-span section and the pressure force coefficients evaluated therefrom.

4. Three-Dimensional Model Results

4.1 Lift

The spanwise distribution of 'pressure lift' loading induced by T.E. blowing, with the wing at zero incidence, seems little different from that given by simple lifting-line theory (see Fig.3a) or that due to wing incidence without blow (Fig.3b).

The total lift C_L at zero wing incidence is plotted against $C_J^{\frac{1}{2}}$ in Fig.4a, both with and without transition wires and for various windspeeds. At C_J-values below unity, the experimental results lie reasonably close to the straight line $C_L = 1.4\, C_J^{\frac{1}{2}}$, and at higher C_J-values are slightly above this. The relative magnitudes of the jet reaction and pressure force contributions to the total lift are also indicated. Curves of C_L against $C_J^{\frac{1}{2}}$ for other incidences are plotted in Fig. 4b for the case with transition wires; the slope $dC_L/dC_J^{\frac{1}{2}}$ at a prescribed C_J is seen to increase with incidence. The C_L-values obtained without transition wires are in most instances not more than 0.1 different from those with.

Lift-incidence curves for a range of C_J-values with transition wires are shown in Fig.5. As C_J is increased from zero there is no significant loss in stalling incidence; at C_J-values above unity there is even some increase in stalling incidence which, though possibly peculiar to the low Reynolds number and particular wing configuration of the tests, is at least encouraging. The value of $dC_L/d\alpha$ for small incidences rises steadily as C_J increases, from 0.055/deg without blow to about 0.1/deg at $C_J = 2$. The increase is roughly proportional to $C_J^{\frac{1}{2}}$, and is made up of contributions from both the jet reaction and pressure force components. With α measured in degrees,

$$dC_L/d\alpha = 0.0175\, C_J \cos(\theta + \alpha) + dC_{Lp}/d\alpha \qquad \ldots\ldots(2)$$

$$\simeq 0.015\, C_J + dC_{Lp}/d\alpha \text{ for small } \alpha \qquad \ldots\ldots(3)$$

The removal of the transition wires had little effect on $dC_L/d\alpha$, except for the results without blowing, when the value became extraordinarily high. This seemed to be associated with the presence of a thin laminar boundary layer right back to the T.E. at the low test Reynolds number combined with the unusual slotted T.E. shape.

4.2/

---

[x] The tip increased the wing area by only about $1\frac{1}{2}\%$.

4.2 Pitching Moment

Fig.6 gives curves of total pitching moment C_M about the half-chord axis plotted against the corresponding total lift C_L, for a range of values of α and C_J, from the tests with transition wires.

Probably not more than broad conclusions should be drawn from the results, in view of the few static pressure holes in the vicinity of the slot. It is seen that the mean slope $(dC_M/dC_L)_{C_J}$ of the curves for constant C_J (α varied) is about 0.25 at low but non-zero values of C_J, so that the aerodynamic centre is located close to the quarter-chord position. As C_J increases, the value of $(dC_M/dC_L)_{C_J}$ decreases so that the aerodynamic centre tends to move further aft, say by about 0.04c as C_J is raised from 0.2 to unity. The C_M - C_J curves for zero C_J are, however, somewhat unusual in that the slopes both with and without transition wires differed appreciably from 0.25, being respectively greater and less. This peculiar behaviour in the absence of blowing was again accredited to the unconventional T.E. shape and low Reynolds number of the tests.

As C_J increases with α constant, the nose-down pitching moment becomes steadily larger*, because the induced suction forces on the wing upper surface are much higher near the T.E. than the L.E. (see later discussion on pressure distributions). The chordwise location of the centre of total lift is plotted against C_L in Fig.7, and in general moves rearward appreciably as C_J is increased at constant incidence or as the incidence is decreased at constant C_J.

4.3 Drag

The total drag coefficient C_D on the wing, as defined by equation(1) of §3, is plotted against C_J in Fig.8a, for a range of wing incidences both with and without transition wires. Again the drag results do not warrant more than a qualitative examination.

It will be recalled that the drag is made up of the chordwise components of the direct jet reaction and the pressure forces on the aerofoil surface; the relative magnitudes of the two contributions are indicated in Fig.8a for the zero incidence case. Thus, without blowing, C_D includes the conventional form drag of the wing sections and the induced drag arising from downwash effects, but excludes the skin-friction drag. With blowing, we might therefore regard C_D as comprising a chordwise component $-C_J \cos(\theta + \alpha)$ from the direct jet reaction, a form drag together with any recovery of thrust which manifests itself in the pressure distribution, and an induced drag resulting from downwash effects over the wing. For ideal conditions, i.e., potential flow in the mainstream flow and no mixing, it can be shown that the direct jet reaction and thrust recovery terms taken together contribute the amount $-C_J$ corresponding to the gross thrust. In our measurements the so-called form drag, induced drag and thrust recovery terms are of necessity lumped together as pressure drag. Fig.8a shows that the rate of decrease in C_D with C_J is appreciably less than the amount $C_J \cos(\theta + \alpha)$ associated with the direct jet reaction. Thus, because of the low aspect ratios and small jet angle, the combined form and induced drag contributions to the pressure drag completely outweigh and mask any negative contribution arising from thrust recovery.

For comparisons with the pressure drag associated with more conventional methods of producing pressure lift on a wing, namely by incidence and camber, the value of C_{Dp} for the present jet flap wing

has/

---

*On a complete aircraft with tail this could at least be partially trimmed out by the increased downwash over the tail.

has been plotted against C_{Lp}^2. Fig.8b, for the wing at zero incidence shows that for C_J-values below 0.5 the points lie close to the straight line

$$C_{Dp} = 0.013 + 0.14\ C_{Lp}^2$$

while for C_J-values up to 2 the value of C_{Dp} does not exceed $0.013 + 0.16\ C_{Lp}^2$. Fig.8c, giving results for other incidences, shows that up to 11° the trend is also much the same. The combined form and induced drags of a conventional wing of aspect ratio 2.75 producing corresponding pressure lifts at the same Reynolds number would not in fact be greatly different from the above (see § 6).

4.4 General Flow Characteristics and Pressure Distributions

Tuft and china clay observations were made to visualise the flow about the model. For C_J-values up to 2.1, with the wing at zero incidence, no separation was evident on the upper surface due to the adverse pressure gradients at the front[7]. As the wing incidence was increased a small bubble of separated flow appeared, at the inboard sections first, being formed by separation of the laminar boundary layer close to the L.E. with subsequent reattachment as a turbulent boundary layer ahead of the transition wire. Without blowing, the bubble did not expand appreciably chordwise until the incidence exceeded 10°, after which the position of reattachment moved steadily rearwards, again at the inboard sections first. The behaviour with blowing operative was similar, but the wing incidence at which the bubble began to expand decreased somewhat as C_J was increased.

Some representative pressure distributions with the wing at zero incidence and transition wires on are shown in Figs.9a and 9b for the chordwise sections at $y/s = 0.20$ and $y/s = 0.95$, and selected C_J-values up to 2.1. It is seen that they are similar in shape to the pressure distributions on the main part of a wing when a T.E. flap is deflected. In order to obtain some idea of the variation in pressure distribution with incidence as well as C_J, the values of the peak suctions occurring near the L.E. and T.E. of the two chordwise sections have been plotted against incidence for C_J-values ranging up to 2.1 (see Fig.10). As the incidence increases at constant C_J the peak suction on the nose grows more rapidly at the inboard than the outboard section, so flow separation may be expected earlier inboard which agrees with the deduction from flow visualisation experiments. Furthermore, although the peak suction near the T.E. of the outboard section grows with increasing incidence, that at the T.E. of the inboard section varies little at first and eventually diminishes. As C_J increases at constant incidence, the T.E. peak suctions grow much more rapidly than those near the L.E., partly because the latter are much reduced by downwash effects.

Some total head traverses of the jet were carried out at various distances downstream of the T.E. and at a few spanwise locations, but unfortunately the tests had to be severely limited. Fig.11a shows the mean line of the jet (locus of maximum total head) and also the distribution of the total head in the wake downstream of the mid-span station (6 in. from the root), for the wing at zero incidence with $C_J = 0.5$. It is seen that the width of the wake increases rapidly near the slot exit, being about 1 in. at a quarter-chord behind the T.E., by which time the inclination of the mean-line to the chord has fallen to about 15°. Fig.11b compares a few measurements of the mean-line of the jet downstream of the mid-span station with those further outboard. Spanwise variations are clearly evident further outboard than 10 in. from the root, i.e., beyond about 85% span.

5./

[7] In the absence of transition wires, laminar flow seemed to persist right back to the T.E.

5. Quasi Two-Dimensional Model Results

The pressure force coefficients were derived from static pressure measurements at the mid-span section only, since the lift loading was sensibly constant across the span‡. The curves of total lift, pitching moment and drag for the quasi two-dimensional model (effective aspect ratio ≈ 6.8) are generally similar in character to those already discussed for the three-dimensional model.

At C_J-values below unity, the results for the total lift C_L at zero incidence both with and without transition wires, lie reasonably close to the straight line $C_L = 1.7\ C_J^{\frac{1}{2}}$ and at higher C_J-values are slightly above this (see Fig.12a). Curves of C_L against $C_J^{\frac{1}{2}}$ for other incidences derived from tests with transition wires are plotted in Fig.12b. Lift-incidence curves for a range of C_J-values are also shown in Fig.13, the value of $dC_L/d\alpha$ at small incidences rising steadily from about 0.075/deg without blow to 0.15/deg at $C_J = 2$.

The total pitching moment C_M about the half-chord axis is plotted against C_L for a range of C_J in Fig.14. At low C_J the aerodynamic centre is located close to the quarter-chord position and moves rearward about 0.06c as C_J increases from 0.2 to unity. The chordwise location of the centre of total lift also moves rearward in general as C_J increases with α constant, or as α decreases at constant C_J (see Fig.15).

The total drag coefficient C_D is plotted against C_J in Fig.16a for a range of incidences. It is immediately evident that the rate of decrease of C_D with C_J at zero incidence is less than $C_J \cos\theta$, so that the increase in pressure drag due to the so-called form and induced drag components again outweighs any decrease from the thrust recovery term. The values of the pressure drag, with the wing at zero incidence and with front transition wires, satisfy fairly well the relation

$$C_{Dp} = 0.015 + 0.068\ C_{Lp}^2$$

for C_J values up to 2 (see Fig.16b). This relation also holds with the wing at higher incidences, up to at least 6.5° (see Fig.16c), and is not far different from that for the combined induced and form drags of a conventional wing of aspect ratio 6.8 giving the same pressure lift (see § 6).

Some representative pressure distributions for the mid-span section with the wing at zero incidence and transition wires on are given in Fig.17 for a range of C_J-values. As the incidence increases at constant C_J, the peak suction near the T.E. varies little at first but eventually diminishes (see Fig.18); the value at moderate incidences is little different from that measured for the inboard sections of the three-dimensional model (c.f. Fig.10). The peak suction at the nose of course increases with incidence, until a certain maximum value ($-C_p \simeq 5$) is reached. For any prescribed incidence below that corresponding to this maximum value, the peak suction in general exceeds that measured on the three-dimensional model. The maximum is reached at a lower incidence, as would be expected because of the smaller downwash effects, but its value is not vastly different.

The mean line of the jet and the distribution of total head in the wake downstream of the T.E. are plotted in Fig.19 for the wing at zero incidence with C_J-values of 0.18 and 0.5.

6./

---

‡This was also checked for us theoretically by Miss Weber of the R.A.E., Farnborough.

6. General Conclusions on Finite Aspect Ratio Effects

The investigation described in the present report was a preliminary and first attempt to explore the effects of finite aspect ratio on the jet flap scheme. The experiments were not intended to provide comprehensive data for detailed project studies nor to establish fundamental postulates for a three-dimensional jet flap theory, but simply to give some idea of the magnitude of finite aspect ratio effects, particularly in relation to lift. Nevertheless, in summarising the results obtained for wing aspect ratios in the vicinity of 2.75 and 6.8, it is at least worth considering them in the light of simple aspect ratio correction factors for conventional wings without T.E. blowing*.

6.1 Summary of Experimental Results

(a) Total Lift (Figs.4 and 12) - For zero incidence, and $C_J < 1$, the results for the aspect ratio 2.75 and 6.8 wings lie close to the values

$$C_L = 1.4\ C_J^{\frac{1}{2}} \text{ and } C_L = 1.7\ C_J^{\frac{1}{2}} \text{ respectively,}$$

and are about 0.6 and 0.7 respectively of the corresponding N.G.T.E. two-dimensional values[2]. The appropriate values of the aspect ratio correction factor $[1 + (a_o/\pi Ae)]^{-1}$ for lift on conventional wings are 0.58 and 0.77 respectively, assuming elliptic loading ($e = 1$) and a sectional lift curve slope a_o equal to the flat-plate value of 2π.

(b) Pressure Drag (Figs.8 and 16) - For zero incidence and $C_J < 1$, the results for the aspect ratio 2.75 and 6.8 wings satisfy approximately the relations

$$C_{Dp} = 0.013 + 0.14\ C_{Lp}^2 \text{ and } C_{Dp} = 0.015 + 0.068\ C_{Lp}^2$$

respectively. The corresponding induced (pressure) drag $C_{Lp}^2/\pi Ae$ for conventional wings producing the lift C_{Lp} takes the values $0.116\ C_{Lp}^2$ and $0.047\ C_{Lp}^2$ respectively, assuming elliptical loading ($e = 1$). The remaining contribution ($\doteq 0.015 + 0.02\ C_{Lp}^2$) could reasonably be accounted for as sectional form drag in both cases. The approximate agreement between the measured pressure drags and the corresponding conventional drag estimates (induced and form) may well be fortuitous, but at least it seems that the pressure drag on the jet flap wing is not likely to be much larger than that of a conventional wing producing the same pressure lift.

(c) Lift-Incidence Curves (Figs.5 and 13) - For both aspect ratios the measured slopes $dC_L/d\alpha$ at constant C_J and small incidences are about doubled as C_J is raised from near zero to 2.0, and the increase is roughly proportional to $C_J^{\frac{1}{2}}$. There is also no significant loss in stalling incidence ($dC_L/d\alpha = 0$) as C_J is raised.

(d) Pitching Moments (Figs.6, 7, 14 and 15) - For small C_J-values, the aerodynamic centre is located near the quarter-chord position, and the centre of total lift at zero incidence lies close to half-chord. Both move steadily rearward as C_J increases at constant incidence.

6.2 Fundamental Considerations

The foregoing correlation of the pressure drag C_{Dp} in terms of C_{Lp}^2 would at first sight imply that

(a)/

---

*i.e., with the lift produced by incidence or camber.

(a) the downwash due to trailing vorticity affects only the pressure force contribution to the lift vector.

(b) the downwash is generated only by the pressure lift.

The general consensus of opinion held at present supports the first postulate that the pressure lift only is affected, since there seems little reason for the downwash to have other than small effects on the jet reaction. However, in preference to the second, it is generally considered[1] that the downwash results from the reaction of the total lift on the mainstream. On this basis, the effective downwash angle at the wing is by conventional arguments $\phi = C_L/\pi Ae$ and the corresponding induced drag contribution to the pressure drag is $C_{Lp}\, C_L/\pi Ae$, where e represents an efficiency factor which would be unity for a wing at incidence without blowing and with elliptic loading. The measured C_{Dp} values are plotted against $C_{Lp}\, C_L$ in Figs.8d and 16d respectively for the aspect ratio 2.75 and 6.8 wings at zero incidence. It is seen that, as C_J increases, the efficiency factor e satisfying a relation of the type

$$C_{Dp} = \text{const.} + (C_L\, C_{Lp}/\pi Ae)$$

also increases[/]. This would imply an effective increase in aspect ratio with increasing C_J possibly due to the interaction between the jet and the mainstream[1]. Thus, in general, e may well be dependent on C_J, θ and A as well as on planform.[+]

As far as aspect ratio corrections for lift are concerned it can likewise be argued that the jet produces effectively a change in the sectional no-lift angle, that the pressure lift only is affected by downwash, but that the latter should again be based on the total lift. Simple formulae are then readily obtainable for the pressure lift and the slope of the pressure lift-incidence curve in terms of the corresponding two-dimensional values for the same C_J, but these again involve the product Ae, i.e., the effective aspect ratio.

6.3 Further Work Proposed

Although some attempts have been made to analyse the present experimental data in terms of the above and other arguments, the experiments were not sufficiently comprehensive to permit a careful resolution of fundamental considerations on aspect ratio effects. For this reason, further experiments are proposed on a larger scale model with variable aspect ratio and jet angle. It is intended to determine the forces by balance as well as pressure-plotting measurements, and to make a detailed study of the nature of the three-dimensional flow.

References/

/Note that the value of e derived in this case is lowered by the form drag contribution.

+It can also be argued that the total lift should be used throughout to derive the induced drag, giving a formula of the type $C_{Dp} = \text{const} + (C_L^2/\pi Ae)$. Detailed theoretical studies are being carried out at the R.A.E., Farnborough, to clarify these points.

References

No.	Author(s)	Title, etc.
1	I. M. Davidson	The jet flap. R.Ae.Soc. Lecture, October, 1955.
2	N. A. Dimmock	An experimental introduction to the jet flap. N.G.T.E. Rep.R.175. July, 1955. A.R.C. 18,186.
3	J. Williams	An analysis of aerodynamic data on blowing over T.E. flaps for increasing lift. A.R.C. C.P.209, September, 1954.
4	W. Mangler and J. Rotta	Theory of the three-dimensional aerofoil. Part I - Theory of the supporting line. AVA Monograph F_1. M.O.S. R. & T.1023. A.R.C. 11,553 November, 1947.

Acknowledgements

The writers are much indebted to N.G.T.E. for constructing the model and providing the pumping equipment, in particular to Mr. N. A. Dimmock. The lengthy computations and graphical integrations associated with the reduction of the observations were carried out by Miss E. M. Love, Miss L. N. Esson and Miss A. K. Kernaghan, and the wake traverse gear was designed by Mr. N. Marcus, all of the Aerodynamics Division, N.P.L.

List of Symbols

a_o — slope of two-dimensional total lift-incidence curve

A — wing aspect ratio

c — wing chord

C_{Lp}, C_{Dp}, C_{Mp} — Pressure lift, drag and pitching moment coefficients (about $\frac{1}{2}$-chord); derived by integration of pressure forces on aerofoil

C_L, C_D, C_M — Total lift, drag and pitching moment coefficients (about $\frac{1}{2}$-chord); derived by adding direct jet reaction components to pressure forces on aerofoil. See eqn.(1), § 3)

C_J/

C_J jet coefficient = $J/\frac{1}{2}\rho_o U_o^2 S$

C_p static pressure coefficient = $(p - p_o)/\frac{1}{2}\rho_o U_o^2$

e wing efficiency factor. See §6.

h end-plate height

J total jet reaction

p static pressure

p_o, ρ_o, U_o mainstream static pressure, density, and velocity

R mainstream Reynolds number based on wing chord

s span of wing (excluding small ellipsoidal tip)

S area of wing (excluding small ellipsoidal tip)

w width of blowing slot

x chordwise distance

y spanwise distance from root

α wing incidence

θ jet deflection angle relative to wing chord-line

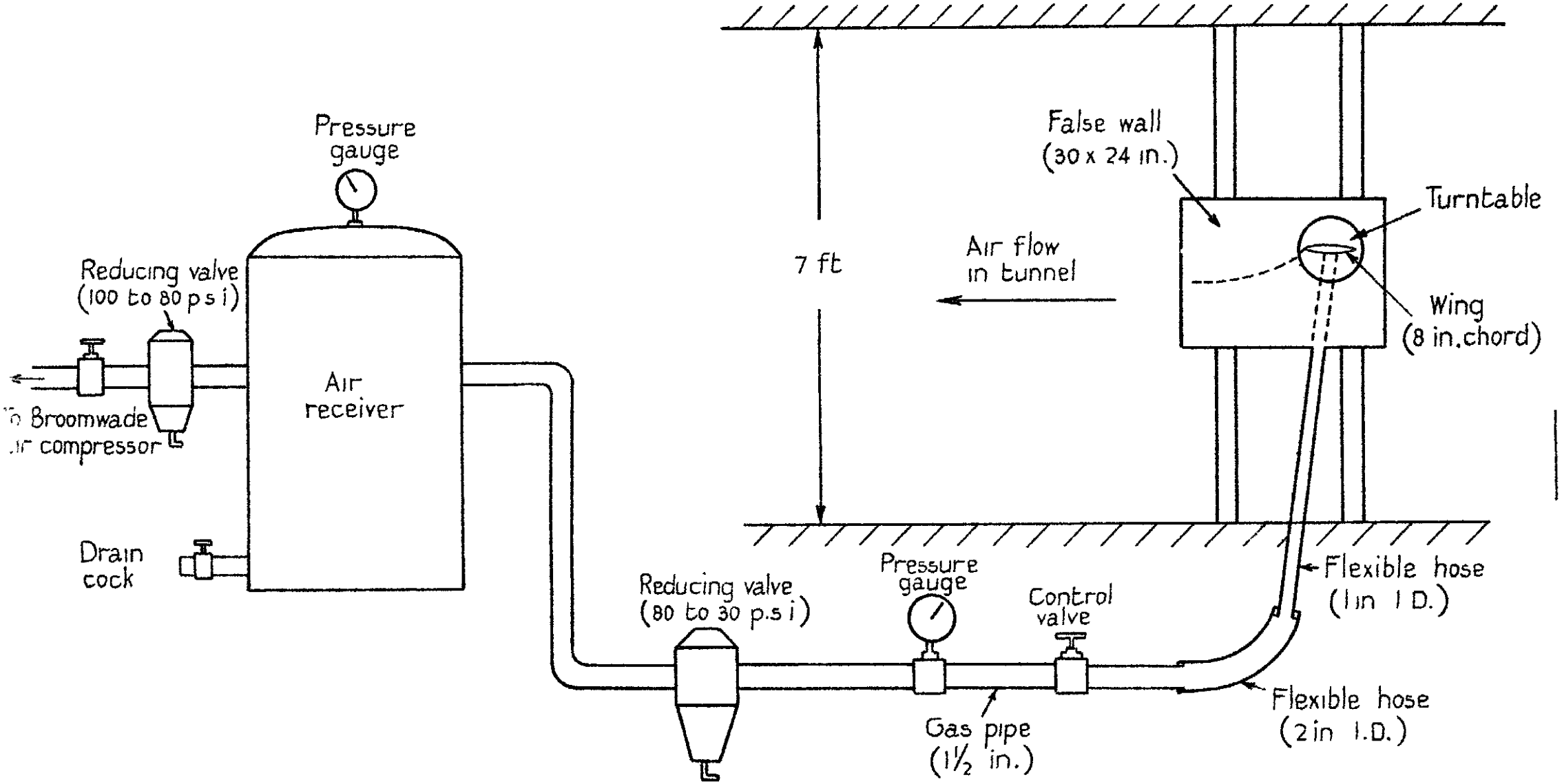

FIG. 1a.

Arrangement of jet flap model and external ducting

FIG. 1b.

Internal structure of three-dimensional jet flap model.

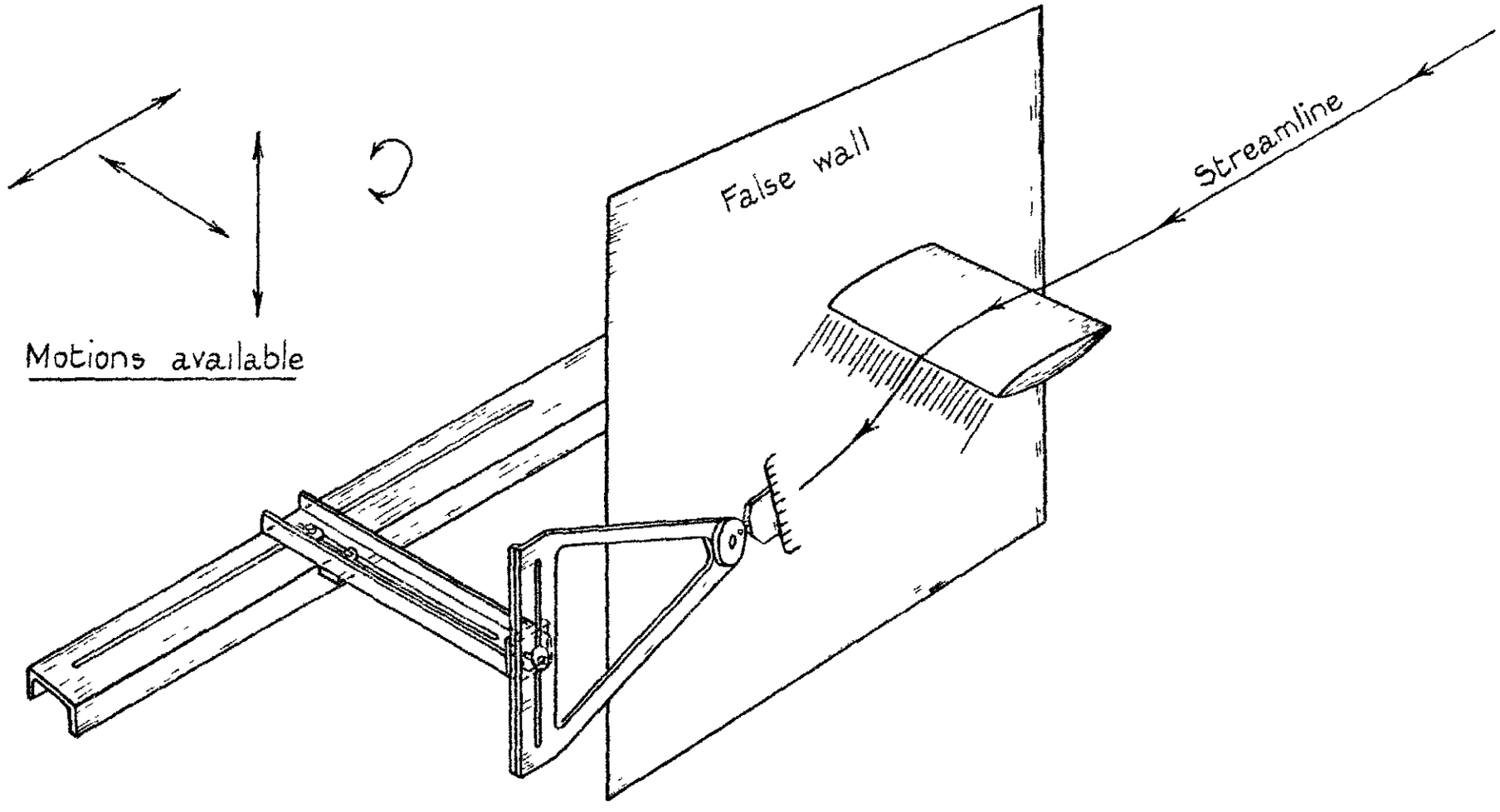

Scale : ≏ 1/10

Pitot comb wake traverse gear.

FIG. 1c

FIG. 2a.

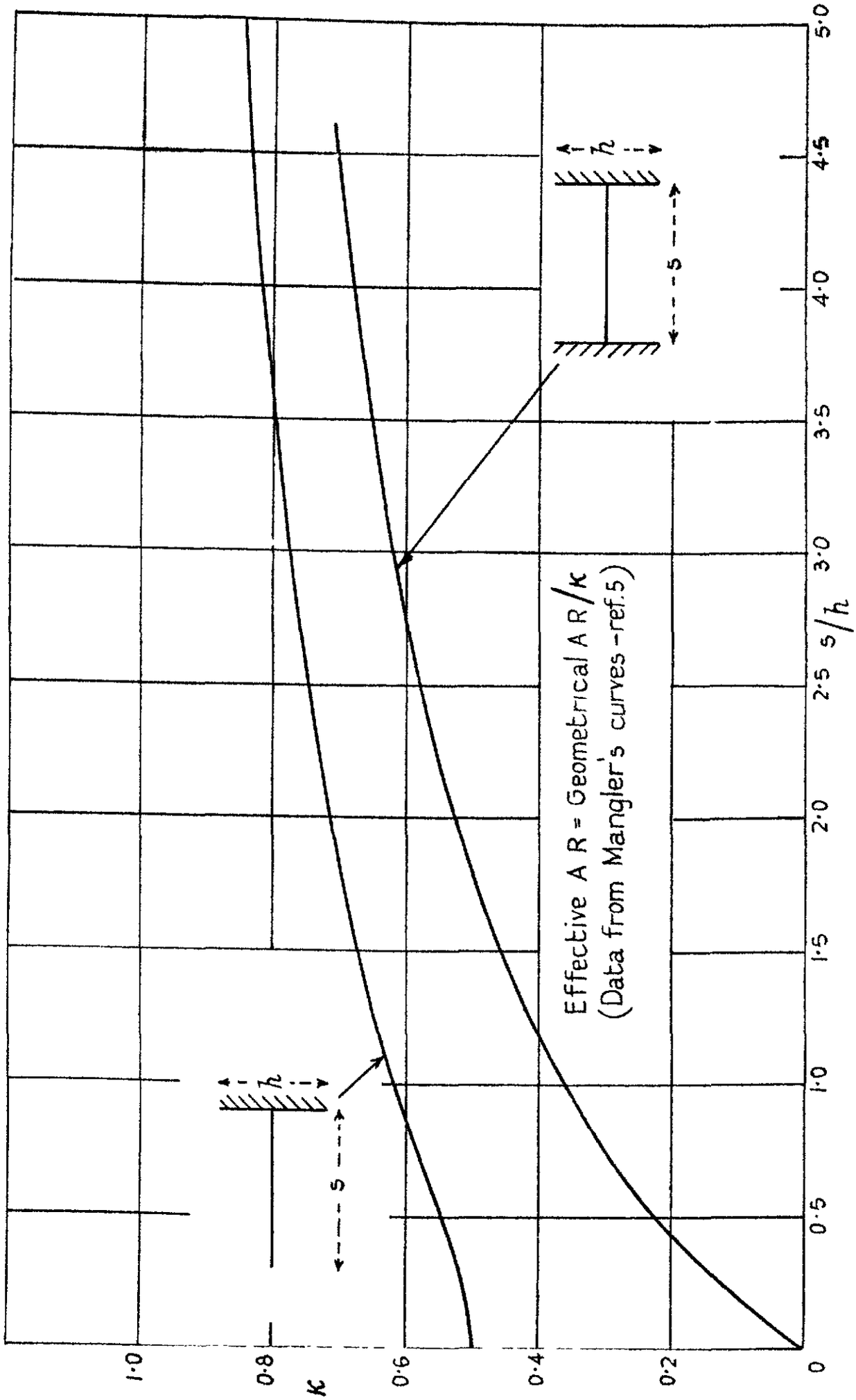

Variation of aspect ratio factor κ with ratio of wing span to end-plate height

Fig 2b.

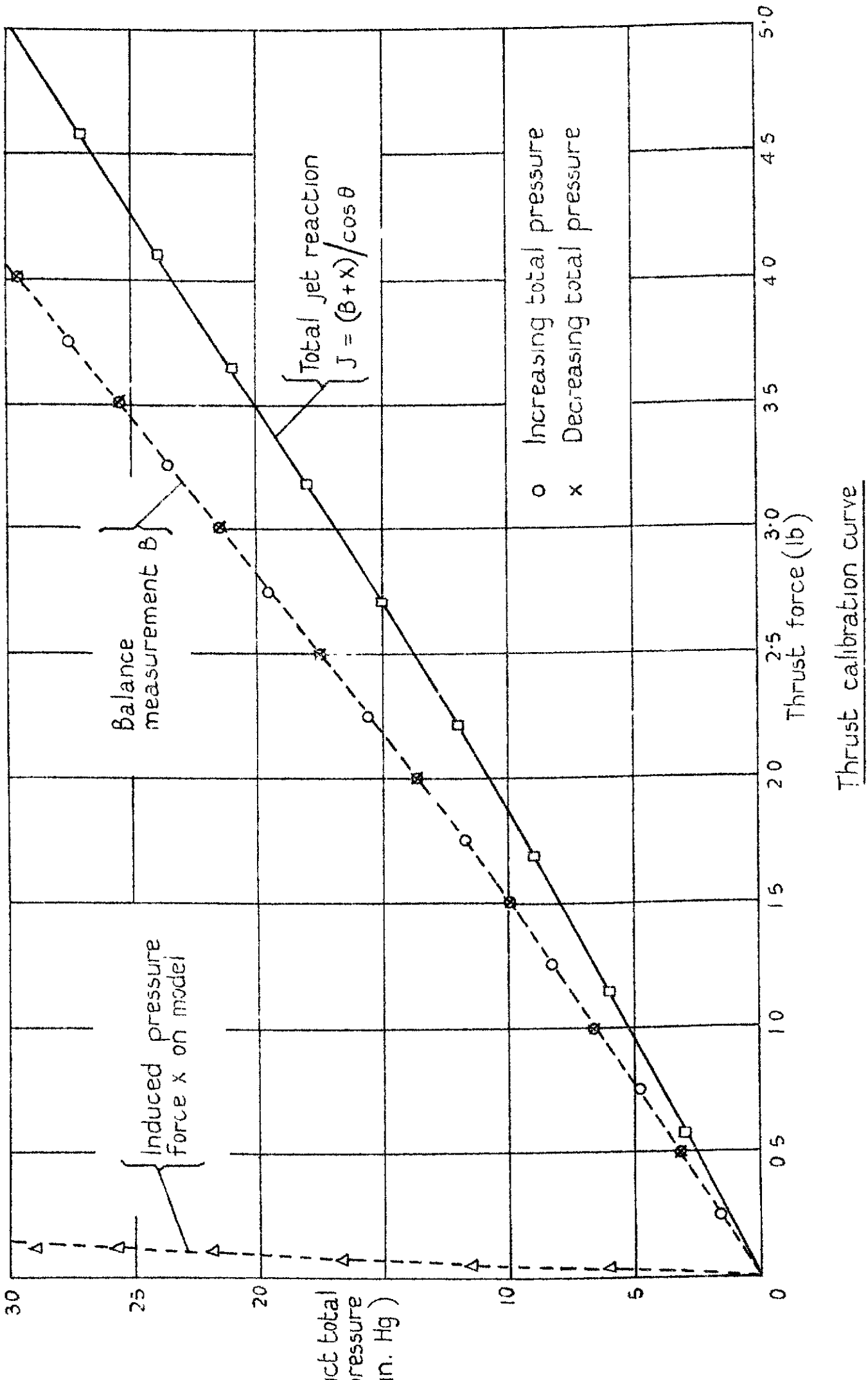

Thrust calibration curve

Fig 3a

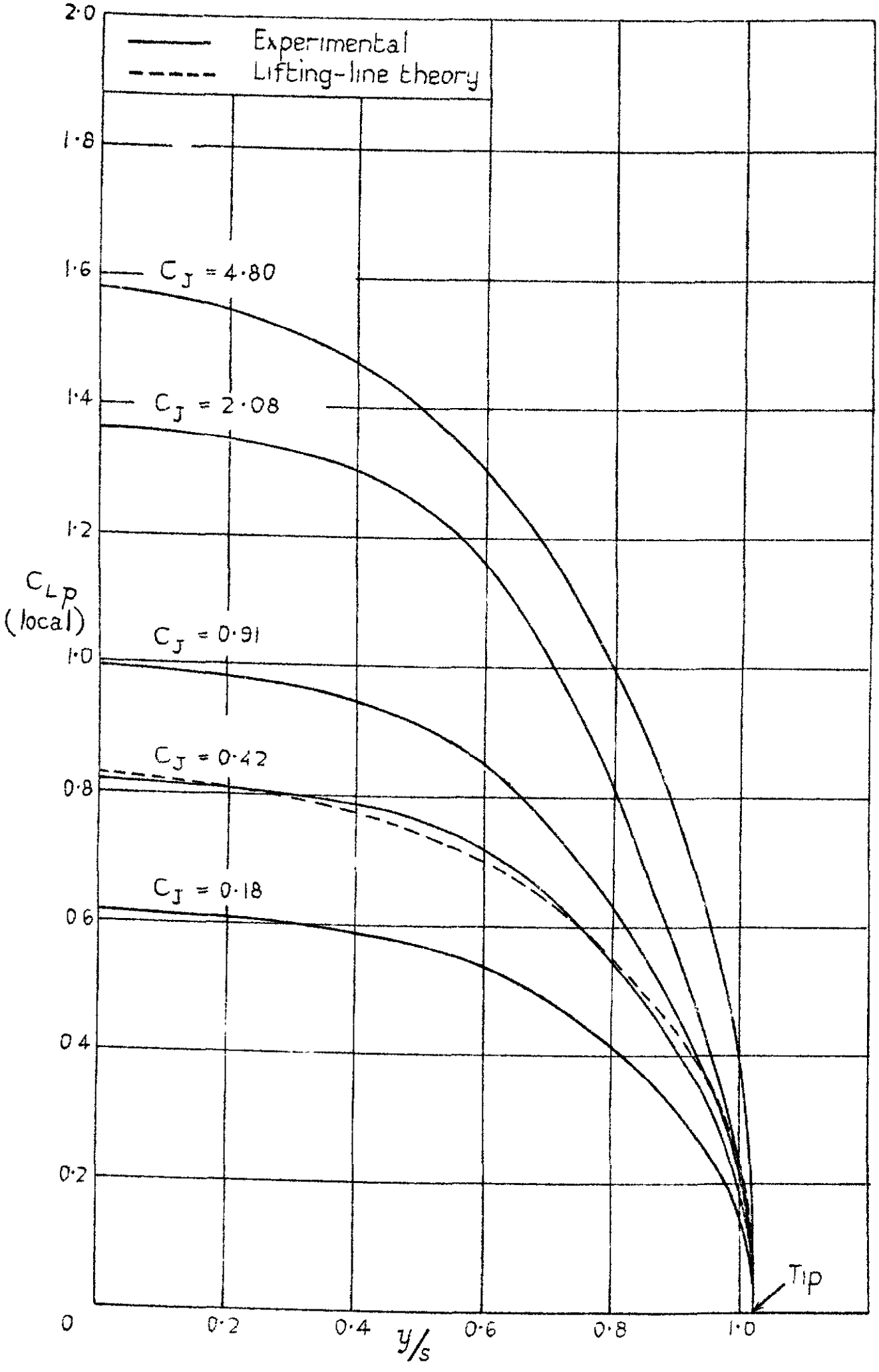

Spanwise distribution of pressure lift at zero incidence – Variation with C_J

Fig 3b.

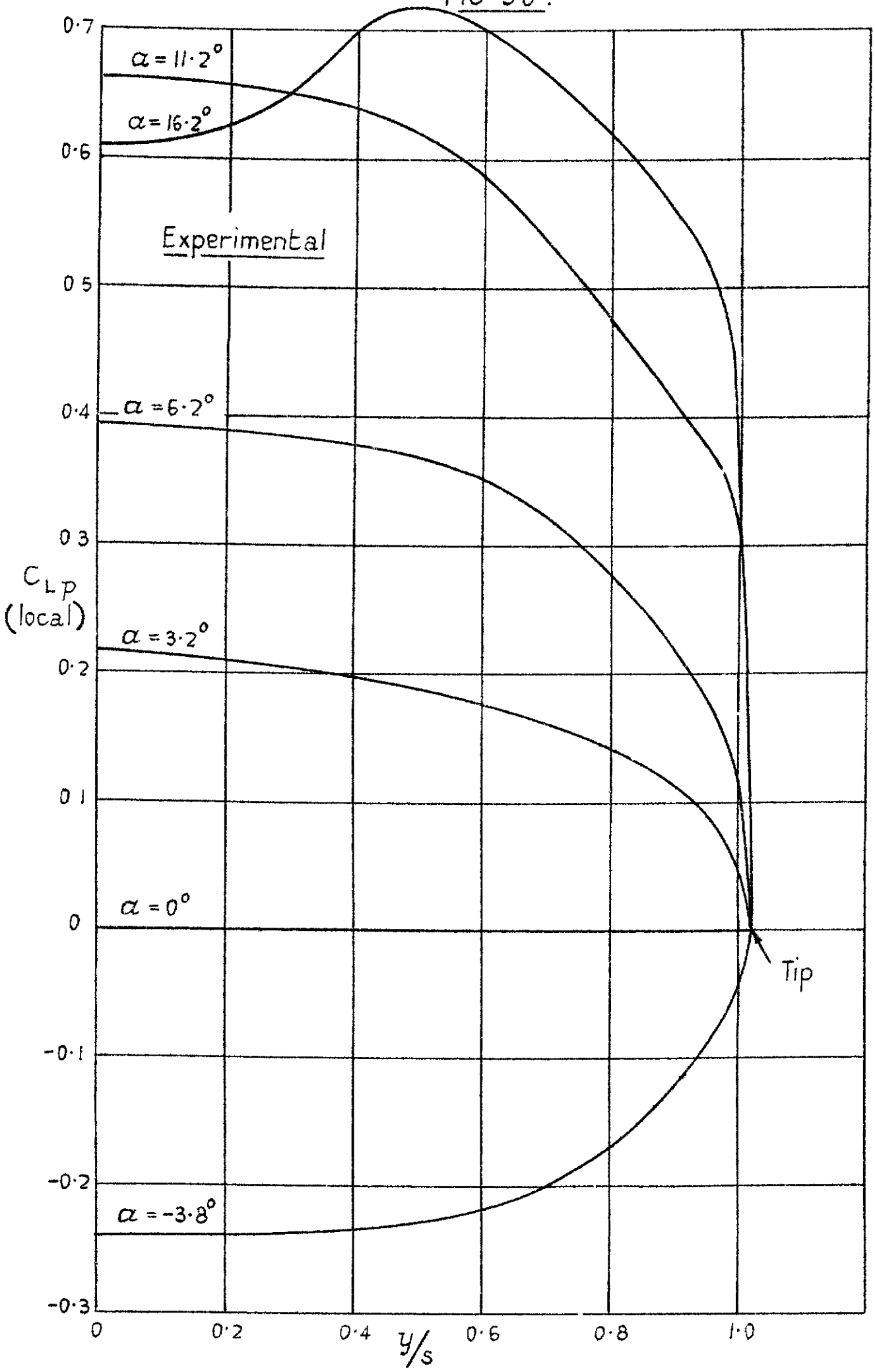

Spanwise distribution of lift without blowing.
Variation with incidence

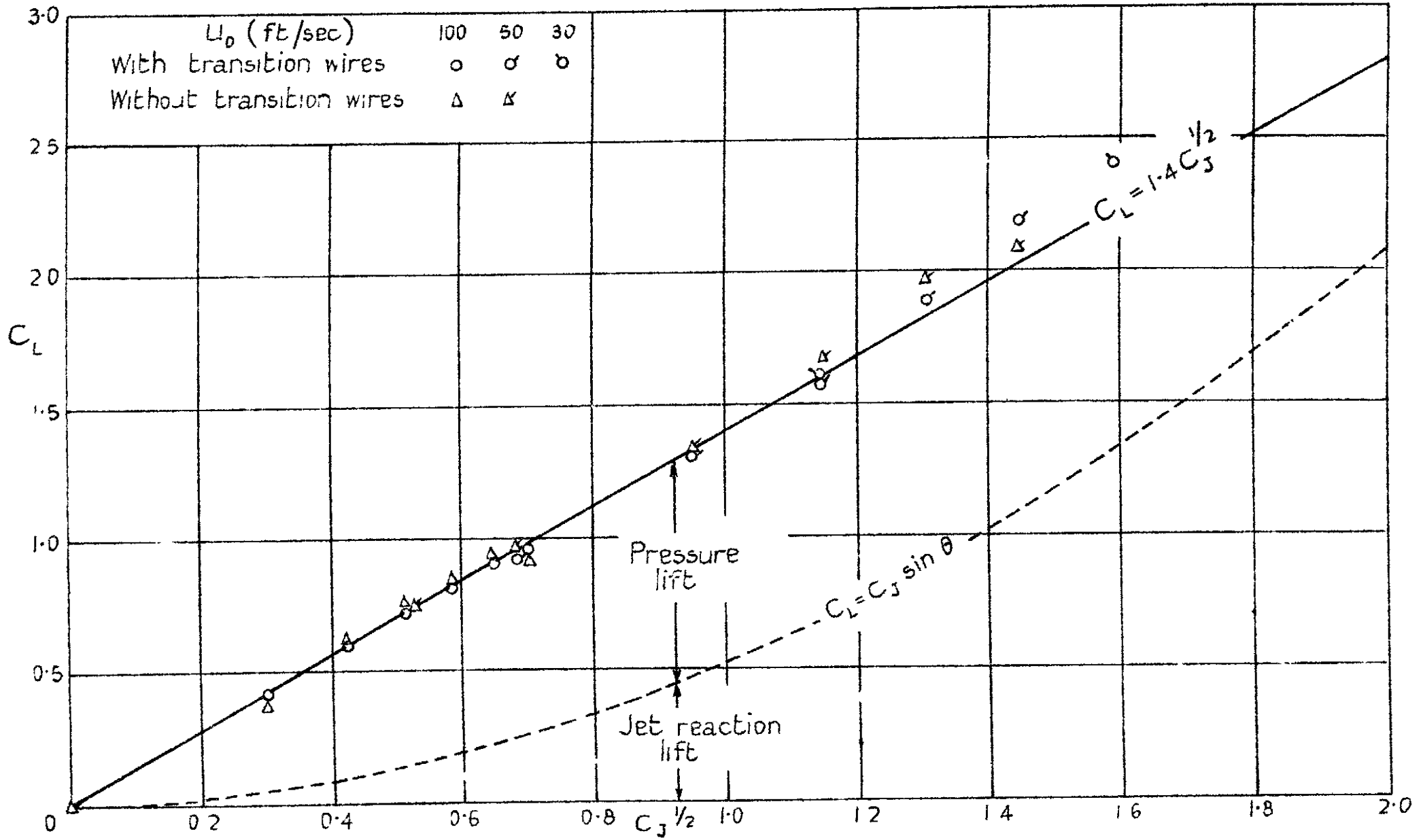

Variation of total lift C_L with $C_J^{1/2}$ at zero incidence

FIG 4a

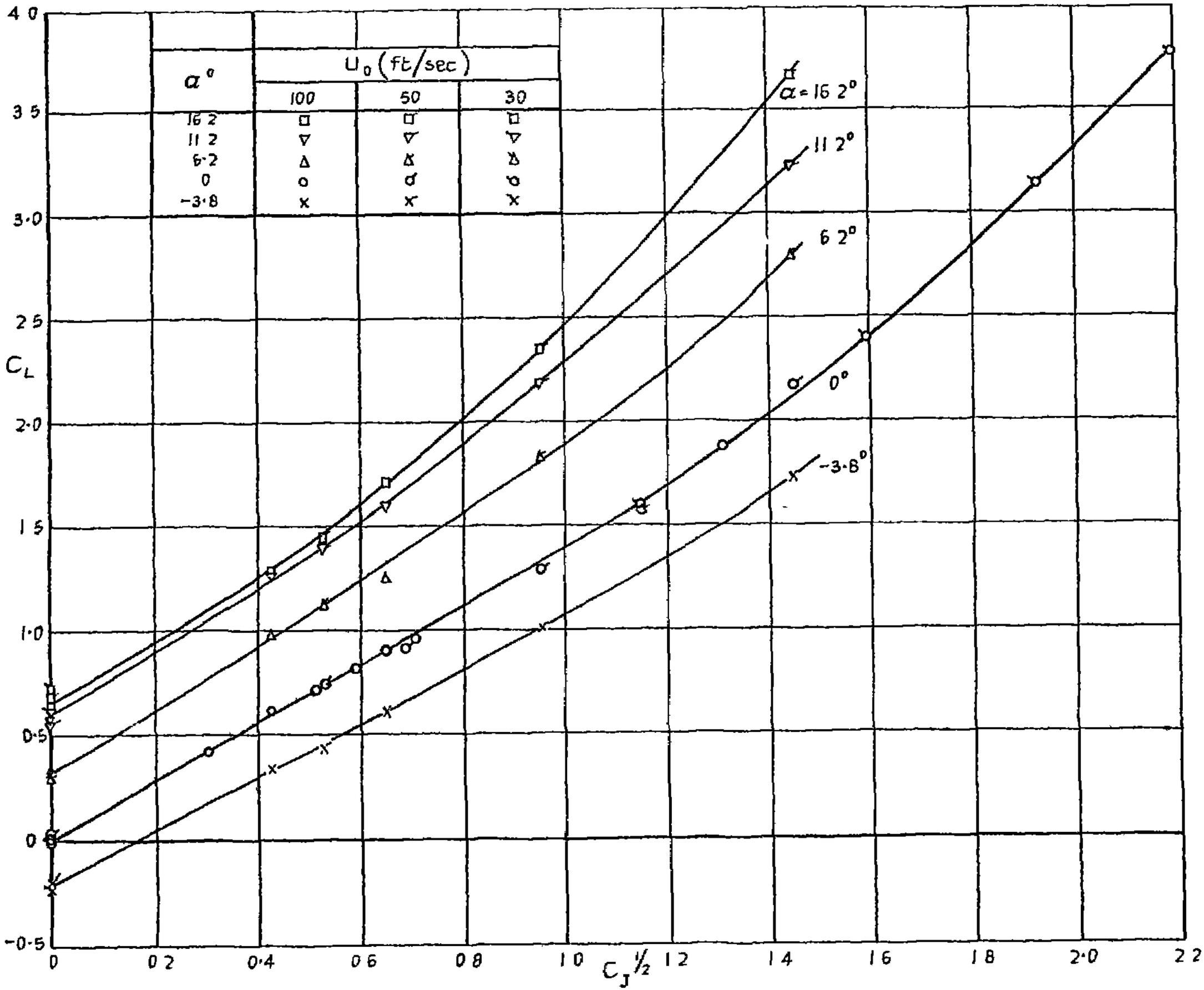

Variation of total lift with $C_J^{1/2}$ at constant incidence

FIG 5.

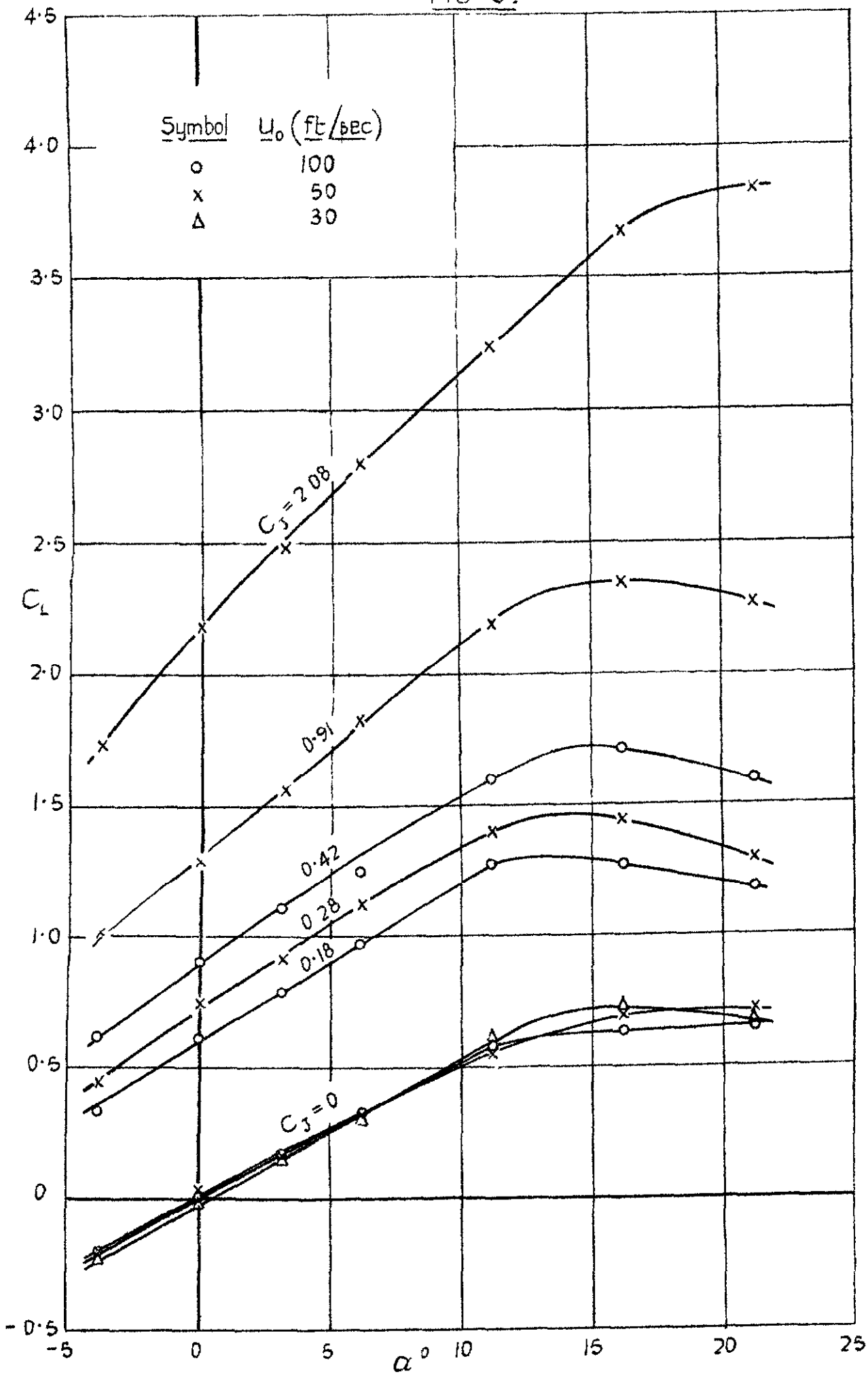

Variation of total lift with incidence at constant C_J

FIG. 6.

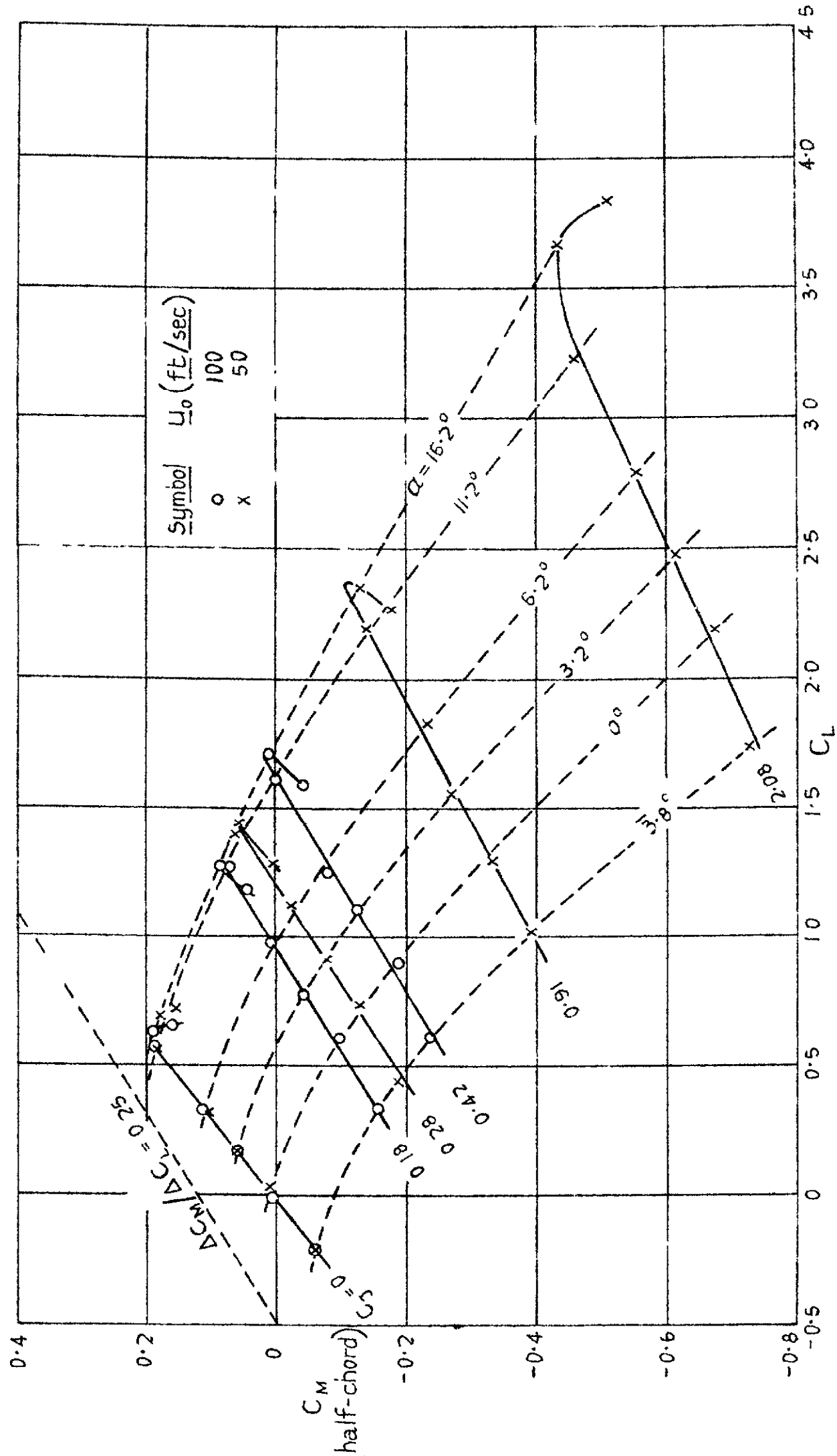

Variation of total pitching moment with total lift.

FIG. 7.

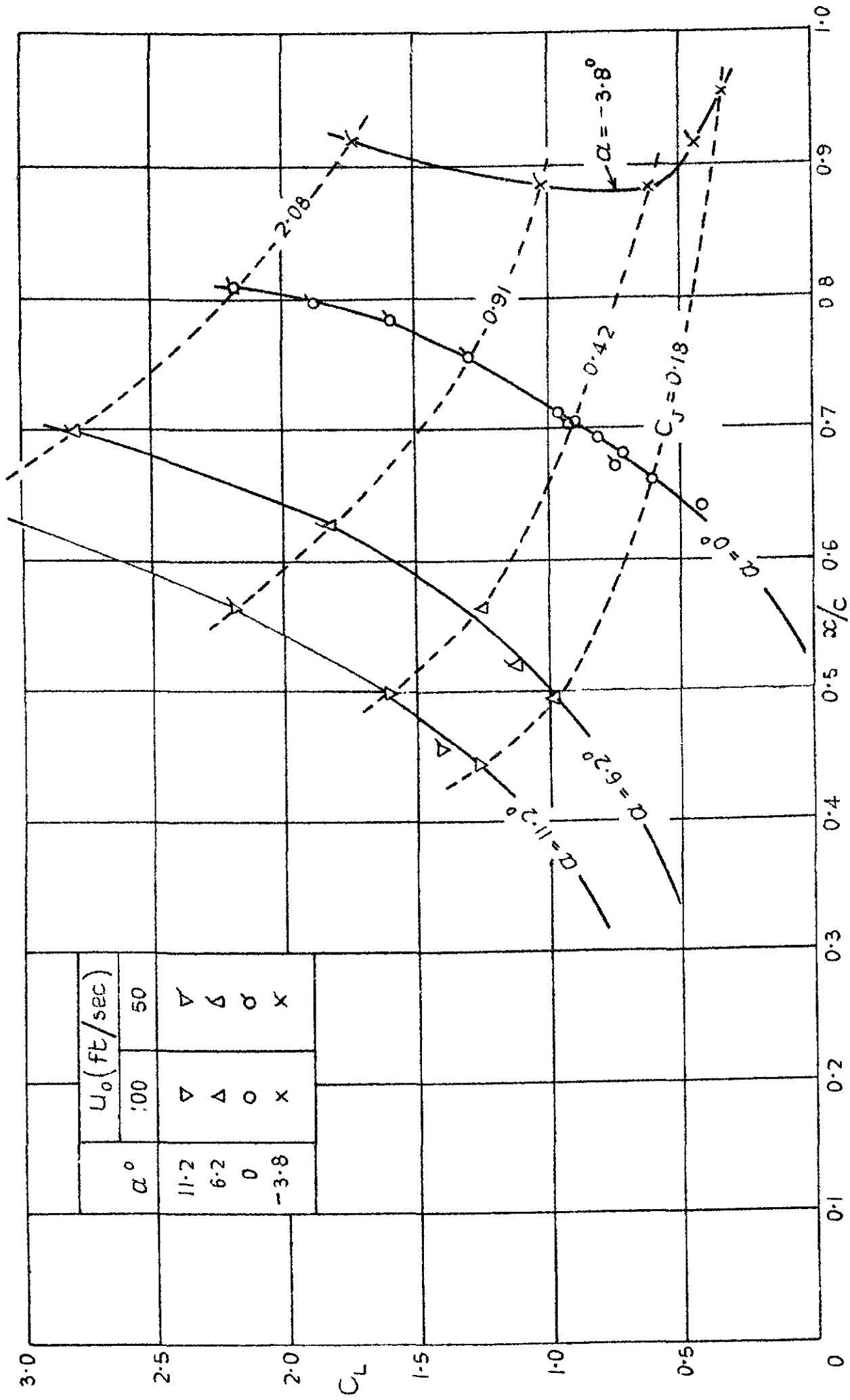

Variation in position of centre of total lift.

FIG. 8a.

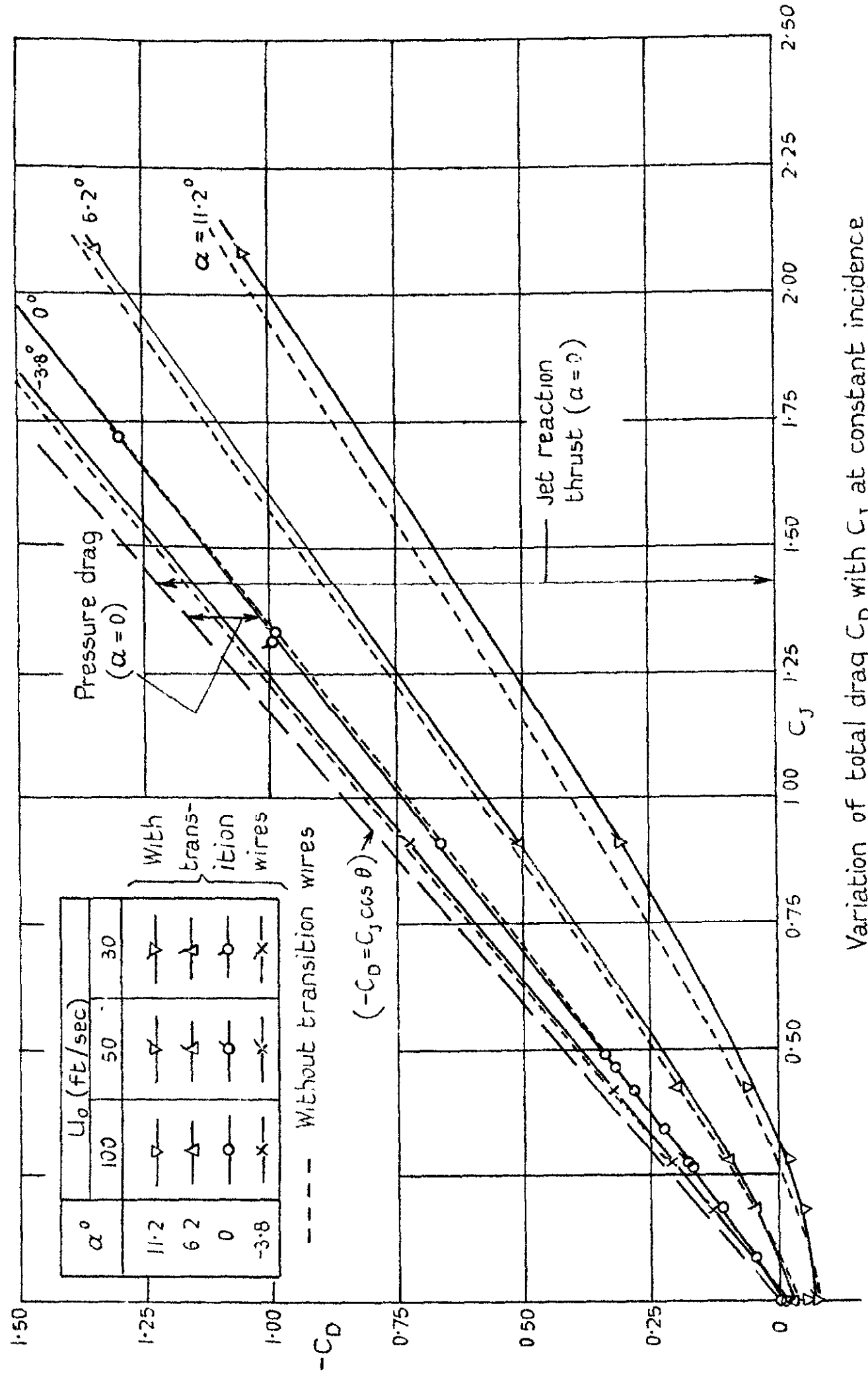

Variation of total drag C_D with C_J at constant incidence

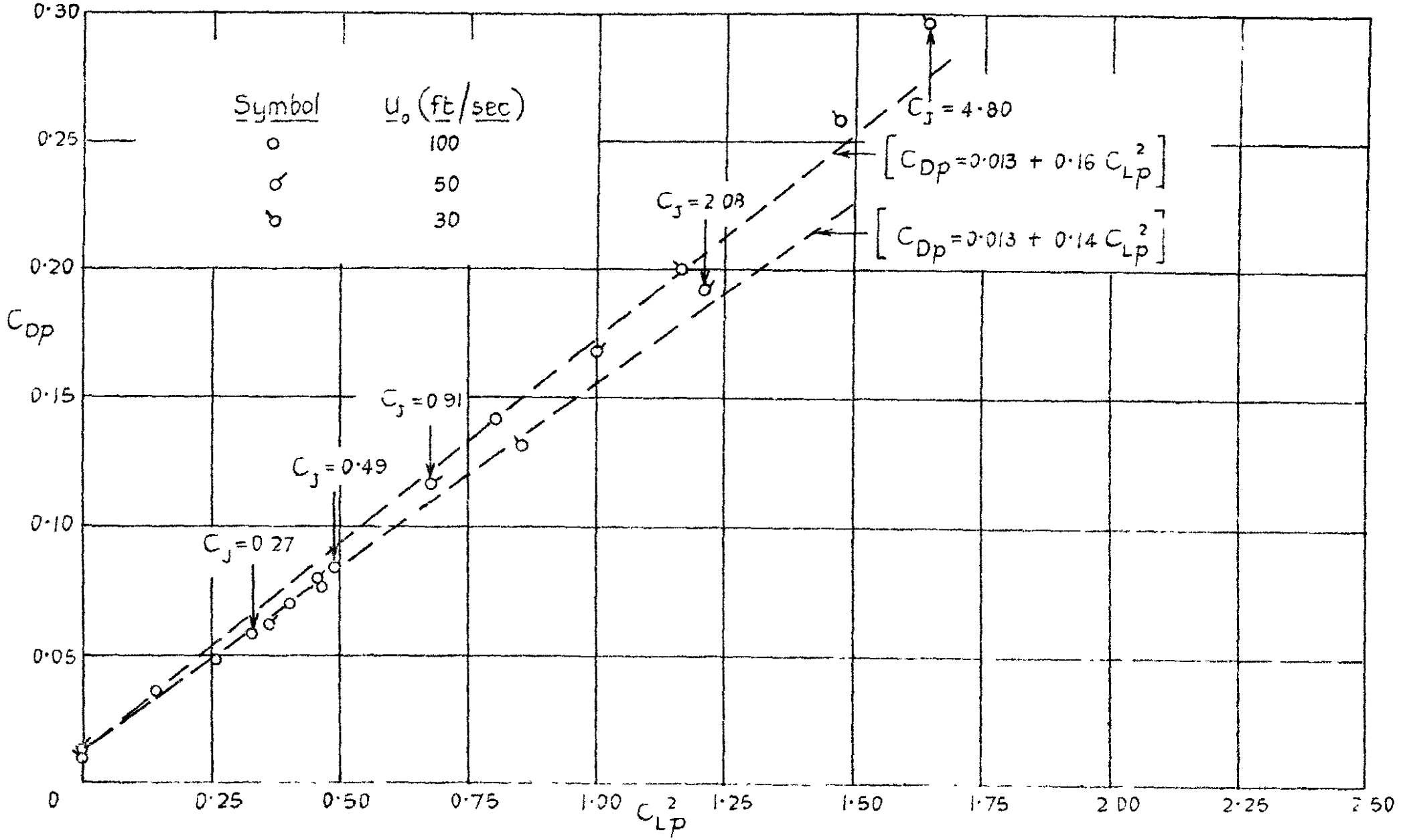

FIG. 8b.

Variation of pressure drag C_{Dp} with C_{Lp}^2 at zero incidence.

FIG. 8c.

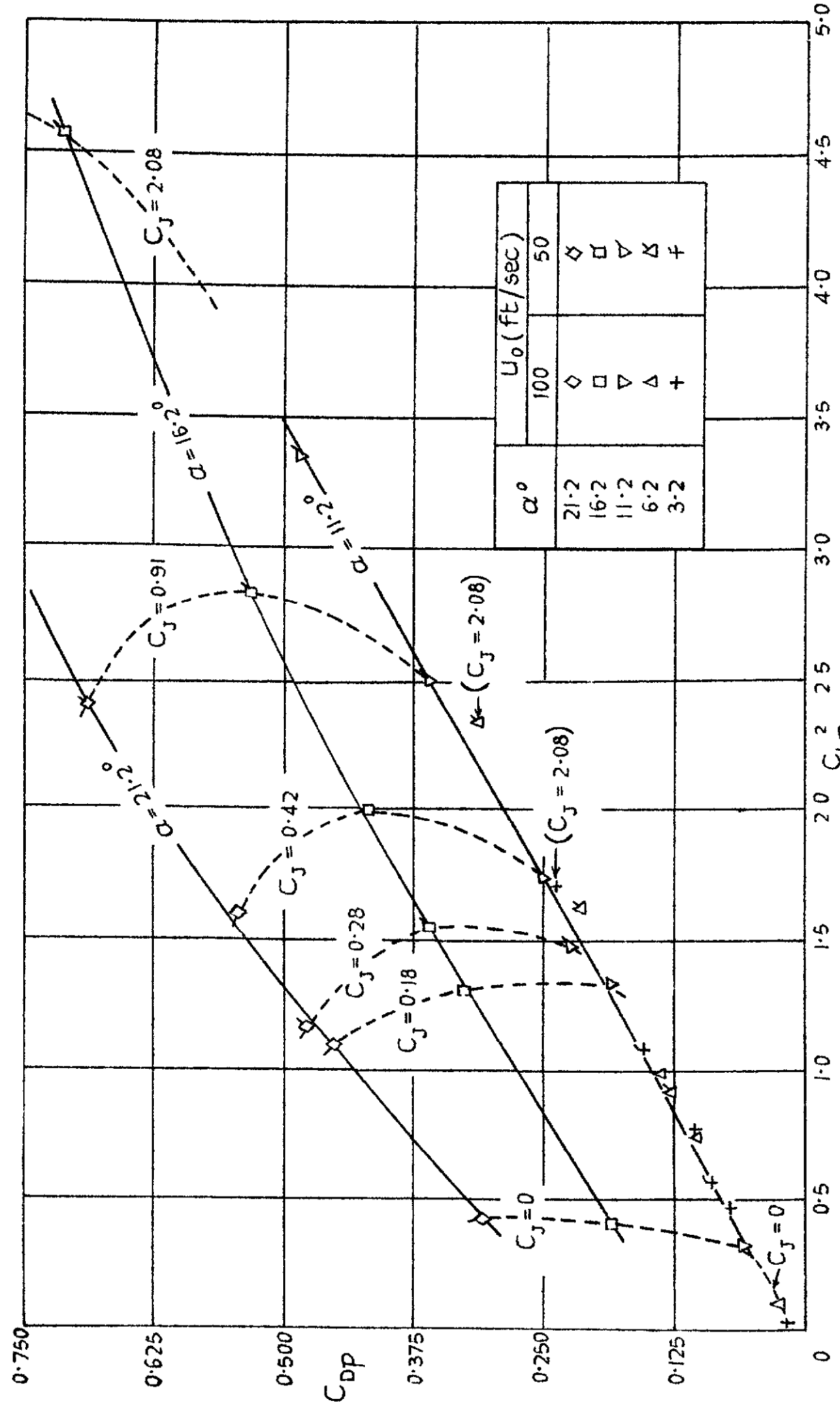

Variation of pressure drag C_{Dp} with C_{Lp}^2.

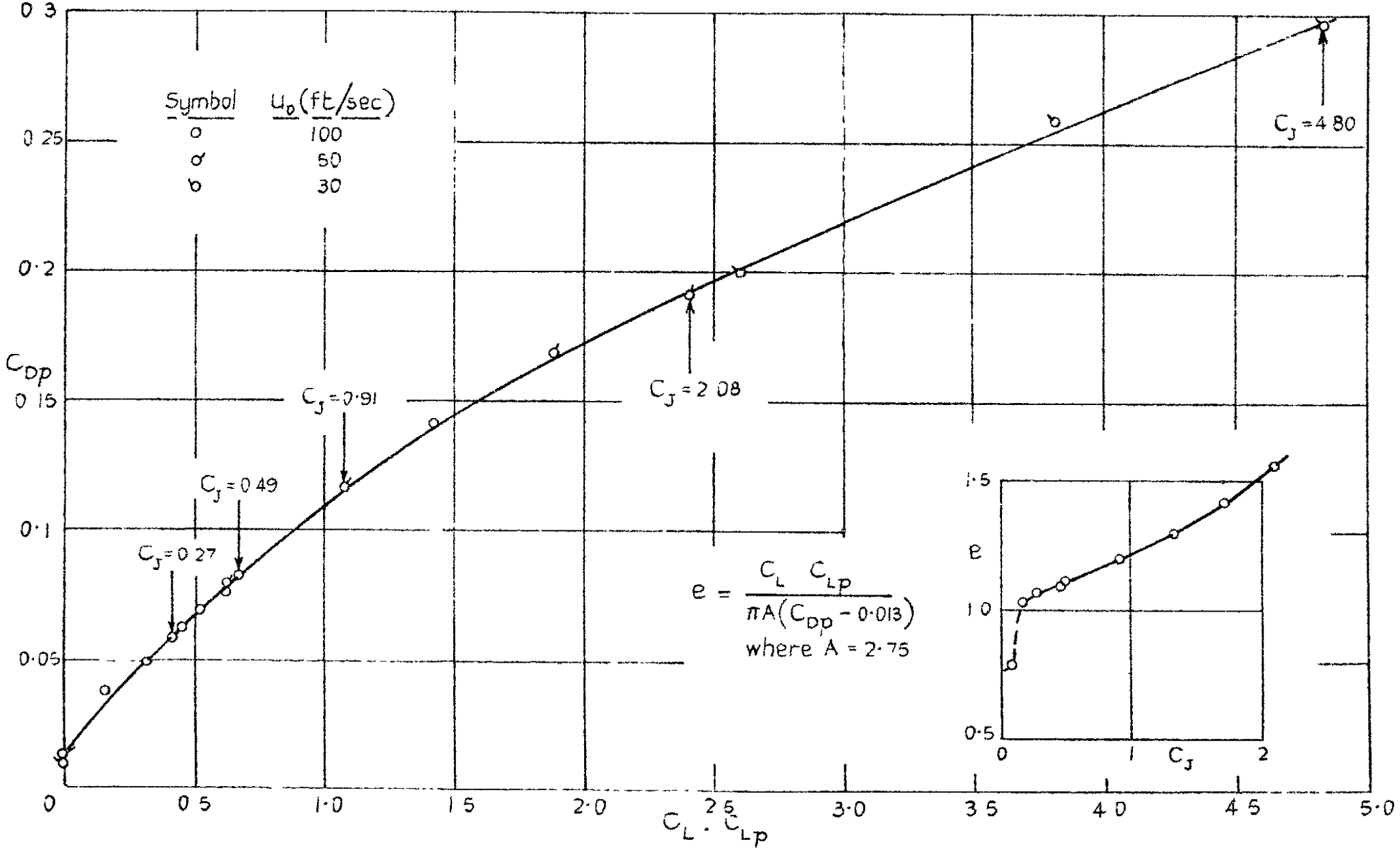

Fig 68

Variation of pressure drag C_{Dp} with $C_L \cdot C_{Lp}$ at zero incidence

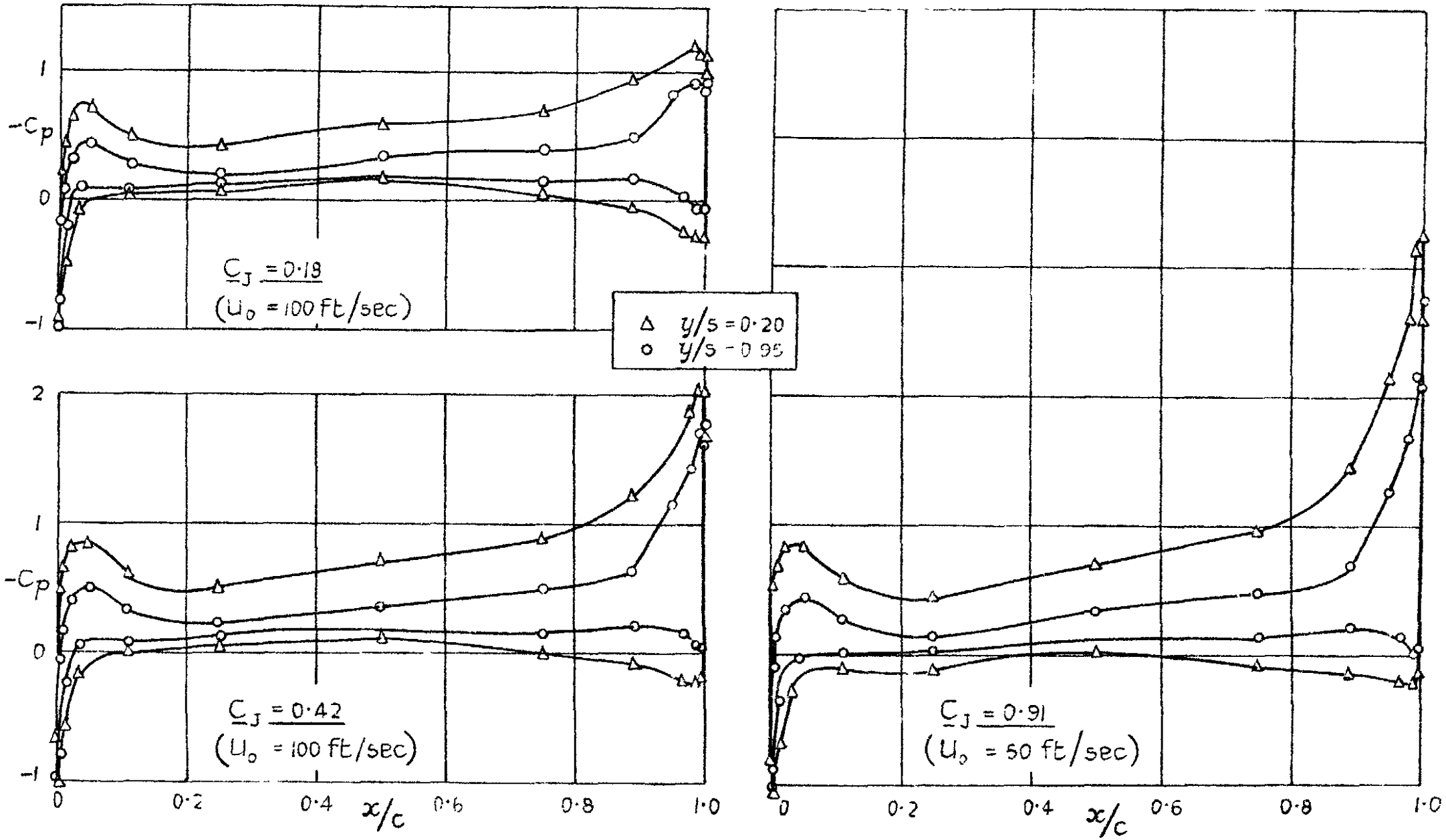

Fig 9.2

Chordwise pressure distributions at zero incidence Variation with C_J

Fig 9b

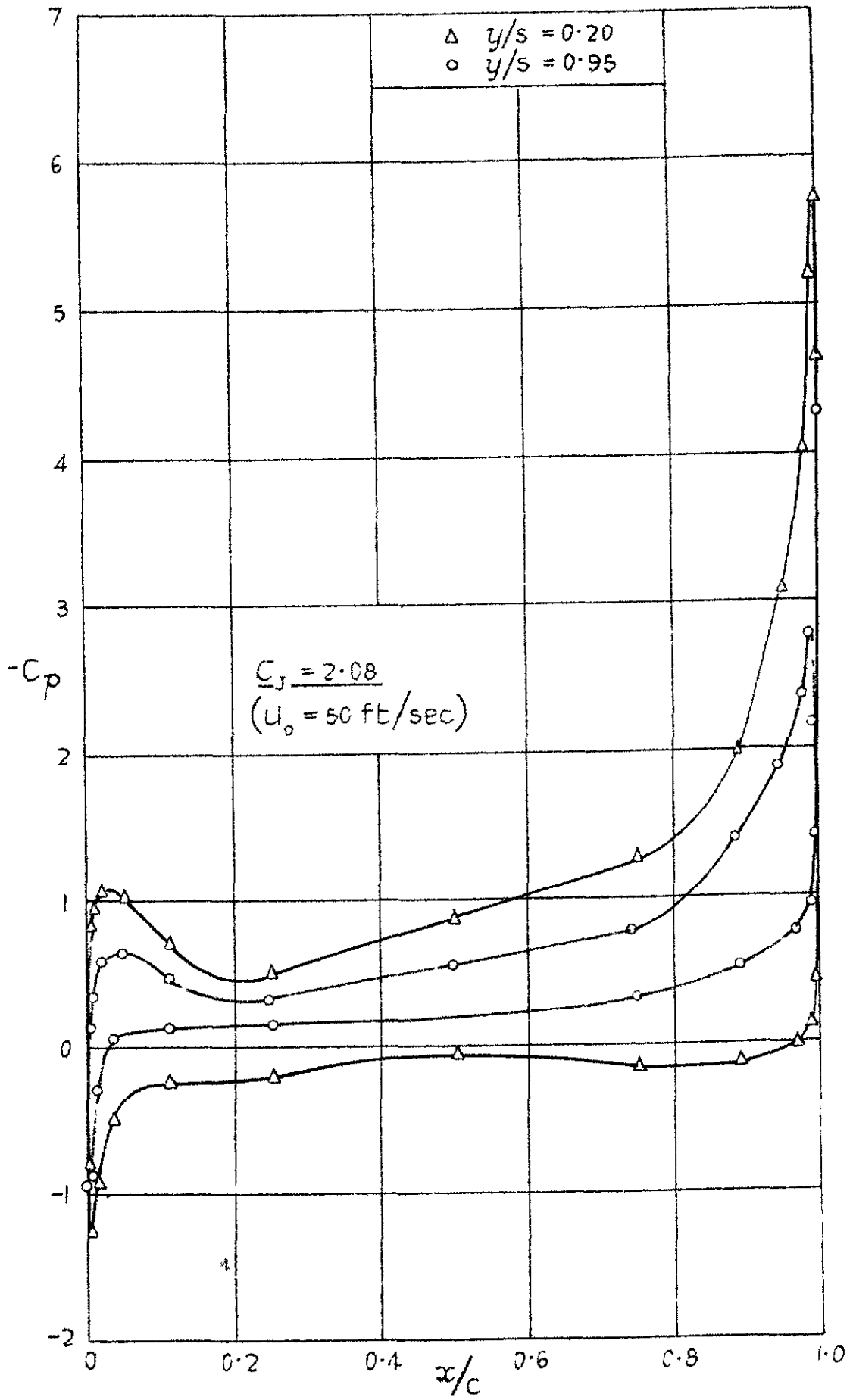

Chordwise pressure distributions at zero incidence
Variation with C_J.

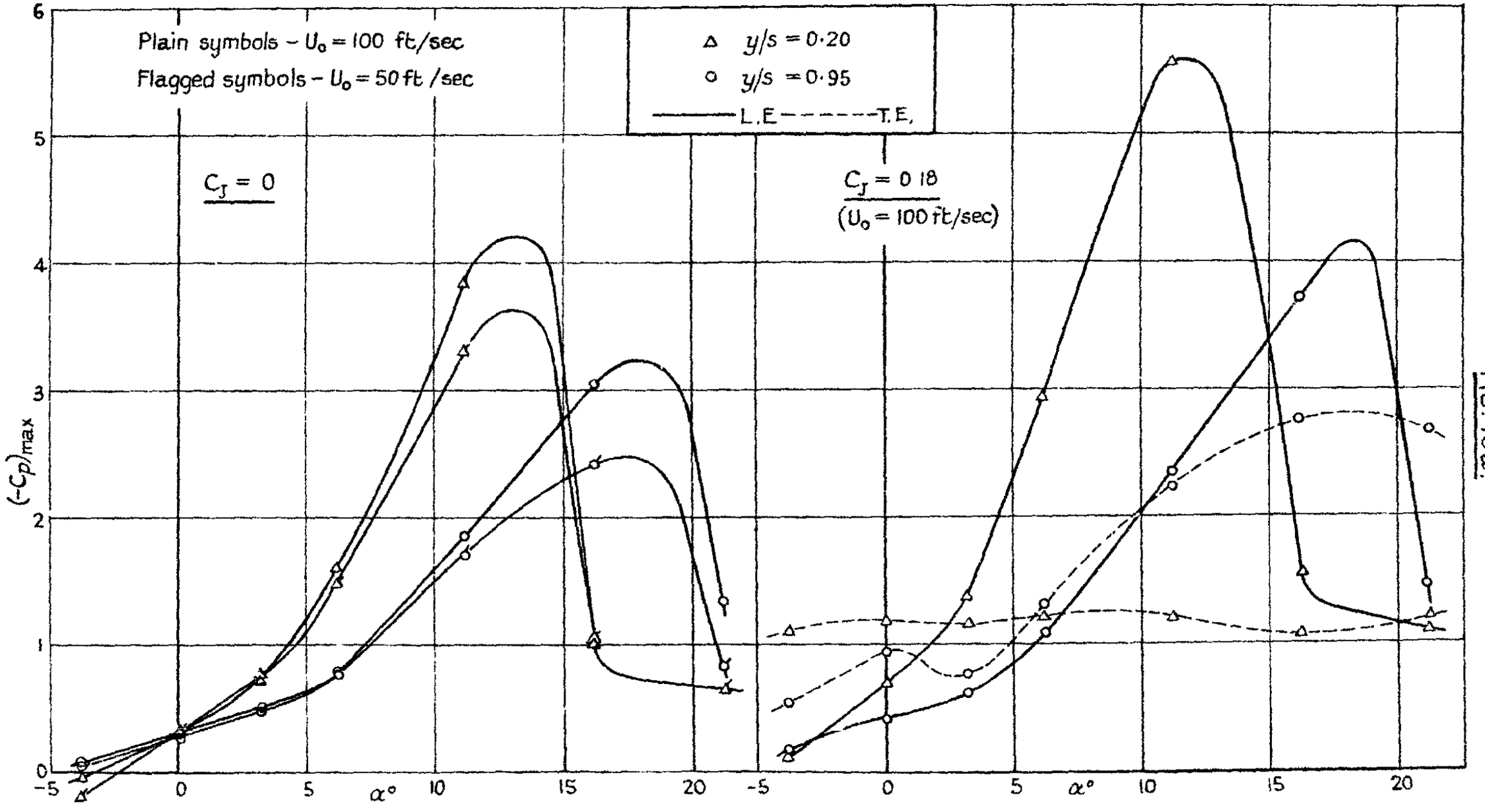

Variation of peak suctions near L E and T.E.

FIG. 10a.

FIG. 10 c

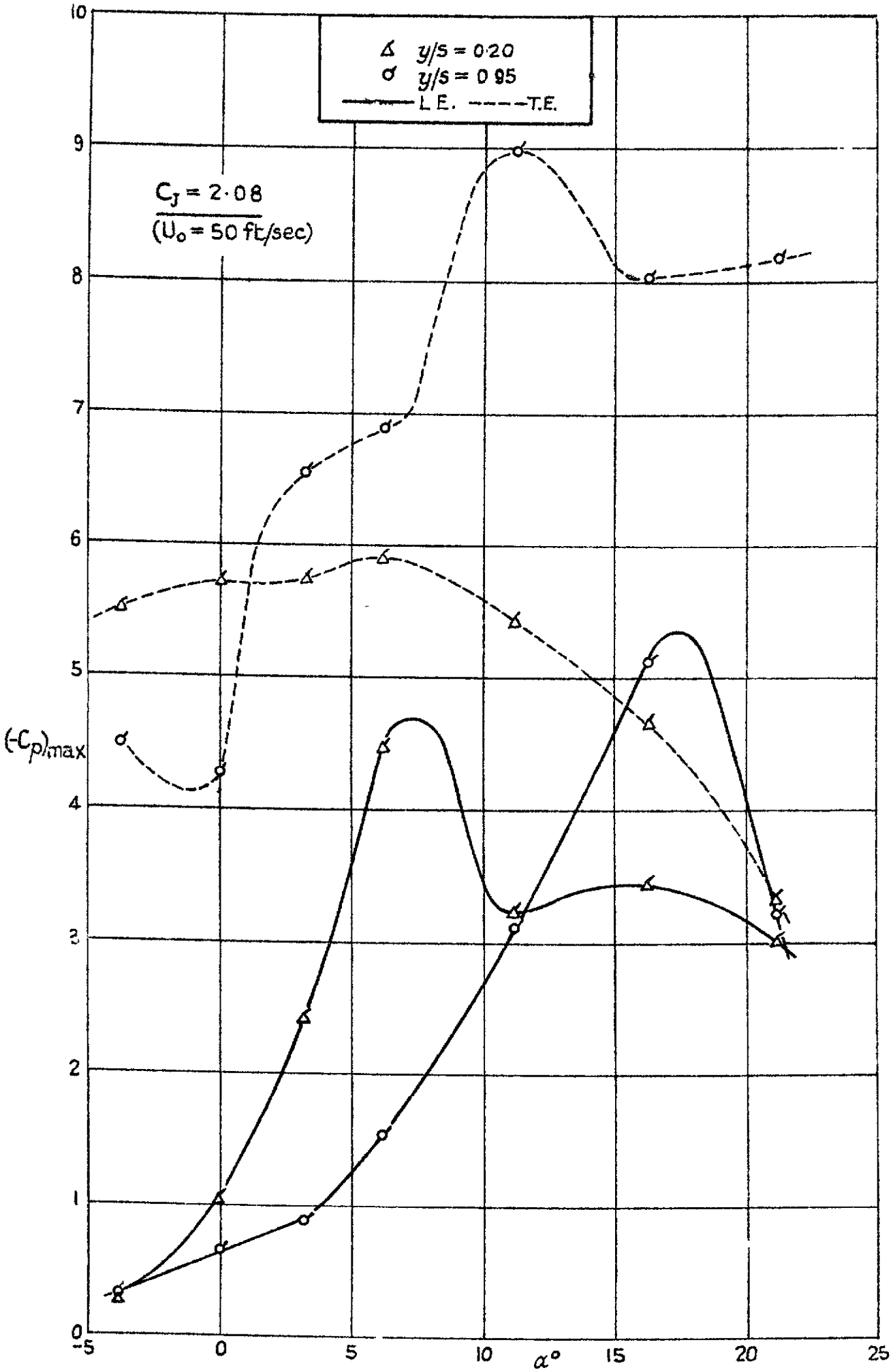

Variation of peak suctions near L.E and T.E

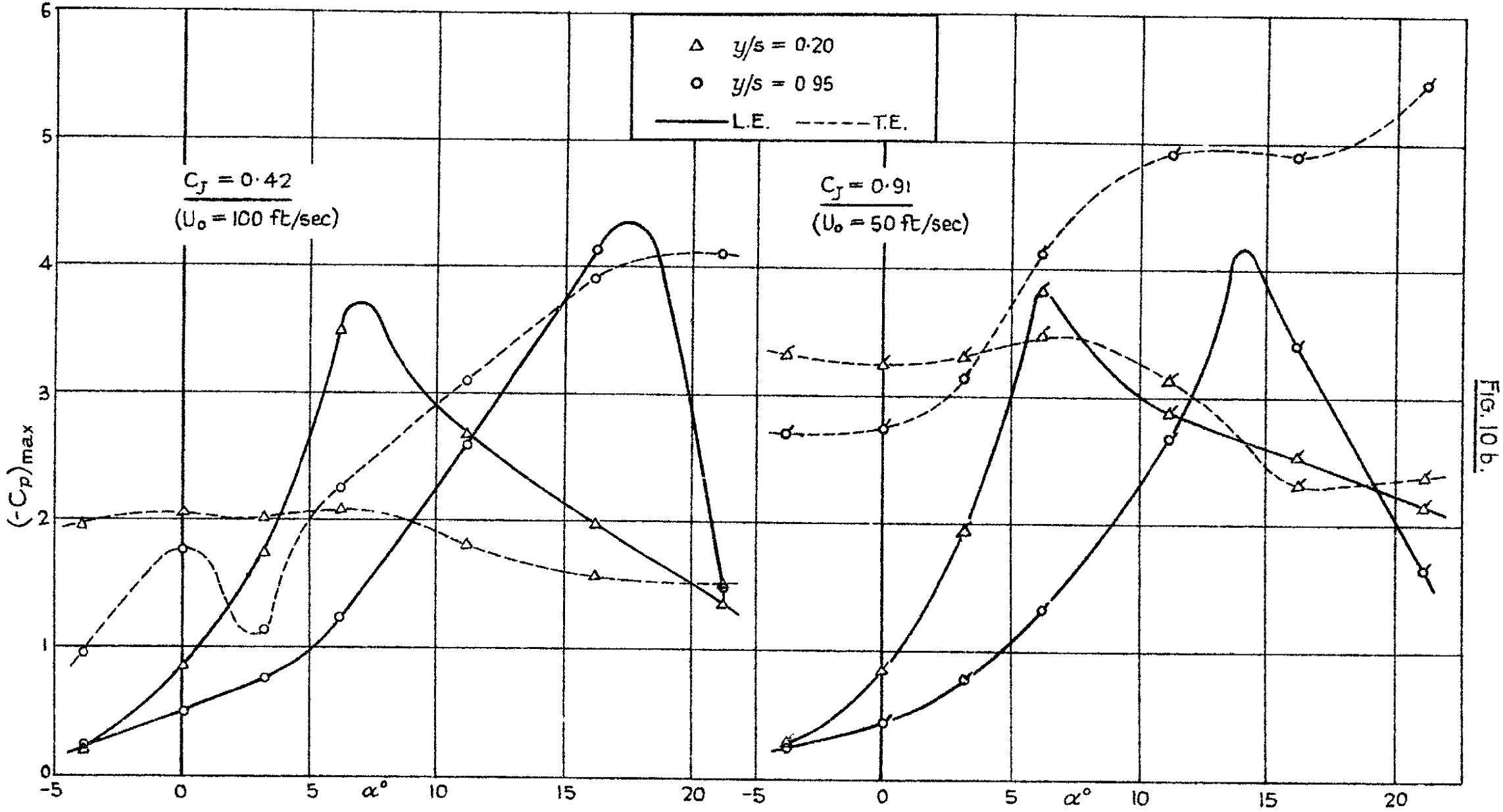

Fig. 10 b.

Variation of peak suctions near L.E. and T.E

FIG. 10 c

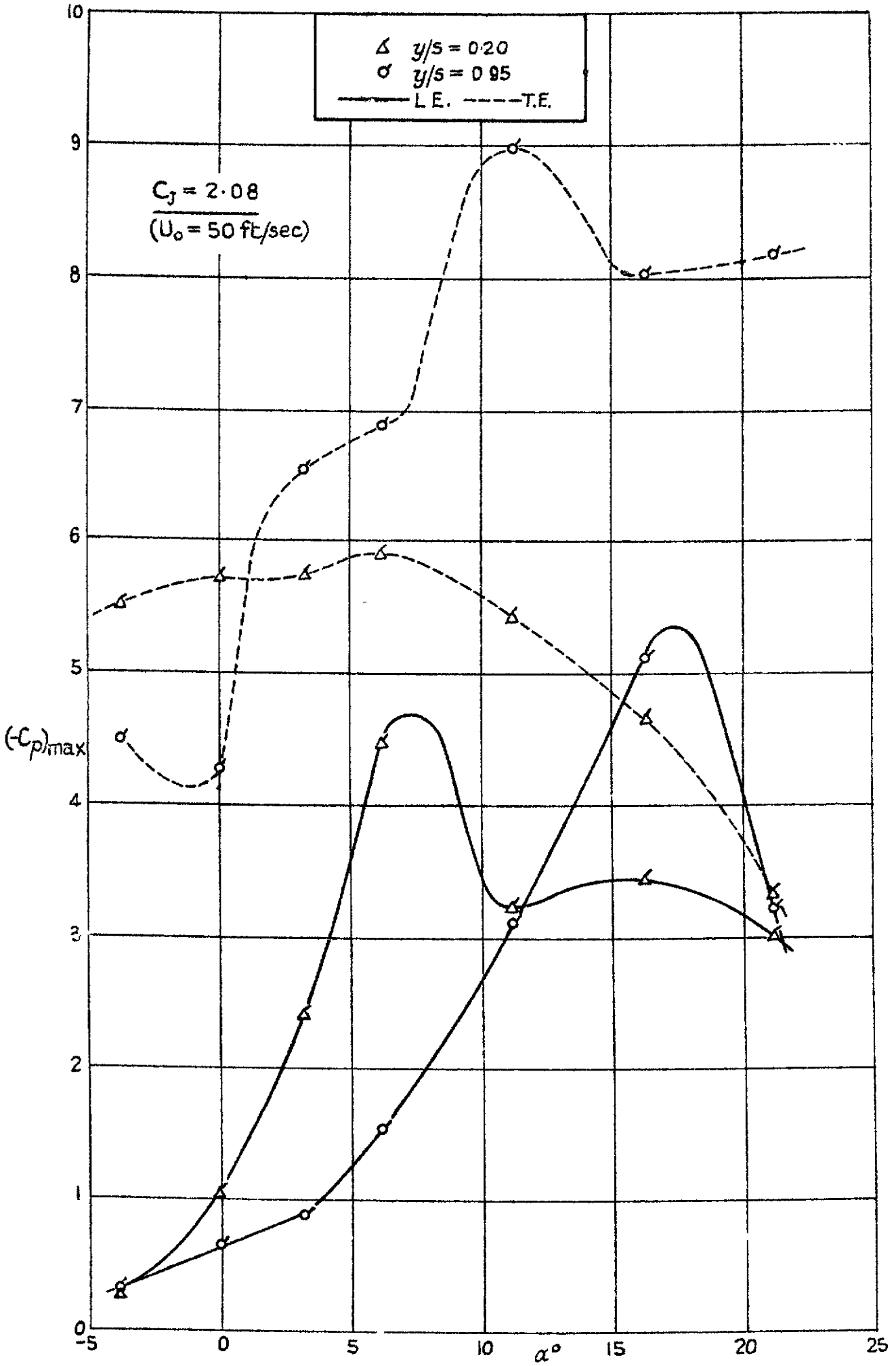

Variation of peak suctions near L.E. and T.E

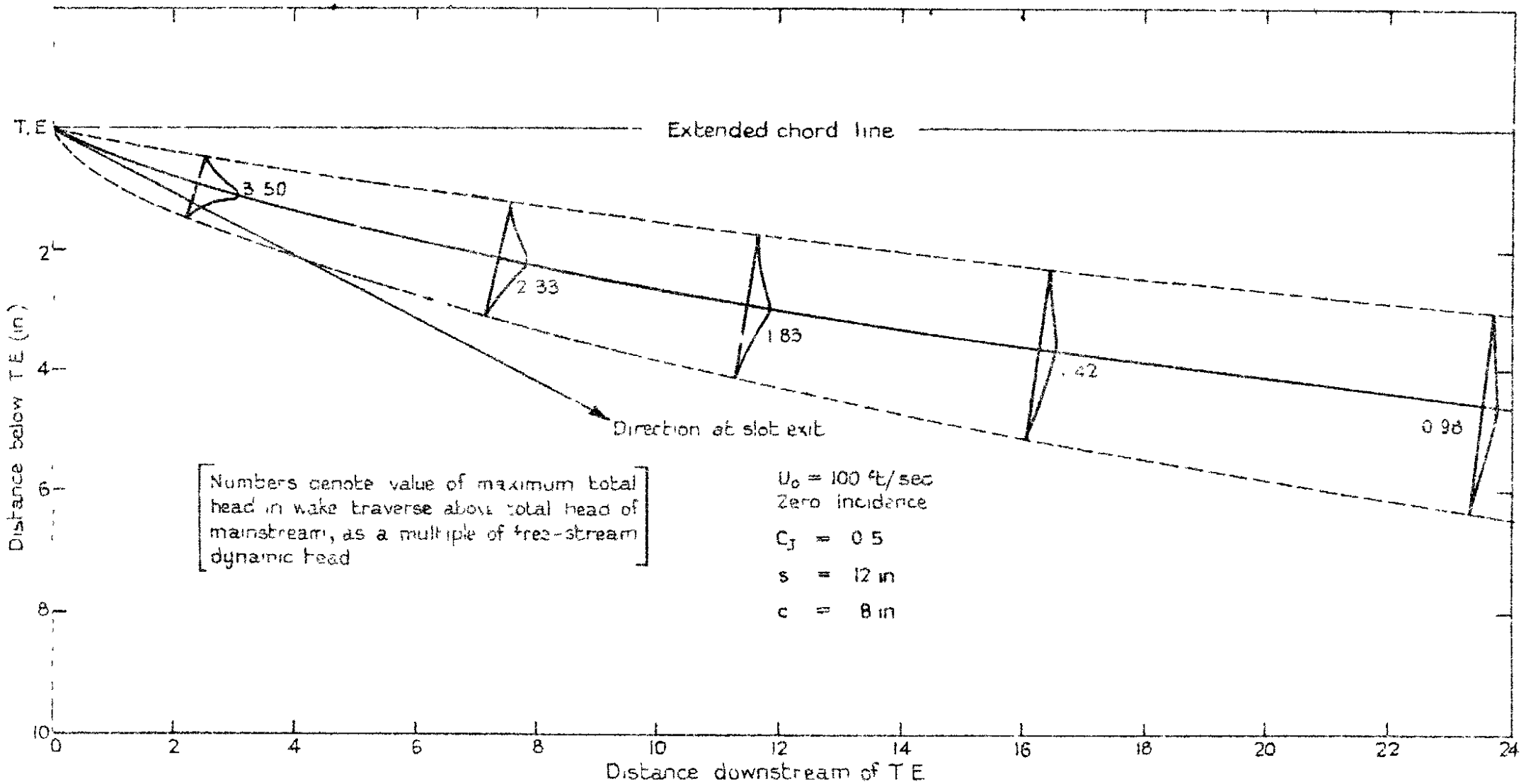

Fig 11a

Mean line and total head profiles of jet at mid-span position

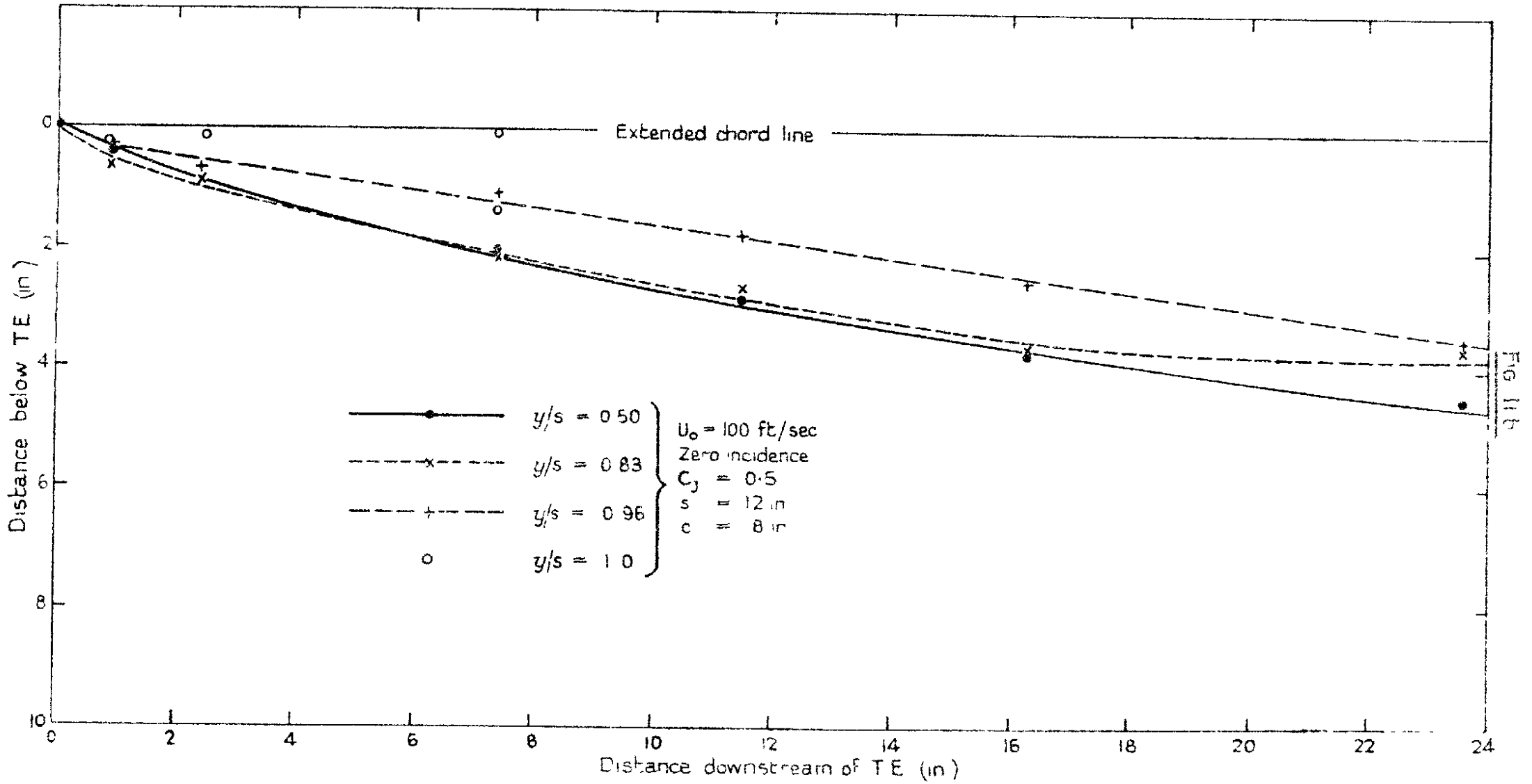

Fig 11b

Spanwise variation of mean line of jet

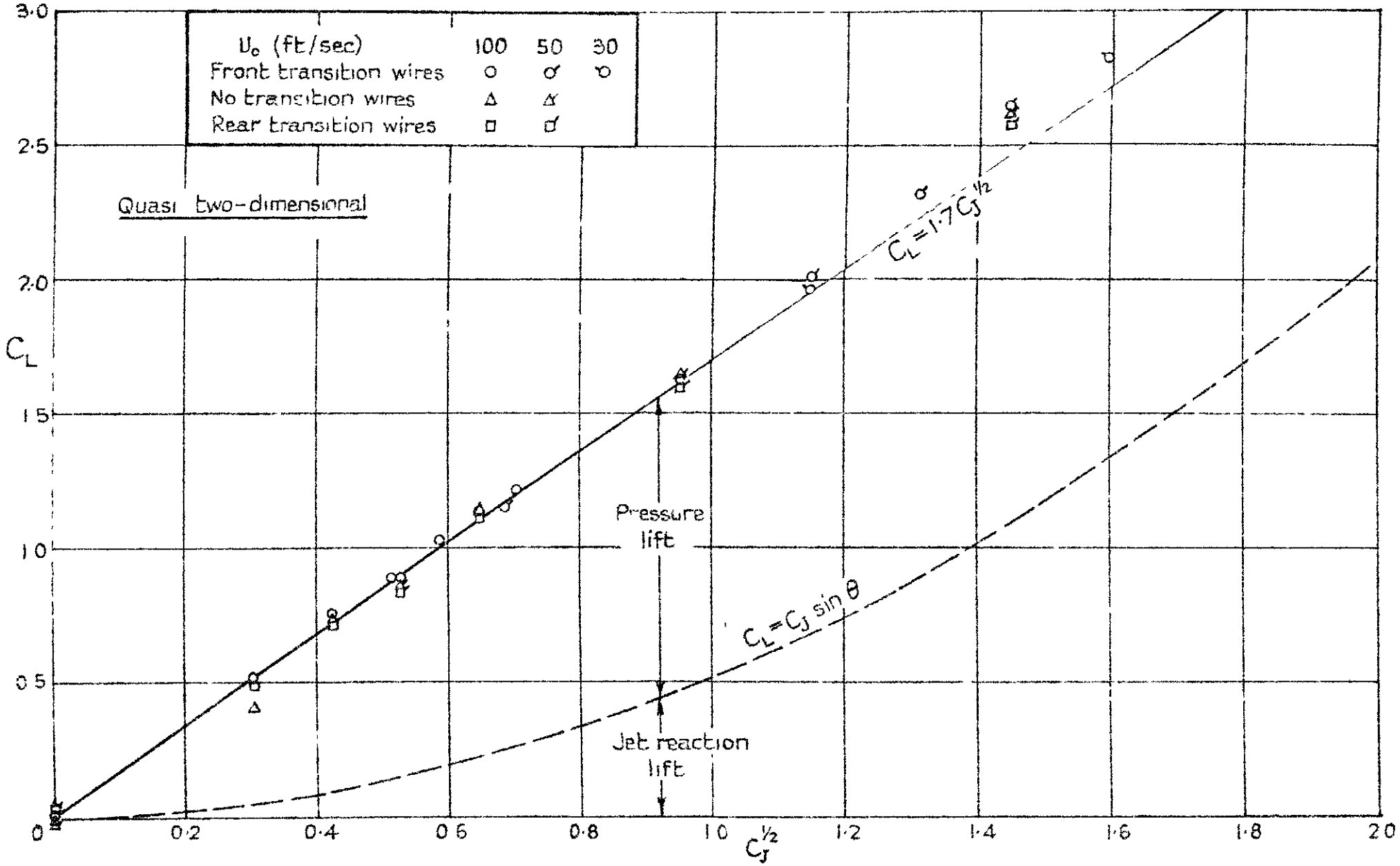

Variation of total lift C_L with $C_J^{1/2}$ at zero incidence

FIG. 12a

Quasi two-dimensional

$\alpha°$	U_0 ft/sec	
	100	50
11 5	▽	▽
6 5	△	△
0	○	○
−3 5	×	×

$\alpha = 11\,5°$

6 5°

0°

−3 5°

C_L

45 40 35 30 25 20 15 10 05 0 −0 5

0 0·2 0·4 0·6 0·8 1·0 1·2 1·4 1·6 1·8 2·0

$C_J^{1/2}$

Variation of total lift C_L with $C_J^{1/2}$ at constant incidence

Fig 13.

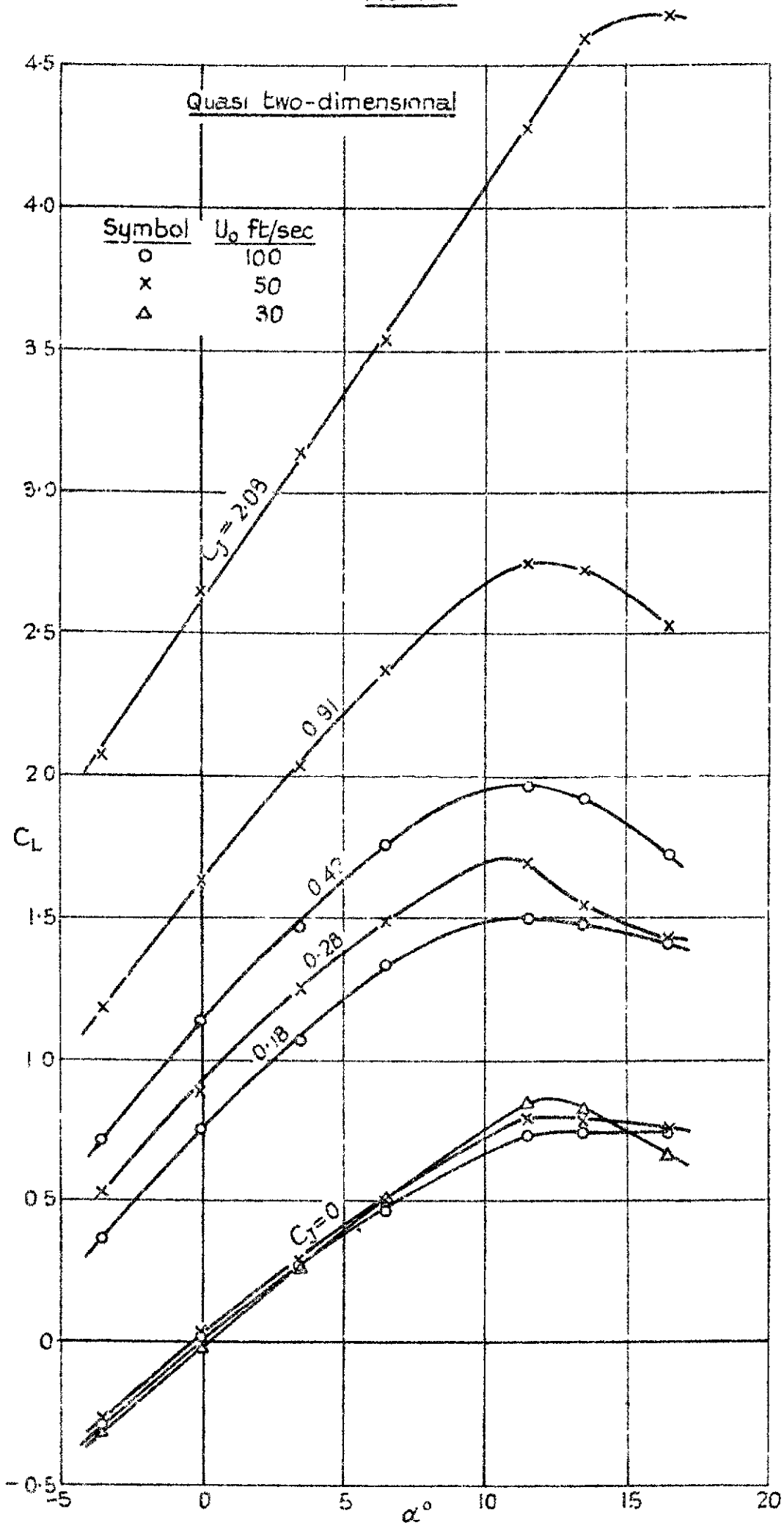

Variation of total lift with incidence at constant C_J

(Ref. 4A/6/18)

FIG. 14.

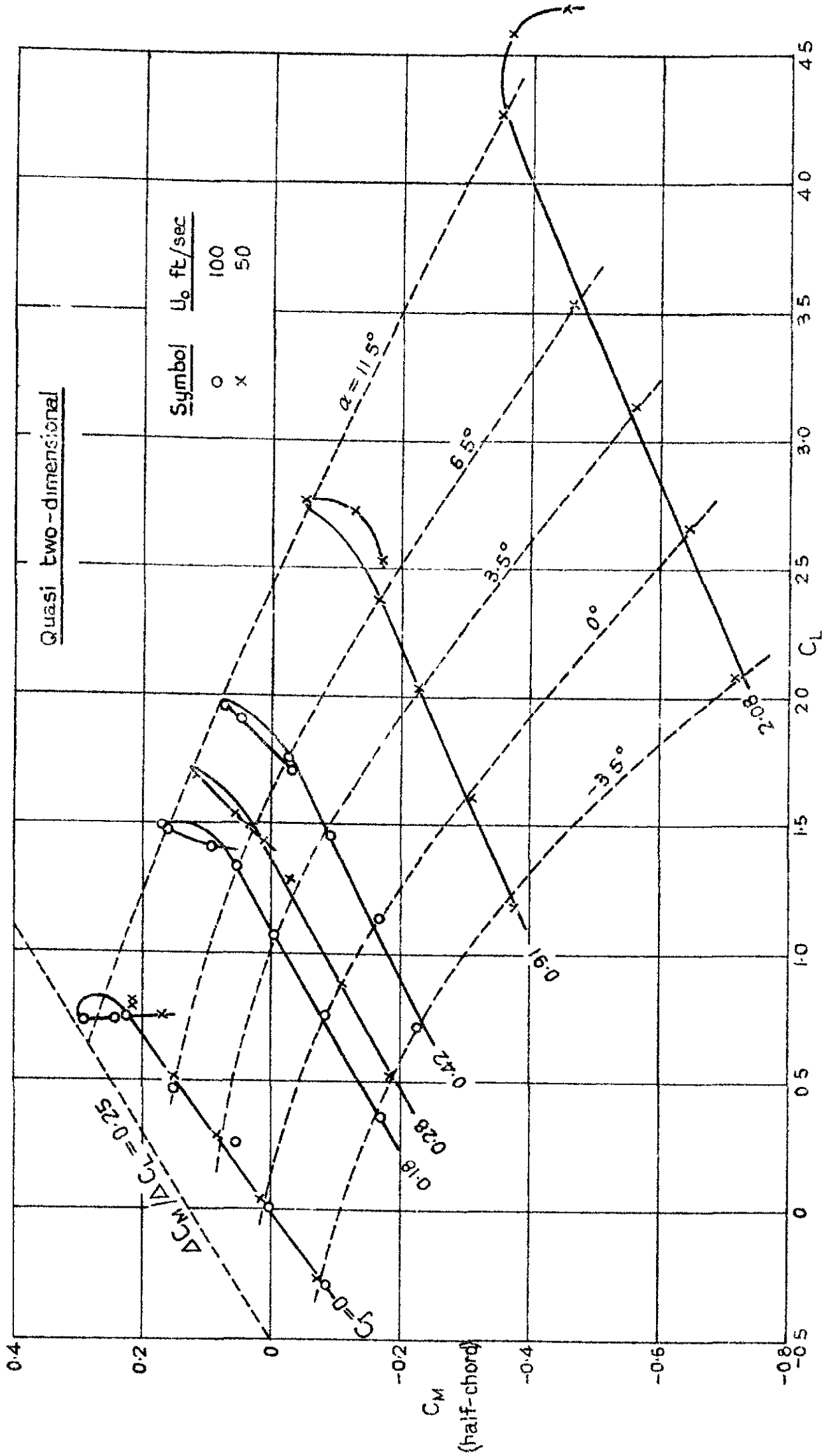

Variation of total pitching moment with total lift

FIG 15

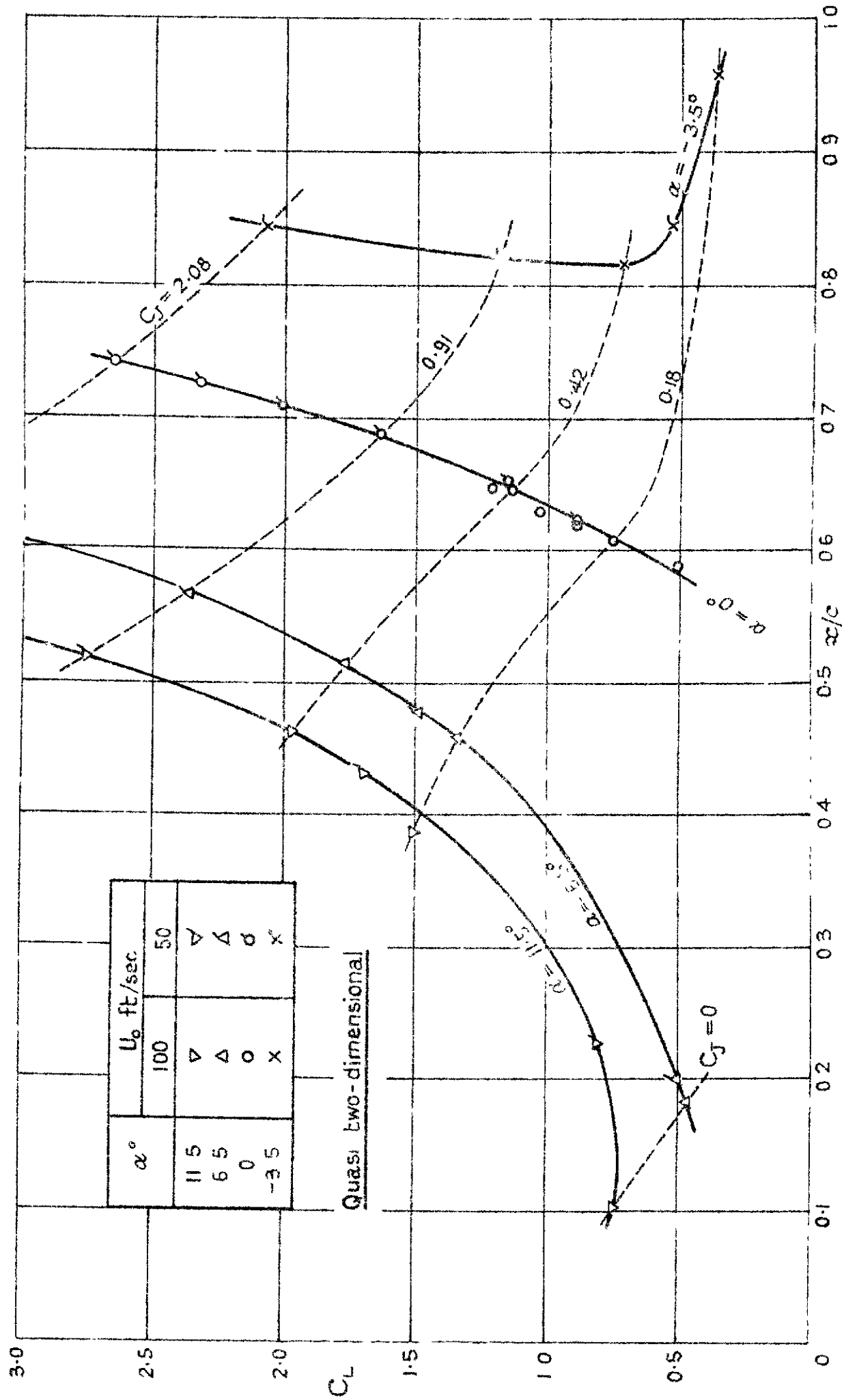

Variation in position of centre of total lift.

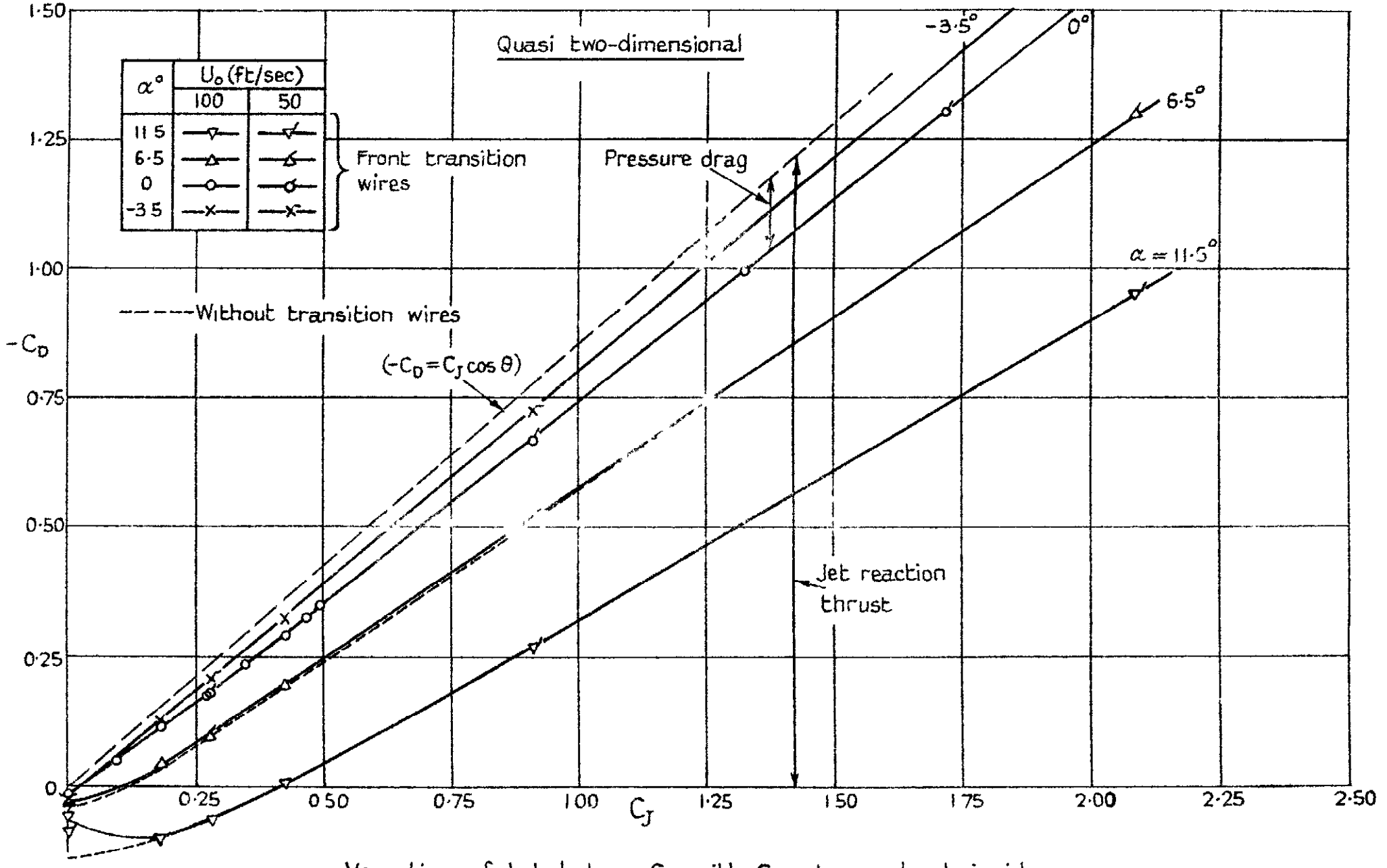

Variation of total drag C_D with C_J at constant incidence

Fig. 15 a.

Fig. 16 b

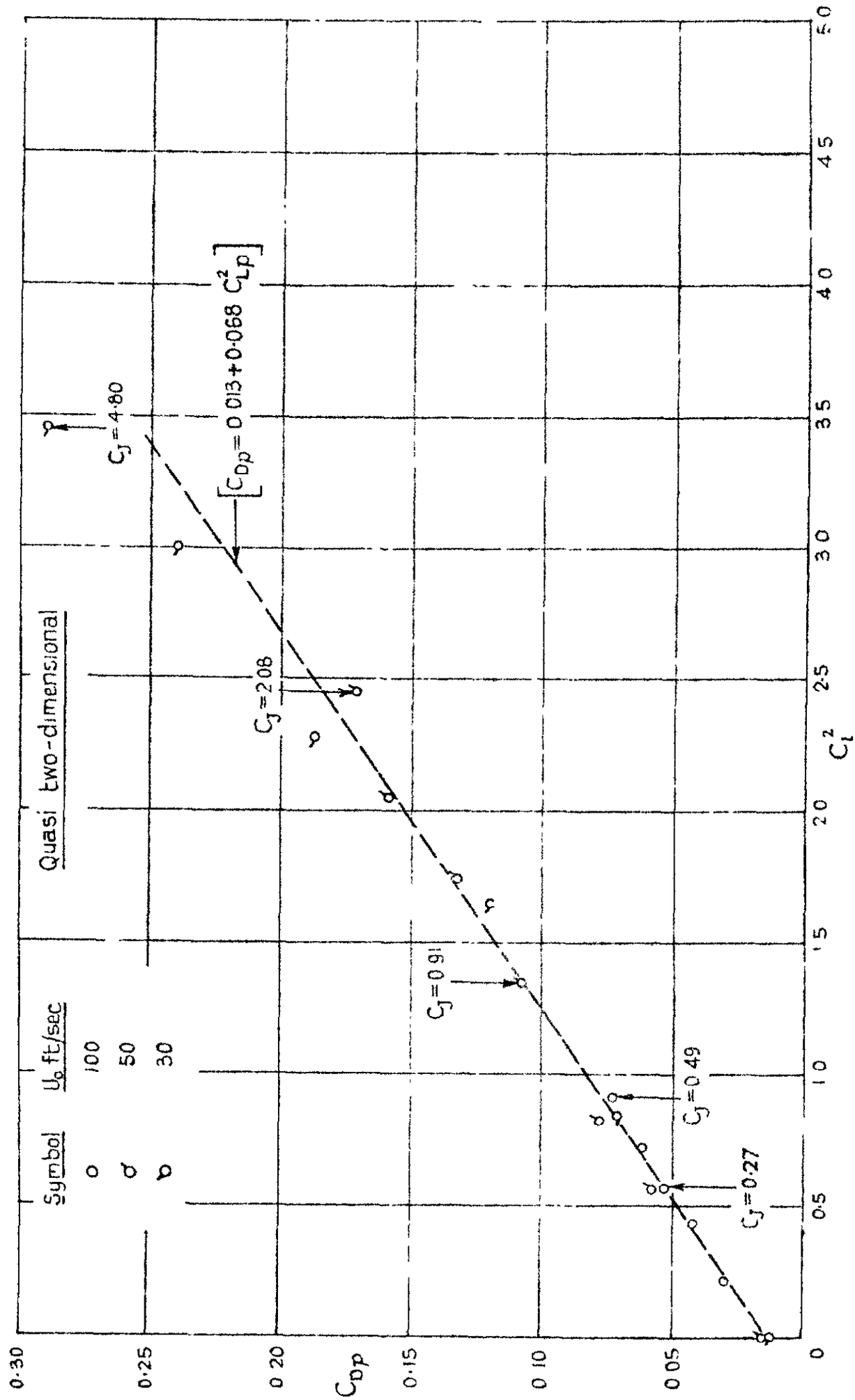

Variation of pressure drag C_D with C_l^2 at zero incidence.

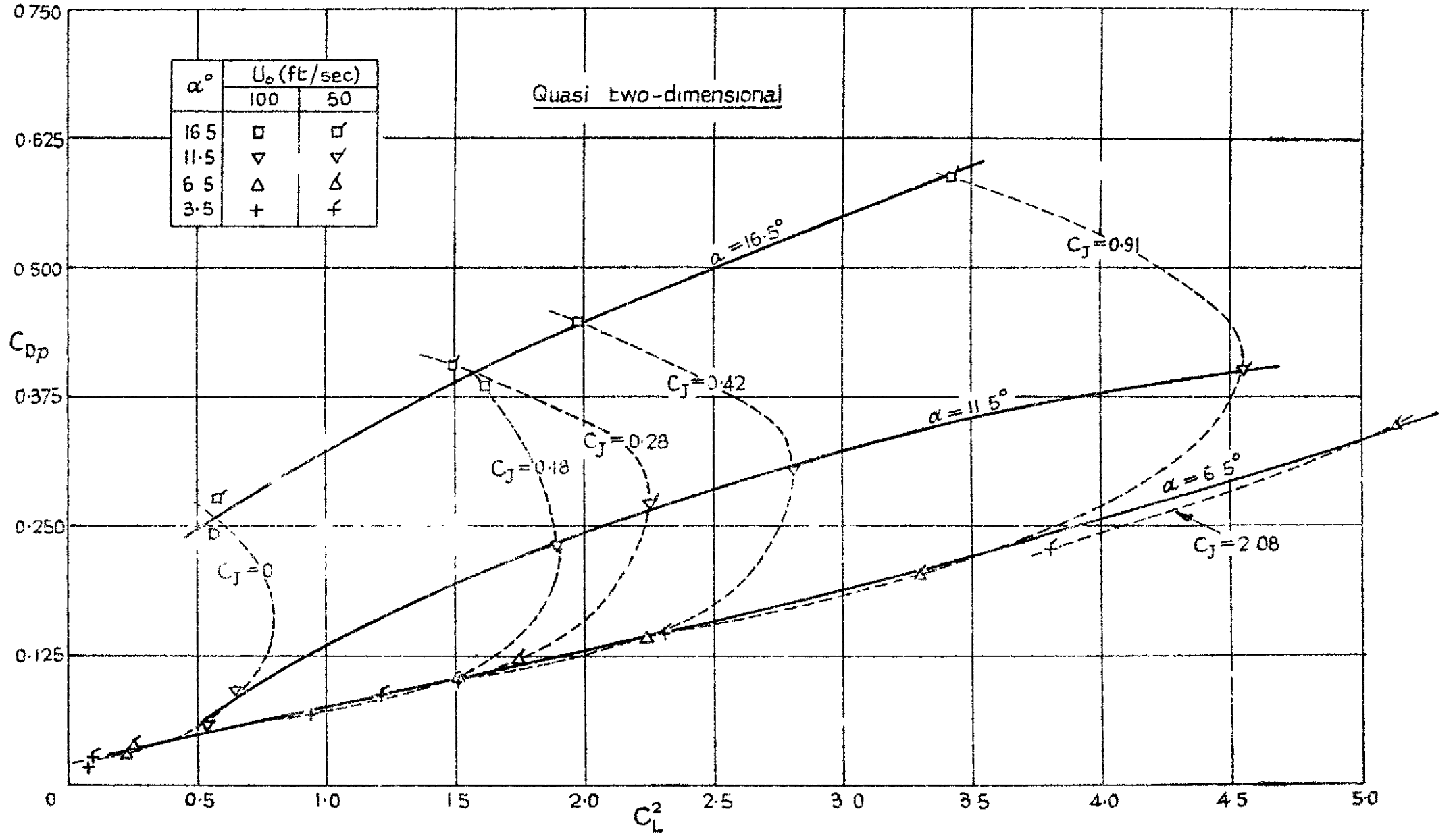

Fig. 16c

Variation of pressure drag C_{Dp} with C_{Lp}^2

FIG. 16 d

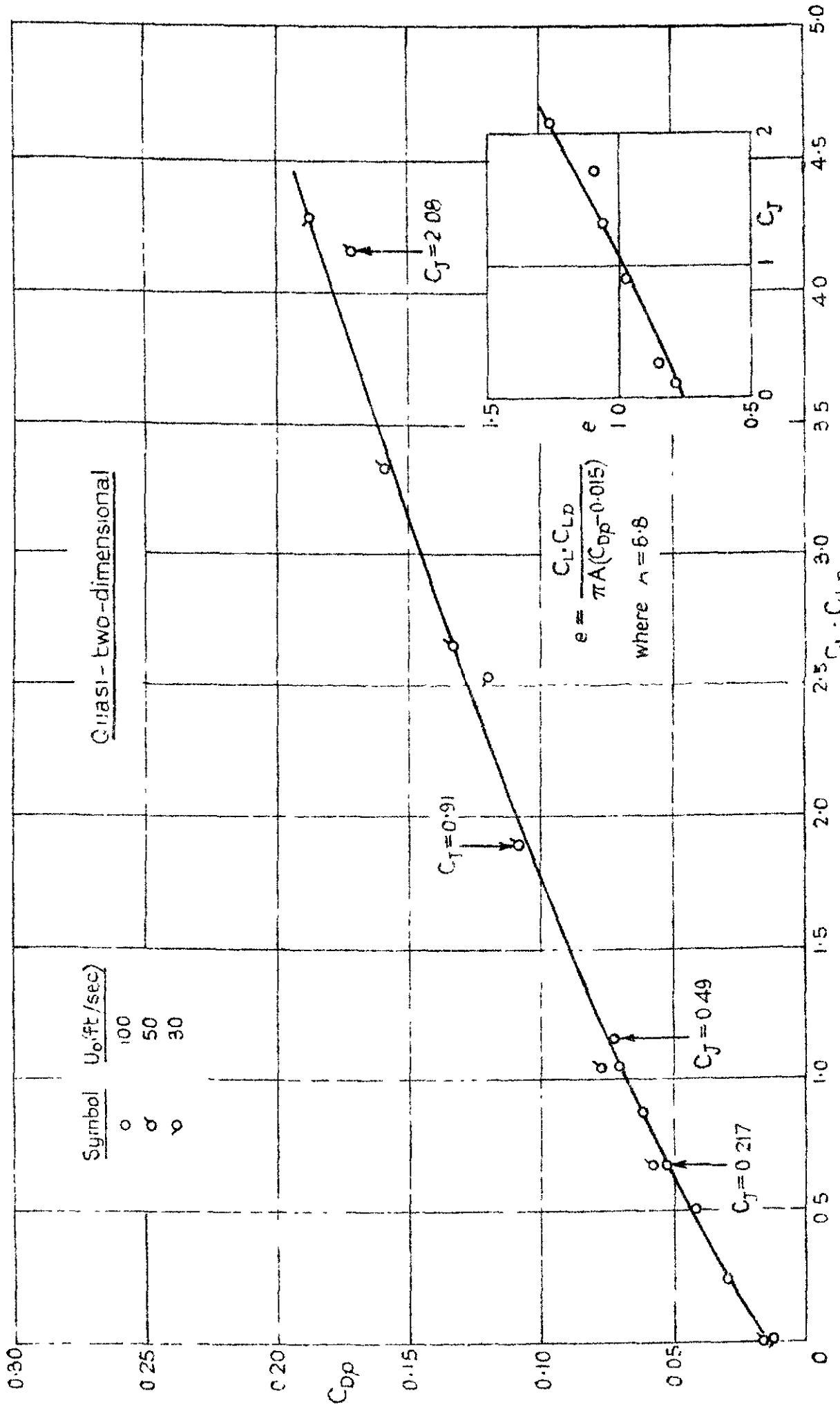

Variation of pressure drag C_{Dp} with $C_L \cdot C_{Lp}$ at zero incidence

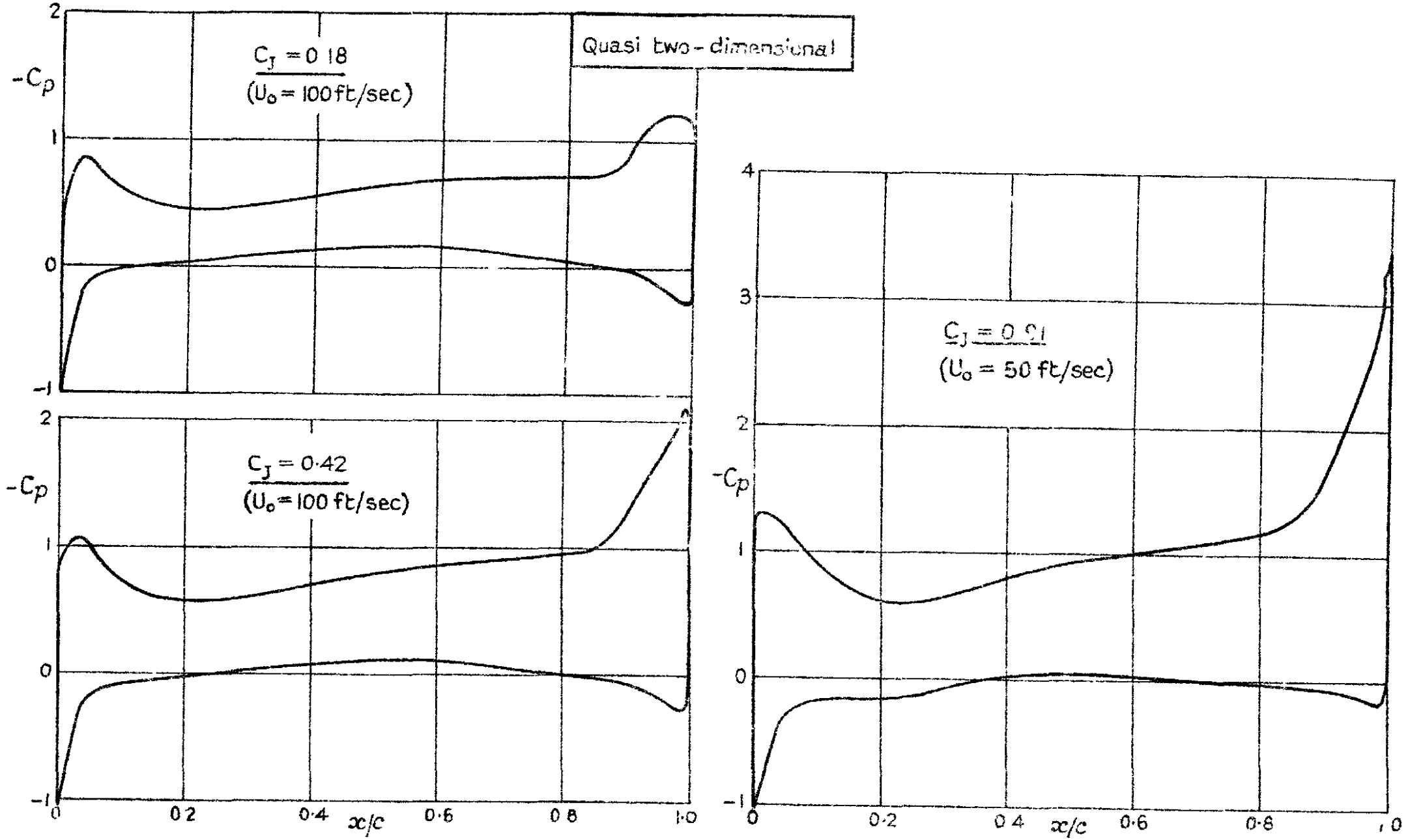

Fig. 17 a.

Chordwise pressure distributions at zero incidence – Variation with C_J.

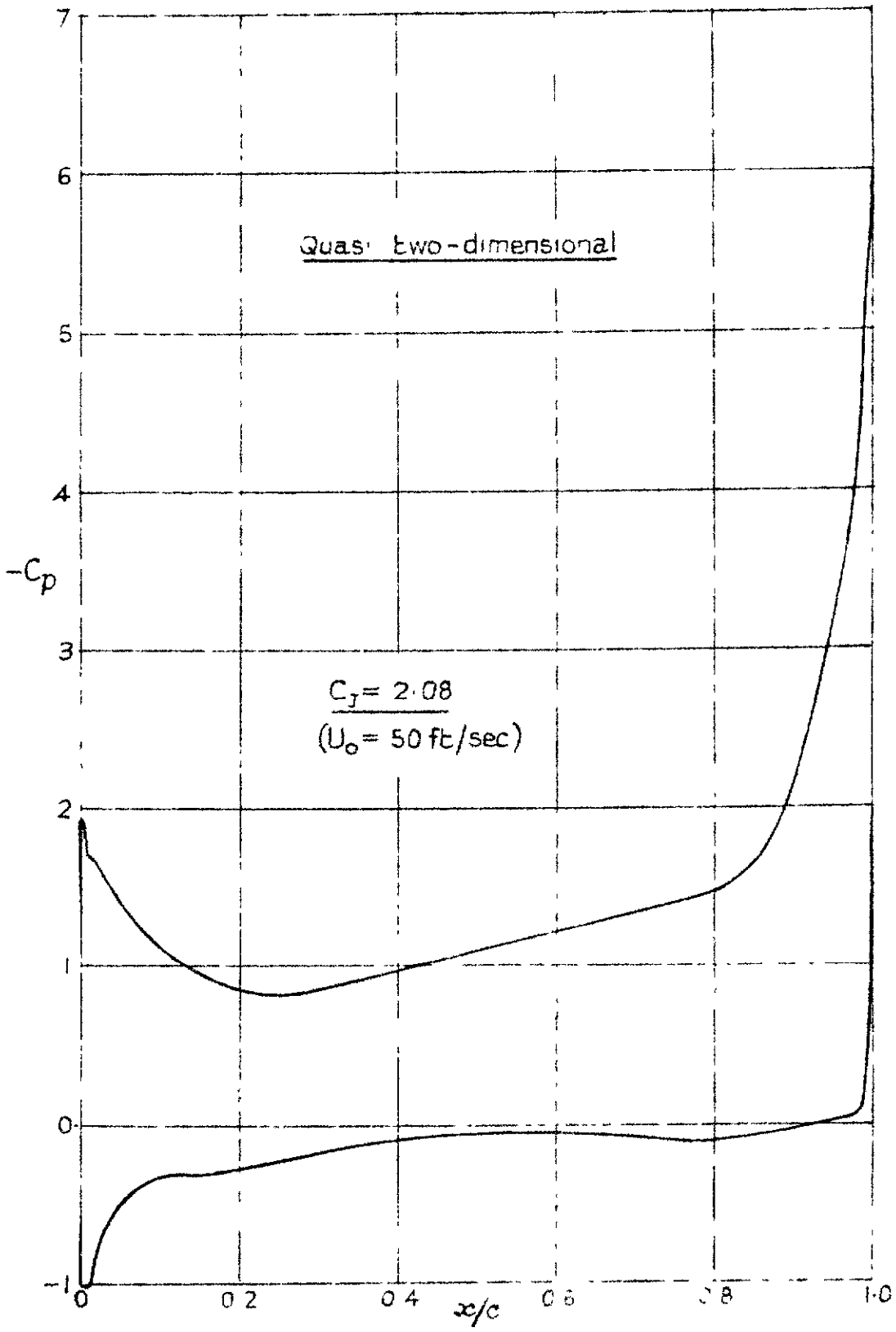

Chordwise pressure distribution at zero incidence – Variation with C_J

FIG. 18 a.

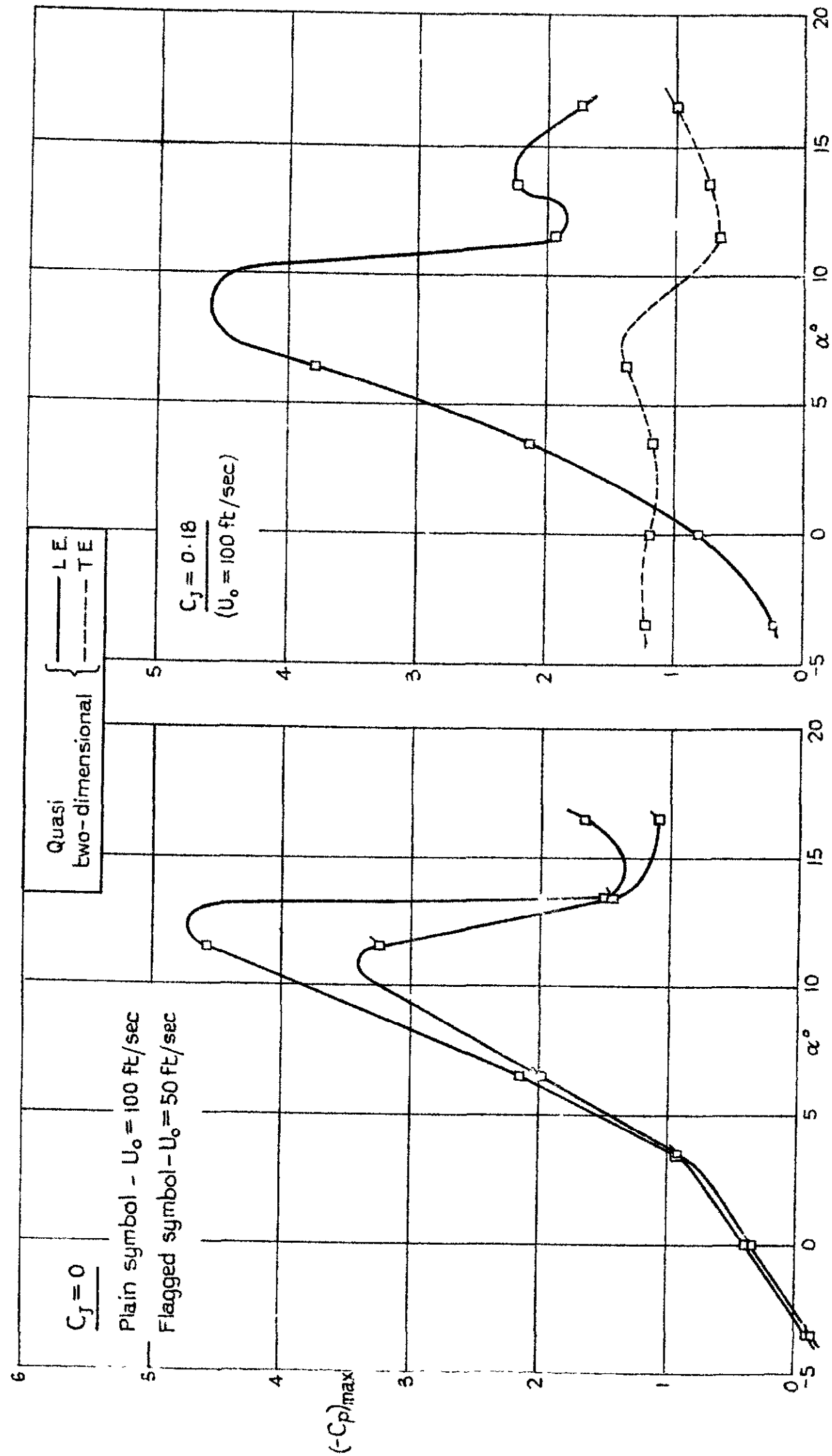

Variation of peak suctions near L.E and T.E.

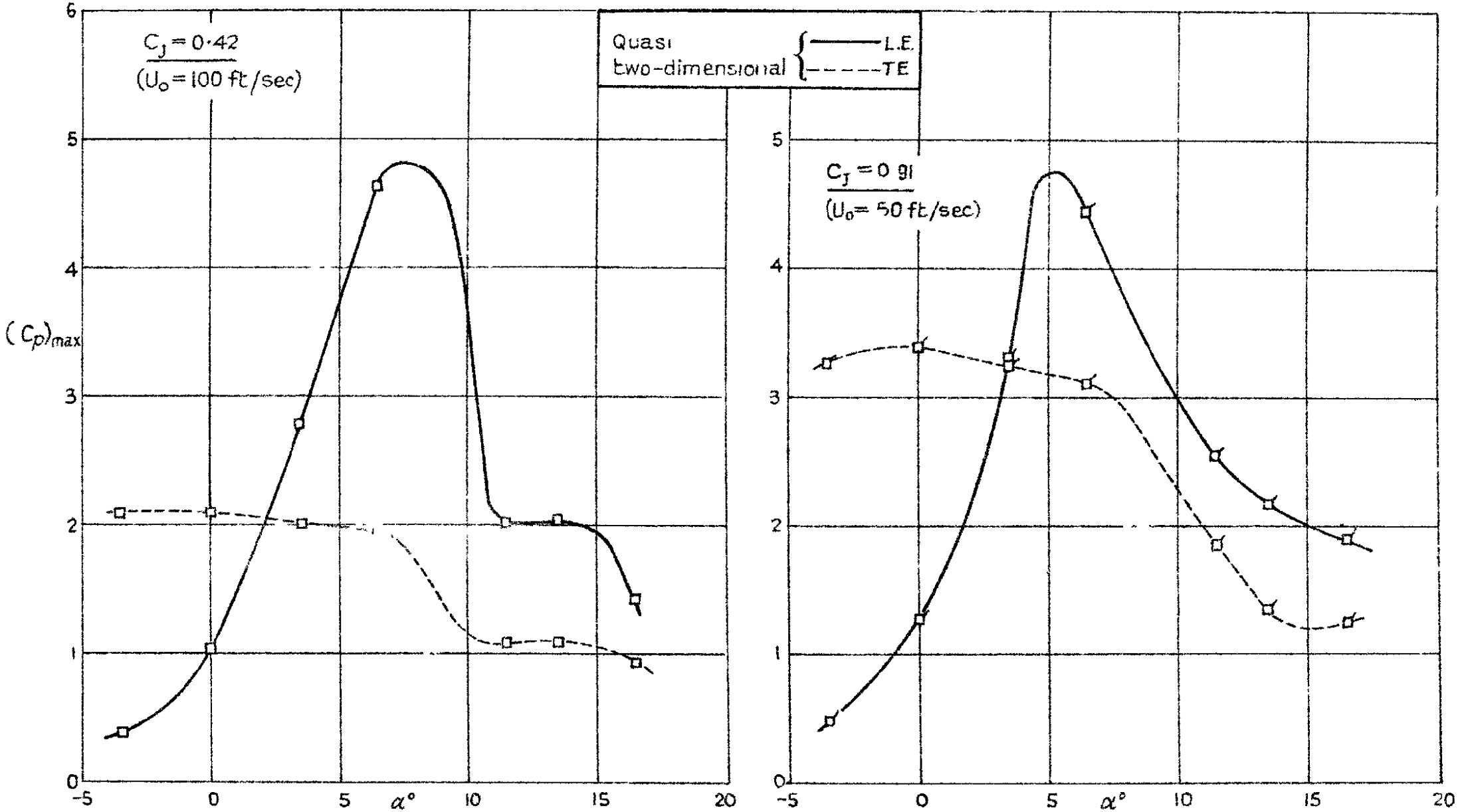

Fig. 18b

Variation of peak suction near L.E. and T.E.

FIG. 18c.

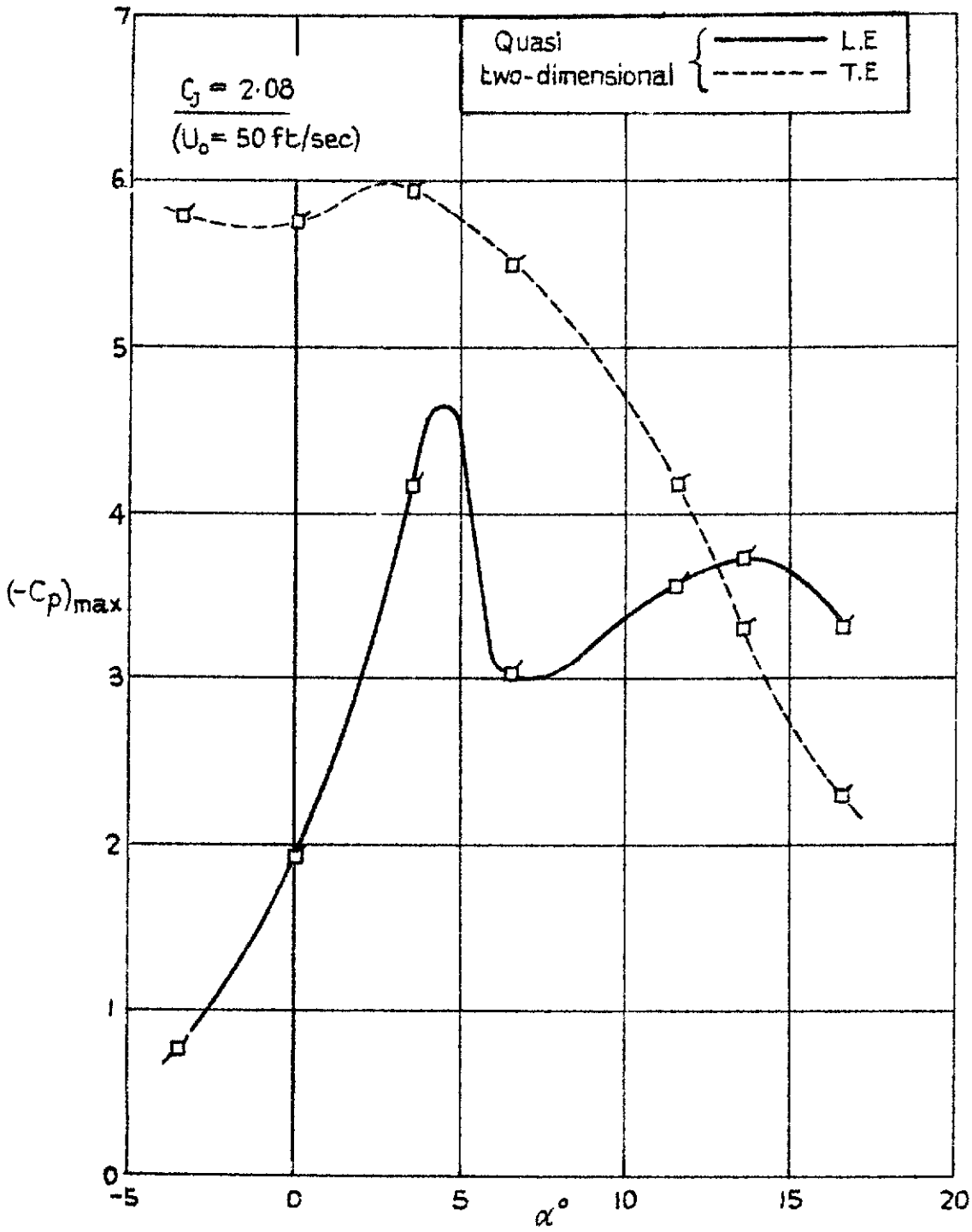

Variation of peak suction near L.E. and T.E.

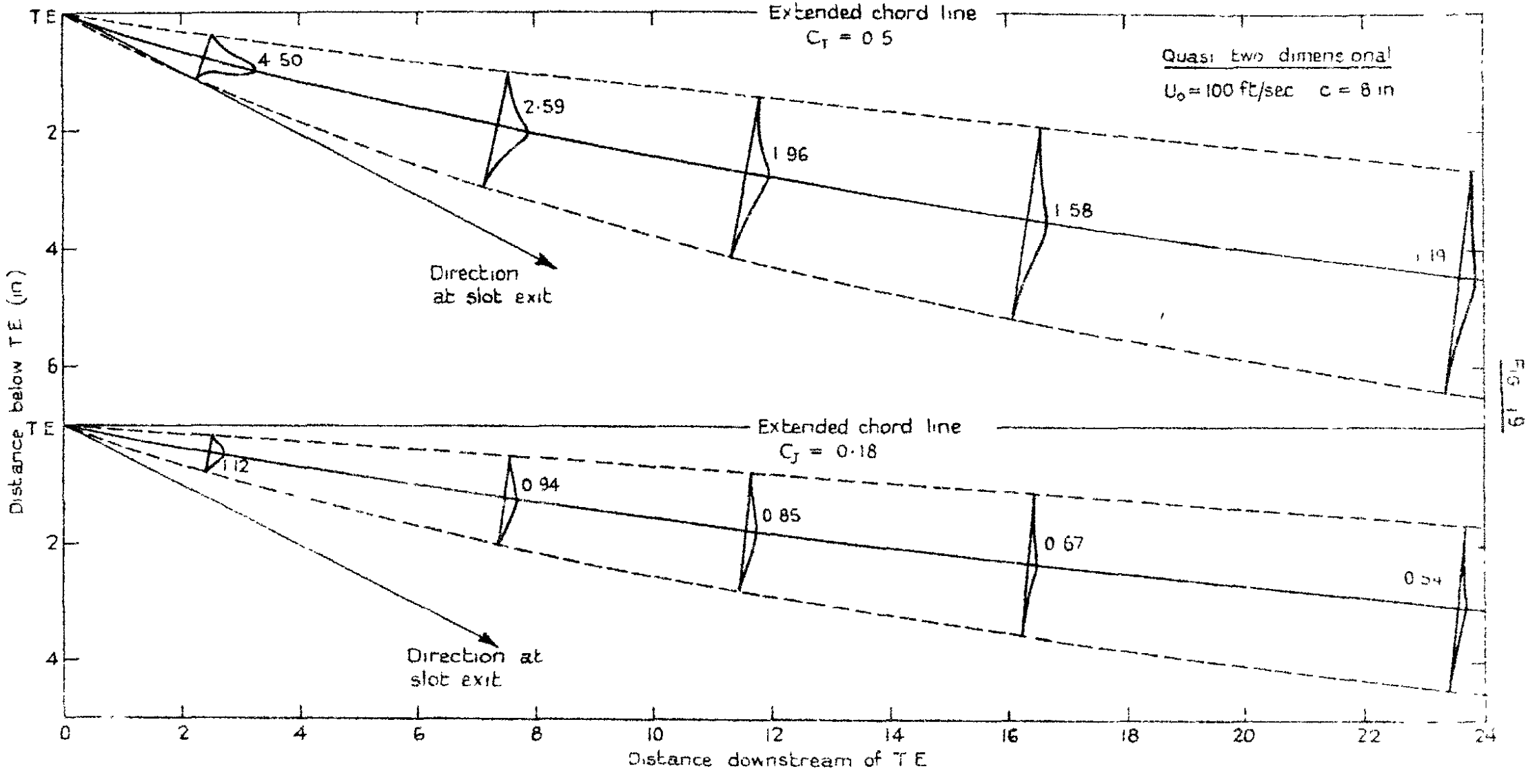

Fig 19

Mean line and total head profiles of jet

C.P. No. 304
(17,990)
A.R.C Technical Report

Printed and published by
HER MAJESTY'S STATIONERY OFFICE

To be purchased from
York House, Kingsway, London W C 2
423 Oxford Street, London W.1
P O Box 569, London S.E.1
13A Castle Street, Edinburgh 2
109 St. Mary Street, Cardiff
39 King Street, Manchester 2
Tower Lane, Bristol 1
2 Edmund Street, Birmingham 3
80 Chichester Street, Belfast
or through any bookseller

Printed in Great Britain

S.O Code No. 23-9010-4

C.P. No. 304